Optimisation of a Three-phase Partial Core Inductor

John H Morris

A thesis submitted in partial fulfilment
of the requirements for the degree of
Master of Engineering
in
Electrical and Computer Engineering
at the
University of Canterbury,
Christchurch, New Zealand.

30 July 2018

ABSTRACT

Three-limb partial core inductors are studied by observing the effects of combining three, single-limb partial core inductors in close proximity, and energising them in a 3-phase circuit. The observed effects include an increase in magnetising reactance in each winding due to a lower reluctance path between the limbs, and an increase in *ac* resistance, becoming more significant at higher frequencies. Increased inductor resistance at higher frequencies was found to be an important consideration in applications where harmonic current may be encountered.

The research characterises the behaviour of 3-phase partial core inductors and empirical deductions are made to estimate the effects of winding proximity. A new formulation for 3-phase magnetising reactance is developed based on a modification to the air reluctance calculation for the single-limb partial core inductor.

Power loss measurements of a split winding show that heating effects at the ends of partial core windings are due to eddy current loss in the winding conductor and are not primarily due to *ac* conduction loss. Further observations by calorimetric measurements confirm that orthogonal flux components give rise to eddy current loss resistance in both the core and in the winding, and become more significant in a 3-phase partial core inductor. Winding eddy current losses were generally more significant than core losses at frequencies above 150Hz in the units tested. A modification to the transformer equivalent circuit model is proposed by introducing two new resistance terms for winding orthogonal eddy current resistance and core orthogonal eddy current resistance in the case of a 3-phase partial core inductor.

With the inclusion of the new loss terms and modified magnetising reactance in the model, a new design process is developed to optimise the efficiency of a 3-phase partial core inductor. It turns out that the optimal cost-performance for any partial core inductor is determined by the choice of winding conductor width. To confirm this analysis, two designs for a 3-phase partial core project inductor were built and tested. The project inductors were compared to a good quality commercially built unit of the same specification.

The results show that for the smaller values of inductance examined in this thesis, a partial core inductor with a single layer winding of optimal conductor width, produced the most cost-efficient design. A two layer winding of optimal conductor width produced

a design with the lowest material weight and cost per unit inductance, but with poorer efficiency and therefore a significantly higher temperature rise.

Partial core inductors were observed to have reduced efficiency at mains frequency compared to full core inductors due to having more windings per unit inductance. This results in the winding having a higher winding *dc* resistance and therefore, greater power loss at rated current. However in the units compared, the partial core inductor with a single layer winding was more efficient at harmonic frequencies than the commercially built unit and particularly at the 5^{th} and 7^{th} harmonic orders. Usefully, this reduced heating effects in the project inductor application chosen.

CONTENTS

LIST OF FIGURES

LIST OF TABLES

ACKNOWLEDGEMENTS

The journey over the last four years has been filled with tremendous learning experiences and has been a roller coater ride to say the least. Due to earthquake repairs, the department's research facilities have moved all over campus from the old wing to the Warehouse and Kirkwood Village, the HV lab and then finally to the wonderful newly renovated research labs. If anything, a number of the department's members have become expert electric tuk tuk drivers! But for me, the real ride has been wrestling with the harsh reality of the laws of electromagnetism. Model and build something you think will work, but the laws teach you some more about the truth and beauty of the invariant nature of things. The understanding gained by incremental trial and hard learned experience has been invaluable, and reinforces and illuminates the theory.

What started out as a project to learn about a resonant transformer prototype, led to the necessity to firstly address the challenge of partial core device efficiency. I am profoundly grateful for the opportunity to do this work and regard it as a privilege to gain an insight into this fascinating subject.

First of all I would like to thank my supervisor Andrew Lapthorn for all your teaching, encouragement and efforts to help me finally finish my thesis! I'm sure at times I've given you reason to wonder what on earth I'm up to now, but enabling my desire to search broadly before narrowing it down has proven invaluable for my learning and I thank you for your patient and supportive approach to supervision. Thank you to my co-supervisor Neville Watson for the occasional conversation, inductor projects, and things to think about along the way. I'm sorry to have not yet developed the filter designs initially proposed, but the path has unfolded in this way. May I also pay my respects to Pat Bodger who inspired my interest from the beginning and has been supportive throughout these last few years. I regard myself as a most fortunate student to attend your last lecture series on the topic before your retirement and I wish you the very best. Thank you also to Bill Heffernan for your encouraging words and advice on all those weekends our paths crossed while in the lab. Good luck with your endeavours.

I would also like to offer my gratitude to the department's technical team who have accommodated my needs and provided many hours of support and encouragement. To Edsel Villa, Ken Smart, Jac Woodberg, Paul Agger, David Healy, Helen Devereux and a cameo appearance by Malcolm Gordon; you're a helpful talented team, thank you.

As a part-timer on campus, I did not associate much with my post-grad' peers, however I would like to acknowledge Andrew Berry for your help with experimental work and the various discussions and correspondence we have had. I wish you well with your work.

A great deal of the experimental work carried out would not have been possible without the support from two major sources of funding. First of all, a Return on Science grant was won based on this partial core research, and this has led to a stronger understanding of device efficiency, something identified as a first hurdle. Secondly and most importantly, I would like to thank Parcor Technology Ltd, and in particular Mike Ashburn for your tremendous support. Together we have developed a solid foundation for building opportunity going forward.

I would like to also make a special mention to an old (ok, not so old) friend Ian Lester who has provided the vital can-do attitude to building the many prototypes along the way. I very much appreciate what you have enabled Ian, and I could not have made so much progress without your effort and skills. Thanks mate.

My decision to return to university was supported by the flexible approach of my employers at IC Switchgear. Des, Marie, Steve and Chris, thank you for your good-will and encouragement. I would also like to thank my colleague Patrick O'Brien for the very nice geometric drawings and 3-D renditions provided in this thesis.

From the industry I would like to acknowledge the team at TWS Energy Controls who have been very helpful. Thanks Tony, John A., John D. and Graham for your procurement support and practical advice. I would also like to thank Allan at kVAr Correct for the loan of reactors and helpful perspective on the industry. Don't worry, I'll get those loan units back to you, I promise! I would also like to thank ABB and in particular, Peter and Bruce for the use of the workshop and varnishing facilities.

On a personal note, I must thank my long enduring family for your support and patience. There have been times where I have been distracted by this work and I'm very grateful for your understanding. To the lads, in particular Paul, Nick and Mark, I thank you for those evenings of philosophical discussion on completely unrelated topics!

And finally, to my loving mum and dear late dad, I hope I've done you proud in all of this. Thank you for everything you have done for me.

Having begun an interest in partial core transformer technology back in the formative years when the Transflux fluid induction heater was first patented, I worked on the early prototypes, and knew this was the path I really wanted to be on. It wasn't to be at that time however, but coming back to it nearly twenty years later, I am humbled by the wealth of research and theory development that has occurred over the years. So many of the building blocks have been pieced together in the theory of partial core transformer technology, that it has been a great platform upon which to scale, and hopefully, stand.

"The universe so vast, Would I ever find a place to be, It all moves too fast to see"

PREFACE

An investigation into power engineering applications for inductors with a partial core has produced a wealth of experimental data on a wide range of devices. Numerous inductors have been designed to suit applications such as detuning reactors for power factor correction capacitors, low resistance inductors for laboratory testing applications and inductive load banks. The results of experimental work show that modelling the *ac* resistance of partial core power inductors is crucial if efficient and useful inductor designs are to be achieved.

The approach taken in this work has been to model partial core inductor devices based on formulations developed through departmental research in the field of partial core transformers. Particular attention was paid to the consistent discrepancy of *ac* resistance in the power frequency spectrum between modelled predictions and experimental observations. Measurements show that the ac resistance is always higher than predicted, with the discrepancy becoming more significant as frequency increases.

Experimental work has demonstrated the great beauty of electromagnetic phenomena so readily observed in the partial core inductor. The presence of a stray magnetic field surrounding such devices, particularly at the ends, gives rise to induced effects in neighbouring metallic objects, but also of course, in itself. Induced loss effects in the winding for example, become very pronounced at higher frequencies of excitation, and indeed, it has been shown that by studying these effects across a wider spectrum of frequencies, a more accurate estimation of loss components can be determined at lower frequencies. For example, eddy current loss resistance is reasonably constant for the frequencies (up to $800Hz$) used in this work, and therefore it has a single characteristic resistance based on the physical construction of the device at hand. By adding this single value of resistance into the model, the correction applies to the whole range of measured frequencies confirming the optimal value to be achieved by formulation. When such corrections are attempted at only $50Hz$ say, the errors can be large and it is not certain if modelled predictions bear any relevance to the often very small changes produced in modelled resistance at $50Hz$.

This thesis does not offer a treatise on theoretical electromagnetics. It does however provide a picture of the electromagnetic forces at play based on the real effects observed in over thirty 3-phase inductors constructed and tested over the course of

this research. Progressively by experimental deduction, refinements in constructional methods demonstrate how to produce the most efficient 3-phase partial core inductor. The outcome is a device that behaves remarkably well when compared to a good commercially built unit and shows that practical and commercially viable designs are within reach. The benefit of this being a significant reduction in material required to build devices which in certain aspects, perform better than the full core counterpart that was tested.

Chapter 1

INTRODUCTION

1.1 GENERAL OVERVIEW

National electric power systems of today are sophisticated systems designed to reliably distribute electrical energy to consumers within a relatively tight supply voltage tolerance. Yet despite significant advances in technology and computerisation of control systems, the essential features of the *ac* electric system are the same today as they were in the original late nineteenth century systems; being electric generation, transformation and distribution of alternating current.

Of transformation, there have been significant advances in the technology of power transformers since the early times, and efficiencies better than 99% are not just achievable, they are required under the prescriptions set out by international standards governing the manufacture of large power transformers. However, the fundamental operation of transformers remains as unchanged as the principle of induction discovered by Faraday in 1831. The advance of power electronics and the so called solid state transformer, while having a lower device efficiency, have theoretical advantages in power transformation when considering the benefits to load flow and overall system efficiency. This technology may well be the way of the future as suitable transistor technology is developed.

In the same way as power transformers, inductors used in power systems have also undergone technological improvement as better materials and a deeper understanding of their inner workings have developed. Largely though, they have remained unchanged in over one hundred years and it is often advances in related technology that have driven improvement. For example, steel core manufacture has improved with lower loss steels and innovations such as distributed gap core technology due to the ability of automated machinery to precisely cut and fold laminations to form interleaving core sections in an economic way. This has the effect of lowering reluctance in the core, reducing leakage effects and reducing weight and assembly times which enable more efficient use of core and winding material and lower construction cost. At the complete opposite end of the spectrum of innovation regarding the minimisation of leakage effects, sits the open or partial core transformer or inductor. These devices were in fact the very

first manifestation of transformation devices invented by a team of engineers lead by K. Zipernowsky, O. Blathy and M. Deri from the Ganz factory in Budapest in the 1800s. These guys later went on to invent the closed or full core, shunt connected transformer. Due to the greater efficiency that could be achieved with full core devices, they have developed into the mainstream technology employed in power systems today.

In recent decades at the University of Canterbury, attention has returned to the partial core transformer as it has been shown that a significant reduction in material and device weight can be achieved in certain applications when compared to equivalent full core designs.

In the case of this thesis, an application is chosen to test the feasibility of applying partial core technology to a 3-phase power inductor application. By applying the current understanding of single-limb (1-leg) devices, and comparing this with the experimental results obtained when three such devices are brought together to create a 3-phase inductor, empirical analysis has enabled the optimisation of a 3-phase device to reduce material weight and achieve acceptable efficiency.

1.2 THESIS OBJECTIVES

The goal of the research is to develop a design process to enable optimisation of the partial core inductor for 3-phase power applications and to verify if feasible designs may be achieved.

To enable optimal design, further consideration is given to the loss mechanisms in the partial core inductor. By empirical means, a contribution to the formulation of the apparent loss mechanisms is sought.

Many applications of power inductors require a 3-phase configuration and therefore modelling of 3-phase devices based on 1-leg device formulations is sought.

The optimised designs are to be built and tested and compared to a good quality power inductor of the same specification.

1.3 THESIS CONTRIBUTIONS

A geometric formulation is proposed to modify the reluctance of a 1-leg partial core inductor to enable modelling of a 3-phase partial core inductor based on core separation.

Experimental observation has proven the existence of winding eddy current loss resistance. An estimation of the winding eddy current resistance is proposed for 3-phase partial core inductors based on a similar approach used to estimate core axial eddy current resistance.

Core orthogonal eddy current loss resistance is estimated based on a volumetric ratio of core to winding.

A modification to circuit theory is proposed to include both the winding eddy current loss and core orthogonal eddy current loss resistances.

An optimisation method is devised and tested to determine the optimal winding formation for a 3-phase partial core inductor.

1.4 THESIS OUTLINE

Chapter 2 In this chapter the relevant background to partial core research is presented. This includes a brief overview of how partial core technology has been applied and the theory developed to account for the differences to conventional transformer technology.The chapter concludes with an overview of conventional inductor applications and a suitable new application for a 3-phase partial core inductor is selected.

Chapter 3 A sequence of experiments is conducted to arrive at the best constructional technique for a 3-phase partial core inductor including:

- Winding formation
- Core length
- Winding aspect ratio
- 3-leg core lamination orientation
- 3-leg winding proximity

Chapter 4 Following the experiments of Chapter 3, the best constructional technique is found and further experiments are conducted to derive an empirical formulation of the reactive and resistive elements of the 3-phase partial core inductor including:

- Estimation of 3-phase device self-inductance
- Identifying the winding eddy current resistance and empirical formulation
- Estimation of orthogonal core loss resistance and empirical formulation

Chapter 5 Based on the formulations of Chapter 4, a new technique is presented which enables design optimisation of a partial core inductor including efficiency and material usage. The design technique assumes there is a target reactance at a prescribed current and frequency. Conductor size, shape and formation are defined and a target peak flux density is set. The design routine then computes the core cross-sectional area required for each increment of winding turns within a specified range maintaining the target peak flux density. The output from the algorithm is a range of inductors of incremental winding turns with the required core cross-sectional area for each. From this range the required inductance can be found along with its performance, weight and cost. Because the routine is also able

to compute the total power loss at each increment of winding turns, the efficiency can be compared for partial core inductors of any target flux density, type of conductor and number of winding layers that achieve the required inductance. The output of the algorithm enables optimisation of designs for weight, cost and efficiency.

Chapter 6 To verify the design output of the thesis, an application for the partial core inductor is described and analysed in terms of the typical performance of commercially available units. A specification is prepared for a project inductor. The application chosen is a detuning reactor for a 33kVAr, 400V capacitor bank used in low voltage power factor correction systems.

Chapter 7 To conclude the thesis, the new formulations are used to develop a design for the project inductor. Two designs are analysed, built and tested and compared to the results of the design model and a commercially available unit. A conclusion is reached about the merits of the partial core inductor technology applied in this application.

Chapter 8 Conclusion, critique and future work

Chapter 2

BACKGROUND

2.1 OVERVIEW

This chapter begins by defining what is meant by the term "partial core inductor" and its derivation from the current research into transformers with a partial core. An overview of recent research applications is provided. The theory of partial core transformer technology then follows with the relevant contributions from researchers in the field. An overview of the many types of power system inductor is then provided and the project inductor for this work is identified.

2.2 INTRODUCTION TO THE PARTIAL CORE TRANSFORMER AND INDUCTOR

A partial core inductor is a two terminal device based on a single-winding transformer with a partial core. A partial core may be defined as core material that is contained mostly within the winding of the device, and where the magnetic circuit from each end of the core is completed through air or other non-permeable medium. Devices with a partial core have a classical solenoid appearance as shown in Figure 2.1, but unlike this earlier depiction, have magnetic fields that emanate from the ends and sides of the device like the magnetic field of the earth.

Research has shown that partial core transformer designs can provide a dramatic reduction in physical size and weight when compared to the traditional full core equivalent. This is due mainly to the reduction of core steel required by eliminating the top and bottom yokes and side limbs. This work investigates if partial core power inductors can offer comparable performance to conventional full core devices at reduced material weight and cost.

A partial core inductor can be thought of as transformer with only the primary winding. Therefore the modelling used to estimate the values of components used in the equivalent circuit are similar to those used for the partial core transformer with the exclusion of the secondary winding elements.

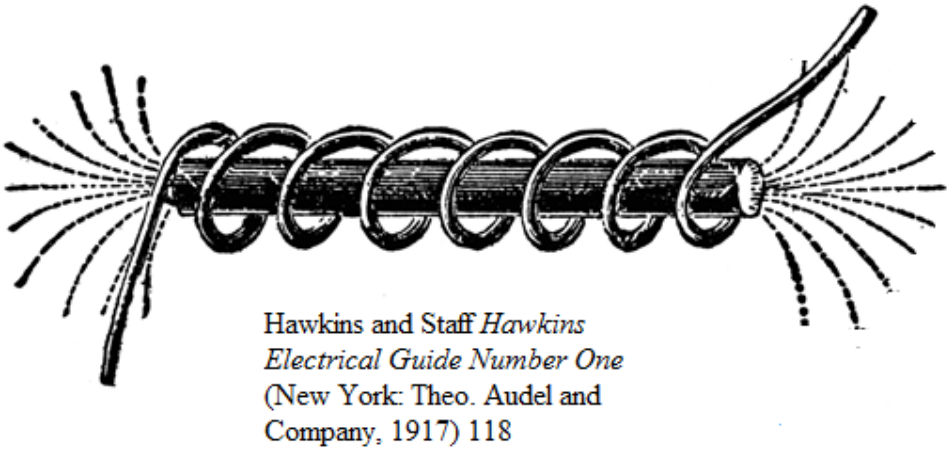

Figure 2.1 Classical depiction of a solenoid

Of particular interest is the estimation of power loss within the device, which his determines if a given design is viable.

2.2.1 Recent applications of partial core technology

2.2.1.1 Fluid heating

The first significant application of partial core technology was of induction fluid heating Bodger et al. [1996], and more recently investigated by the work of Takau [2015]. These devices are essentially transformers with an optimised, near short circuit secondary and core losses which enable optimum power transfer at mains frequency to heat a fluid or gas medium. Losses developed in the primary winding may be thermally conducted toward the fluid medium to improve efficiency in the device, or they may be convected by immersion in oil. The core and secondary losses heat the fluid medium.

This transformation technology is designed to generate heat in the device which is the reverse of typical transformer engineering. Due to the physical construction of the direct heating surfaces of the transformer secondary, surface power densities can be designed to provide an optimal heat transfer gradient to the product being heated in much the same way as conventional two-circuit heat exchanger technology. But rather than requiring a heat source such as steam or hot water to heat the primary circuit, the heat is provided directly by transformer action.

2.2.1.2 High voltage resonant test transformers

The production of high voltage for insulation testing of electric machine windings can be cost-effectively achieved by a partial core transformer, Bell [2008], or cascaded partial core transformers up to $100kV$ Irani [2017]. In these devices a high voltage is produced

by resonating the test transformer with the capacitance of the device insulation under test; such as the stator winding of a machine or cable conductor with respect to earth Irani et al. [2013].

Due to the high voltages applied during the test, the capacitive reactive power is significant and is usually difficult to obtain directly from the local distribution board. Compensation with inductances requires often complicated arrangements and it has been shown that partial core transformers can provide not only the required voltage transformation, but may be readily tuned to resonate with the item under test and therefore reduce the burden of the local supply Enright and Bodger [2005].

The heat generated in these transformers may be significant, but due to the nature of the application requiring only short duration testing, in the order of minutes, the effect of heating is not particularly significant and can be limited by providing cool down periods between tests or some other form of heat removal process. The resistance characteristic of these transformers is significant however in terms of the quality factor at resonance, particularly when transformers are connected in cascade mode. Irani [2017] A poorer quality factor limits the voltage developed at resonance if the resistance of the tuned transformer circuit is too high.

These devices have proven to significantly reduce the size and weight of test equipment used for this purpose Enright and Bodger [2005]. In addition, the transformer construction is of a dry type thus removing the need for a tank and oil Bendre et al. [2007].

Hi voltage potential testing is an ideal application for partial core transformer technology. Equipment must be readily portable and operate on single phase supplies of typically less than 100A. It has been shown that test voltages of up to $100kV$ are now possible which is sufficient for many of the machines tested in New Zealand.

2.2.1.3 Partial core power transformers

The research has also produced a number of power transformers with step down ratios up to $11kV : 230V$. The work of Zhong [2012] showed that it was feasible to built a step down partial core transformer of $12kVA$ rating with a transformation of $11kV$ to $230V$. The results produced a transformer with an efficiency of 90% and regulation of 10%. Whilst these figures might be improved by design, the largest part of the loss was due to winding *dc* resistance. Reducing winding *dc* resistance requires a larger conductor which would therefore have an impact of the overall size and weight of the device.

The other significant feature of this design was the open circuit power rating at around 67% of full load power. In other words, under no load conditions, the apparent power input to the transformer was $8kVA$ against its full load rating of $12kVA$. This is compared to standard full core transformer design where no load power would be in the order of 3 to 5% or $0.6kVA$ in this case. The reason for the high standing load

of the partial core transformer is due to its typically very low magnetising reactance component. This is due to the partial core ends having a high reluctance path and therefore an overall low relative permeability core Liew [2001]. This is another reason why partial core transformers are not used as distribution transformers.

At full load, partial core transformers can achieve reasonable efficiency of up to 98%, but as yet they have not proven to be commercially viable.

2.2.1.4 Superconducting partial core transformer

High temperature partial core transformers have been designed and tested at the University of Canterbury by Bodger et al. [2005] Chew [2010] and Lapthorn [2012]. These devices have proven the benefit of the partial core approach, however the relative cost of refrigeration reduces the overall efficiency of the transformer system and was shown to be uneconomic. Apart from the currently prohibitive cost of the HTS wire, the other main obstacle to partial core superconducting transformer designs, is the radial magnetic field produced at the ends of the windings Bell [2008]. This field causes a reduction in the critical current carrying capacity of HTS wire which may be prone to failure under fault conditions.

Superconductor winding losses modelled by Lapthorn [2012] show they are more significant towards the winding ends due to the influence of intensifying radial fields. These winding losses occur in superconductors due to a number of identified modes, however they may be generally classified as conduction losses as they increase the resistance of that portion of conductor affected by the influence of the local magnetic field. In this thesis, the effect of winding *ac* resistance is studied in particular detail to determine if a similar conduction loss mode occurs in ordinary winding conductors.

2.2.1.5 Fault current limiting partial core transformer

In this work, fault current limiting of high temperature superconducting transformers was investigated Sham [2015]. It was found that there may be an optimal design whereby the leakage reactance of a transformer combined with the sudden increase in resistance due to superconductor quenching may enhance fault current limiting performance in transformers.

This work may lead to designs of power transformers that have good fault current limiting characteristics without the accompanying high leakage reactance typical of conventional designs. The concept however relies on the use of high temperature superconducting methods and has been previously shown, may require a radical new approach for such devices to become viable.

2.3 MODELLING THE PARTIAL CORE TRANSFORMER

To examine the behaviour of devices such as transformers and inductors, a mathematical model is developed which comprises the various mechanisms that give rise to the electrical performance of the device when connected into a circuit.

These mechanisms or electrical elements of the model are linked to the physical parameters of the windings and core. In this way, changes to the physical construction of the device are linked to electrical performance in the model to determine the response characteristic of the device. The method by which a design is developed is to set the physical parameters of the device construction and simulate the device performance under electrical design conditions.

There are two main approaches to producing a model of electrical performance. The first is by means of circuit theory in which a network of passive electrical elements such as reactance, resistance and capacitance are connected in such a way as to produce an equivalent circuit for the device. This approach is the traditional method of analysing the complex characteristic of the device and has been attributed to Steinmetz who applied complex number notation to electrical circuit theory and pathed the way to more straightforward solutions of electrical systems Hase [2013]. The advantage of this approach is the very rapid calculation of device response and is the approach used in this work.

The second method is by means of computational finite element analysis which finds solutions to the to a physical representation of the electromagnetic device under study. This method solves for the electromagnetic state of the device under defined conditions and produces an electrical response characteristic, whilst enabling visualisation of the magnetic field densities surrounding the device. This approach has been shown to produce more accurate results but requires much more computational time, making design iterations more laborious Bell [2008].

To aid the design process, a technique known as the Reverse Design Transformer Modelling Technique is applied to designs in this work.

2.3.1 Reverse design transformer modelling technique

The reverse design technique enables transformer and inductor designs to be prepared based on the actual materials available. A model linking the various physical parameters of the windings and core, to electrical performance enables the designer to change materials and construction to test the effect they may have on the design performance Bodger et al. [2000].

By means of an iterative process, changes are made until the working design converges on the optimal design to suit the application.

2.3.2 Reactive elements

2.3.2.1 Magnetising reactance

Throughout the research journey of partial core devices, one of the more essential contributions has been modelling of the magnetising reactance. In the circuit theory model, reactance is modelled by introducing a new formulation of the effective permeability of the core by taking into account the reluctance of the partial core and the air path at the core ends Liew [2001]. This has enabled designs of transformers of many types to be modelled to very good accuracy.

Circuit theory estimations may also include a magnetising function akin to a Rogowski factor which multiples the magnetising reactance by a factor < 1 to account for the flux leakage in windings with a low aspect ratio. The magnetising function has proven to be useful in some applications but has not been applied in this work.

The most recent advance in this work has been to compare the circuit theory estimations with estimation produced by finite element analysis Bell and Bodger [2007]. This has shown that finite element analysis produces closer estimations than circuit theory despite making a number of assumptions about the nature of the winding, core and surrounding air to reduce computation time.

FEA was not used in this work however as circuit theory has proven to be a straightforward and accurate enough method for modelling of the lower inductances used in this research.

2.3.2.2 Leakage reactance

Leakage reactance has been treated in a similar manner to that used in full core transformers as it is related mainly to the magnetic energy confined within the volume of the winding Liew [2001].

The formulation of a magnetising function for the leakage reactance was not used in this work due to the small contribution that leakage reactance has in the small inductances examined. (In the order of $1mH$) Lapthorn and Bodger [2009]

Due to the nature of the small inductances explored in this work, the leakage reactance is effectively in series with the magnetising reactance which gives the self-inductance of the device.

2.3.3 Resistive elements

2.3.3.1 Conduction losses

Winding *dc* resistance

The winding *dc* resistance is calculated based on conductor cross sectional area, length and resistivity, which is dependent on temperature. Liew et al. [2001] At low frequencies (mains) this is the predominant loss component and is a pure resistance giving rise to conduction losses.

Skin effect and proximity effect

Skin effect is an increase in conductor resistance due to a reduction of the effective cross sectional area of the conductor due to higher frequency currents flowing. Higher frequency currents give rise to an electric field within the conductor which exclude current from penetrating further into the conductor. The effect is not noticeable until the effective skin depth is less than half of the thickness of the conductor. Roddy and Coolen [1981]

The proximity effect is caused by the influence of current in a winding on a neighbouring winding. The magnetic field established about a conductor when a current flows can give rise to a constriction in the cross sectional area of neighbouring turns in a winding. Over many turns this effect can cause a significant increase in winding resistance but is usually more noticeable at higher frequencies above 3kHz, or at lower frequencies where heavy currents flow. Ferreira [1989]

Neither of these effects are accounted for in this work.

2.3.3.2 Induction losses

Hysteresis or Steinmetz core loss

Alternating current losses in the core are significant and must be accounted for. The current approach is to quantify these as hysteresis loss and eddy current loss as they are in the full core transformer loss model. The losses are derived empirically and may be represented by the mass of the core, frequency of excitation and the applies flux density. Nasar and Boldera [1989]

Hysteresis loss is due to the coercive force required to align the magnetic domains within the core steel. Hysteresis loss is therefore proportional to the frequency of excitation and the flux density in the core.

Eddy current core loss

Eddy current loss is produced by currents circulating in each lamination around the axis of the magnetic field. Due to the path of the circulating current being confined to a thin lamination it is well defined, and therefore the circulating current path has a defined resistance no matter what the frequency or flux density in the core. The circulating current is estimated by a notional emf applied across the resistance of the current path of the core lamination. Therefore the effect of increasing temperature increases the core resistivity giving rise to a higher eddy current resistance and therefore a lower power loss develops for a given lamination emf. Slemon [1966]

Conversely, by significantly lowering the temperature of the core at cryogenic temperatures, the skin depth of the lamination is reduced and this also has the effect of increasing the effective eddy current resistance of the core material if the skin depth is less than half the thickness of the lamination. Liew [2001]

In this work, operational temperatures are taken to be at room temperature for all comparative measurements. The effect of temperature is included in the model however by means of a coefficient of resistivity when calculating the core loss resistance components.

Orthogonal eddy current core loss

Research has also identified an orthogonal or radial loss component in the core due to flux bending through the steel at the core ends. The work of Huo [2009] in defining the losses due to orthogonal flux contributions has provided a method for better estimation of these effects. The approach used was to decompose the flux contributions in the core into three planes of effect and derive an empirical formulation for each by applying a magnetic field in each plane. Further assumptions were made about the lengths of the core subjected to each of these effects and in the end, a model was obtained that was supported by the data collected for the experimental cores sampled.

However the model does not account for losses in 3-phase devices where the orthogonal component, as demonstrated in this work, is intensified by the flux contribution of neighbouring cores and windings.

The empirically derived orthogonal core loss components also do not account for observable induced *ac* losses in the winding and therefore their formulation will not have taken this into account. Therefore this approach to estimating core losses has not been used in this work.

Cores constructed with radially stacked laminations produce significantly less heat due to orthogonal flux cutting through less core steel and therefore producing less eddy current loss. Refer to Figure 2.2. Lapthorn and Keenan [2012]

Radial stacked laminations is a technique used where there are increased radial fields due to the construction of a transformer or inductor.This may occur for example in gapped-core inductors where the gap is significant and gives rise to increasing stray fields. Heathcote [2007] As the partial core inductor is the extreme case of this where stray fields are at a maximum, the radial core is a proven technique for reducing core losses in these devices.

Due to the work involved in producing the many cores (in triplicate), radial cores have not been used in the formulations applied to developing 3-phase models in this work. It is acknowledged however, that using radial cores may well reduce core losses but it is not certain if they will reduce total losses when winding losses are taken into account.

Winding eddy current loss

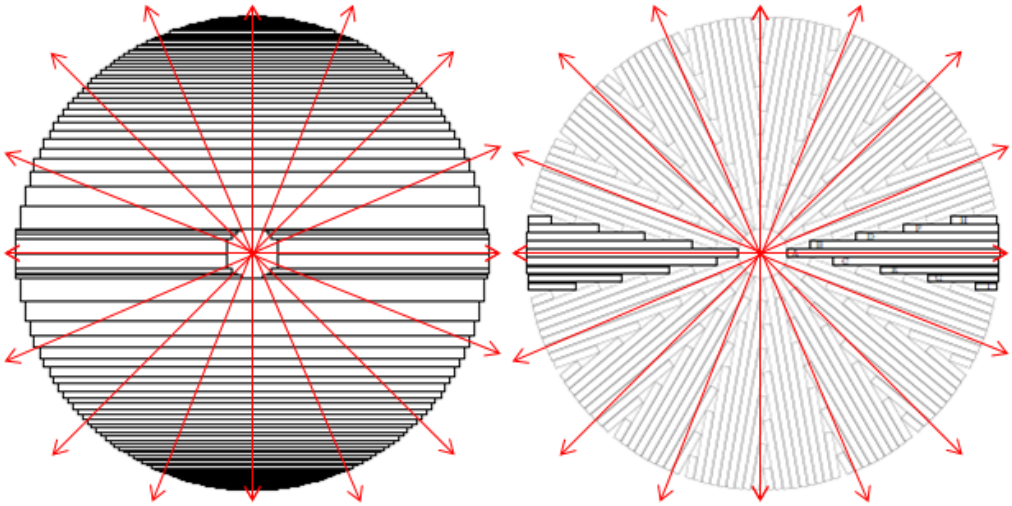

Figure 2.2 Flat stacked laminations and radial laminations

In this work a loss mode has been identified which occurs in the winding of 1-leg partial core inductors, and which is magnified in 3-phase configurations. A definitive study of this loss mode has led to the conclusion that eddy current losses occur in the winding and this loss component may become very significant at higher frequencies.

2.4 APPLYING PARTIAL CORE TECHNOLOGY TO POWER INDUCTORS

Due to the inherent design of partial core devices, it has been shown that a significant reduction in core steel is possible. This is achieved in two ways:

1. Only the limb contained within the winding is utilised eliminating the need for cross members and side members and,
2. a reduction of core cross sectional area is possible due to the usual requirement for an increased number of turns in the winding to achieve a given inductance.

An increased number of turns comes about because of a significantly higher path reluctance due to the open core ends where the field is completed through air. To achieve a given inductance, more turns are required in accordance with:

$$L_m = \frac{N^2}{R} \tag{2.1}$$

where L_m is the magnetising inductance (H)
N is the number of turns
R is the reluctance (At/Wb)

Where a greater number of turns is required to achieve a given inductance, a core of reduced cross section may be used to achieve a specified peak flux density in the core.

Core size reduction requires more turns in the winding to achieve a given inductance however, and this may cause additional winding losses. As each of these parameters has an effect on the other, it is necessary to compute the total effect of changing the physical parameters of the winding and core to produce the optimal design. The question proposed therefore is, can partial core technology benefit the design of power inductors?

Power inductors may operate continuously in service, and good thermal performance is essential for device reliability, especially in applications where harmonic currents may be encountered. Therefore it is necessary to account for core and winding losses to achieve optimal inductor designs.

2.5 USES OF INDUCTORS IN POWER SYSTEMS

Inductance has many uses in electric power systems and may be applied in a variety of ways including shunt and series connected modes. Inductance is packaged in a device generally referred to as a reactor, choke or inductor. The AS/NZS 60076.6:2013 Standard refers to inductances used in power applications as reactors, and that term shall be used in this thesis when it is specifically identifying a 3-phase power inductor. Reactors are a fundamental component of any *ac* network and may operate from a few volts to hundreds of thousands of volts, and have power ratings from a few *VA* to many *MVA*.

The Standard refers to the many different uses for reactors including:

- Shunt and series compensation reactors for managing reactive load in transmission lines
- Current limiting reactors to limit the level of fault current that may flow in a system. These are generally applied when fault levels may be higher than the economic fault levels of protective equipment
- Neutral-earthing reactors connect the neutral point of a distribution system and may be used to monitor earth fault currents
- Filter reactors for tuning or detuning capacitor banks connected to the network. These reactors are designed for high harmonic current.
- Damping reactors for capacitors minimise switching transients when switching capacitors by providing a critically damped circuit and may be combined with resistors to achieve this.
- Capacitor discharge reactors connected across capacitors have a very high reactance at mains frequency, however when the power is switched off, they present a very low *dc* resistance to across the capacitor to quickly discharge it.

- Smoothing reactors are used in *dc* applications to reduce the crest factor or ripple on rectified *ac* supplies.

In this thesis, a filter reactor used for detuning a capacitor bank was chosen as a suitable candidate for applying partial core technology as is explained in Chapter 6.

2.6 CHAPTER 2 CONCLUSION

The partial core inductor is defined as a single primary winding of a partial core transformer.

There is a large volume of research on partial core transformers from induction heaters, transformers that resonate with the load and superconducting transformers.

Power inductors, or reactors, are a fundamental component of *ac* power systems and have many uses. The application of partial core technology to reactor design requires a specific application due to the many purposes for which reactors may be used. In this thesis, the application is a filter reactor for detuning capacitor banks and is discussed in detail in Chapter 6.

Chapter 3

QUALITATIVE CHARACTERISATION OF THE PARTIAL CORE INDUCTOR

3.1 OVERVIEW

In this chapter, qualitative characteristics of the partial core inductor are presented by way of experimental observation along with discussions of their results. The chapter begins by investigating single limb (1-leg) inductors of various winding designs and aspect ratios before progressing to three limb, 3-phase devices.

The experimental work demonstrates many typical characteristics observed in the numerous partial core inductors tested. The work was carried out to better understand partial core behaviour, and, is included in the thesis to explain why it was felt necessary to search for, and quantify ac losses in the winding. The chapter concludes with a best approach to physical construction of a 3-phase inductor as a basis for the project inductor design.

3.2 INTRODUCTION

Numerous aspects of a partial core inductor construction have been found to influence the reactive and resistive elements of the equivalent circuit model used in partial core research. The equivalent circuit model is examined in detail in Chapter 4, however it is considered useful to first observe the general effects such constructional aspects have. Empirical observations of the most relevant constructional aspects are presented to highlight their effect as follows:

- Winding formation (rectangular conductor orientation and sheet conductor)
- Core length with respect to winding length
- Winding aspect ratio
- 3-leg core lamination orientation
- 3-leg winding proximity

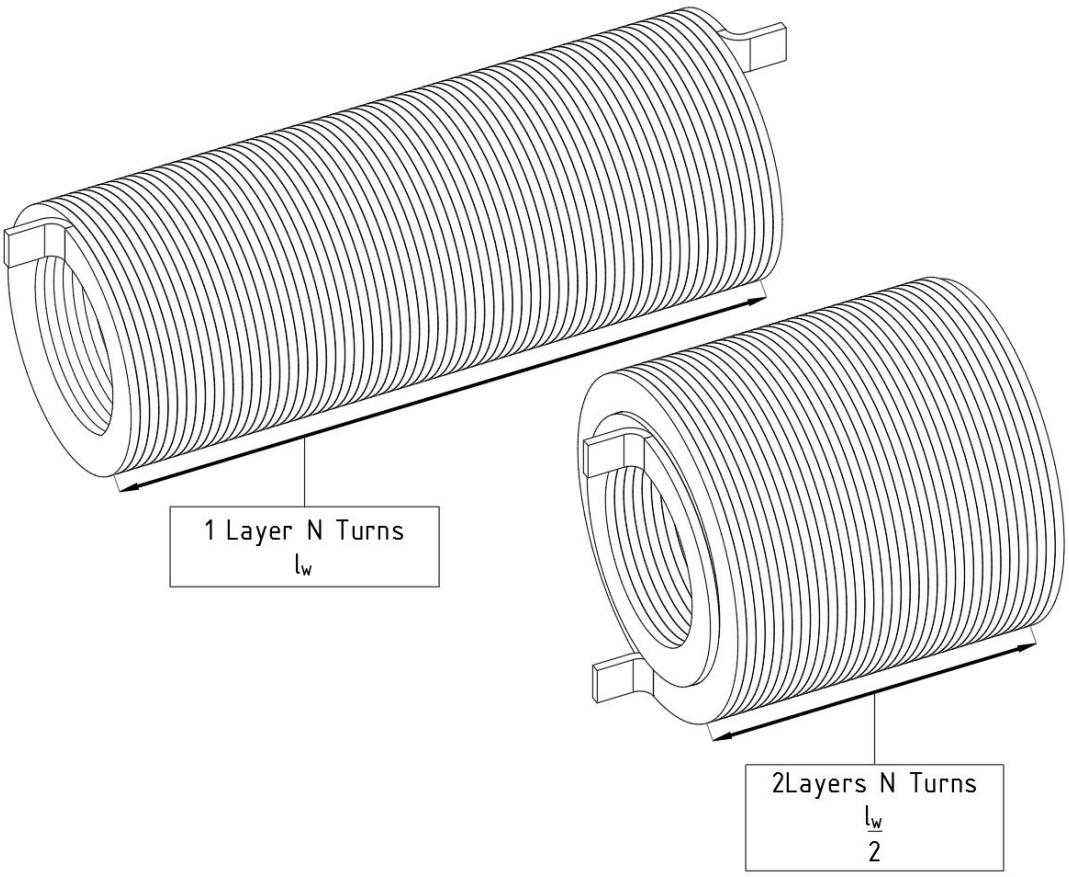

Figure 3.1 Illustration of single layer and two layer winding of half width

3.3 WINDING FORMATION

During experimental trials on partial core inductors it was observed that the more densely packed a winding, i.e. the more turns per winding length, the greater the self-inductance for a given number of turns. For example, if a partial core of a given size has a winding of N turns wound in one layer of length l_w, then let the self-inductance of the winding equal L. If the same number of turns is arranged so that the winding takes up half the length ($l_w/2$) on the same length core, the inductance would be approximately $1.3 \times L$. Refer to Figure 3.1. Note that the cores are not shown for clarity, however they are both the same length as the longer 1 layer winding. Further, for a winding of given length, the self-inductance of the winding increases in relation to core length where the core is longer than the winding.

It was also observed that the equivalent series ac resistance of a given number of turns increased with the number of winding layers, and more dramatically with frequency. Therefore, more layers of winding produced a more compact winding of greater self-inductance, but was accompanied by a greater ac resistance resulting in a poorer quality factor for the inductor.

This general behaviour is compared to that of a full core inductor of given core size,

Figure 3.2 From left to right P1 - flat, P2 - edge & P3 - sheet

where the self-inductance and resistance are dependent mainly on the number of turns, and is not as greatly affected by how the turns are arranged within the confines of the core winding window.

Two questions were initially asked about the partial core inductor:

1. Is there an optimal winding arrangement for a partial core inductor?
2. Is there an optimal core length in terms of quality factor?

In the pursuit of an answer to these questions, it became apparent, particularly at power harmonic frequencies, that the formation of the winding has a significant effect on device performance.

3.4 EXPERIMENT 1 - EFFECT OF WINDING FORMATION

The reactance and total resistance characteristic of three winding formations as shown in Figure 3.2 were tested to determine which winding formation produced the best quality factor. The winding formations are given as:

a. P1 - Flat wound rectangular conductor (widest edge to the former)
b. P2 - Edge wound rectangular conductor (narrow edge to the former)
c. P3 - Sheet wound conductor (sheet full width of winding)

The dimensions of the three conductor types were based on available materials, and to keep the physical dimensions and dc resistance of the windings as similar as possible.

Further, the design of the experiment was to enable differentiation between low inductances and low resistances without being swamped by losses in the core and winding dc resistance loss. To obtain a reasonable differentiation of voltage measurements, a current of 40A was chosen.

The following design criterion were applied:

Table 3.1 Physical parameters of P1, P2 and P3 inductors

Parameter	Flat winding	Edge winding	Sheet winding
Inductor name	P1	P2	P3
Conductor material	Copper	Aluminium	Aluminium
Conductor dimension	$10mm$ W x $4mm$ H	$2.5mm$ W x $30mm$ H	$90mm$ W x $0.7mm$ H
Conductor cross section	$40mm^2$	$75mm^2$	$63mm^2$
Current density	$1.0A/mm^2$	$0.53A/mm^2$	$0.63A/mm^2$
Turns	30	30	30
Winding layers	5	1	30
Winding width	$80mm$	$85mm$	$90mm$
Winding thickness	$23mm$	$30mm$	$31mm$
Winding aspect ratio	3.47	2.83	2.90
Conductor weight	$3.84kg$	$2.66kg$	$2.39kg$
Core length	$100mm$	$100mm$	$100mm$

- Low conductor current density, $J < 0.7A/mm^2$ for aluminium
- Low conductor current density, $J < 1.0A/mm^2$ for copper
- Low peak flux density in the core, $B < 0.1T$ at 40A

Refer to Table 3.1 for an overview of the physical parameters of the three winding formations.

3.4.1 Experimental method

Each winding formation is fitted with a core 100mm in length and injected with a current of 40A to maintain approximately equal flux density at each frequency; 25, 50, 250, 250, 350, 550 and 800Hz. The frequency, voltage, current and power are measured. The total self-inductance and total resistance are calculated as shown in Appendix One - Measurement Technique.

3.4.2 Results

The results are presented in Tables 3.2, 3.3, 3.4 and 3.5 while Figures 3.3 and 3.4 depict the self-inductance and total resistance factor respectively. The total resistance factor is the ratio of total measured resistance to the winding dc resistance - R_T/R_{dc}.

The quality factor for each winding formation is shown in Figure 3.5.

3.4.3 Observations

P1 (flat) has the greatest self-inductance and a higher series equivalent resistance above 250Hz.

P1 copper conductor has a lower dc resistance than P2 (edge) and P3 (sheet) aluminium windings but a much higher ac resistance. This may be due to either or both

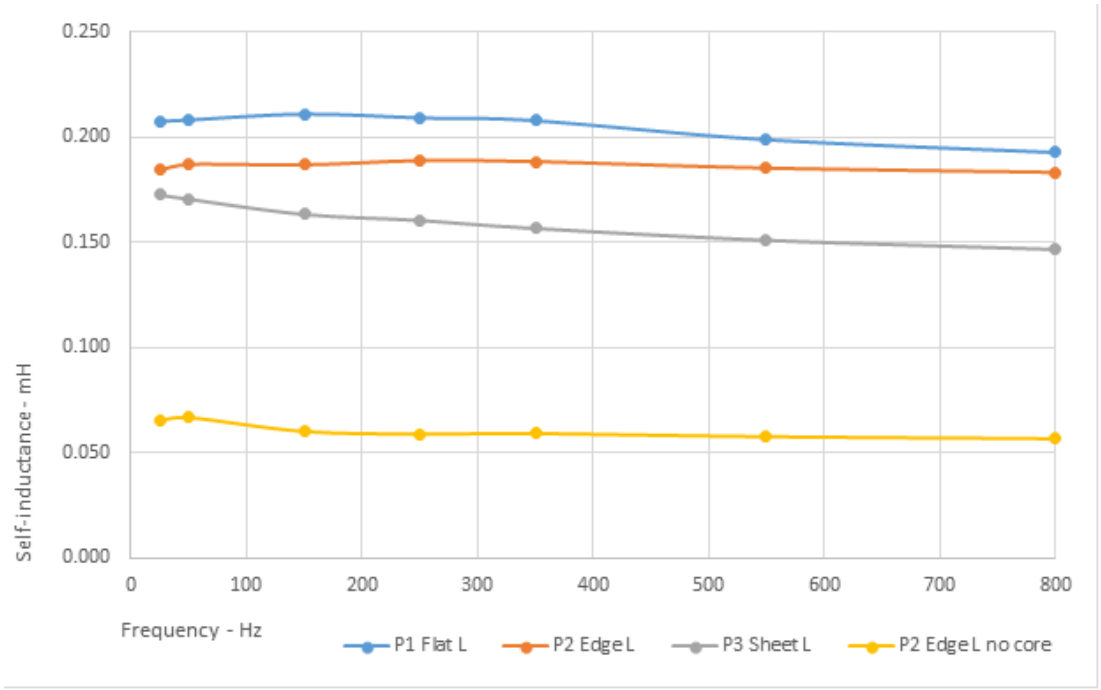

Figure 3.3 Self-inductance for P1, P2 and P3

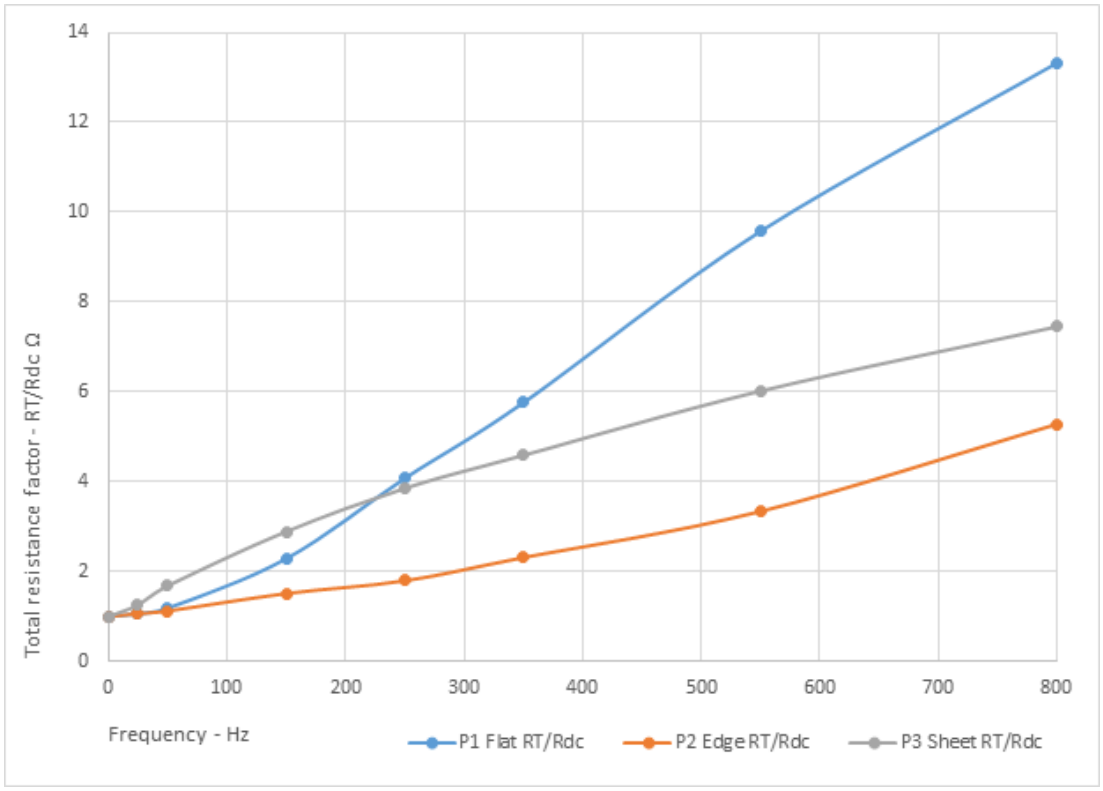

Figure 3.4 Total resistance factor of winding dc resistance for P1, P2 and P3

Table 3.2 P1 flat winding with 100mm core

Frequency	Inductance	Total resistance	Quality factor	Peak flux density
$0Hz$	-	0.0052Ω	-	-
$25Hz$	$0.00021H$	0.0055Ω	5.9	$0.088T$
$50Hz$	$0.00021H$	0.0062Ω	10.6	$0.087T$
$150Hz$	$0.00021H$	0.0119Ω	16.8	$0.089T$
$250Hz$	$0.00021H$	0.0211Ω	15.5	$0.088T$
$350Hz$	$0.00021H$	0.0299Ω	15.3	$0.087T$
$550Hz$	$0.00020H$	0.0497Ω	13.8	$0.084T$
$800Hz$	$0.00019H$	0.0691Ω	14.0	$0.081T$

Table 3.3 P2 edge winding with 100mm core

Frequency	Inductance	Total resistance	Quality factor	Peak flux density
$0Hz$	-	0.0048Ω	-	-
$25Hz$	$0.00018H$	0.0052Ω	5.6	$0.079T$
$50Hz$	$0.00019H$	0.0055Ω	10.8	$0.078T$
$150Hz$	$0.00019H$	0.0073Ω	24.0	$0.079T$
$250Hz$	$0.00019H$	0.0087Ω	34.0	$0.079T$
$350Hz$	$0.00019H$	0.0112Ω	36.9	$0.079T$
$550Hz$	$0.00019H$	0.0162Ω	39.5	$0.078T$
$800Hz$	$0.00018H$	0.0256Ω	36.0	$0.077T$

Table 3.4 P3 sheet winding with 100mm core

Frequency	Inductance	Total resistance	Quality factor	Peak flux density
$0Hz$	-	0.0065Ω	-	-
$25Hz$	$0.00017H$	0.0082Ω	3.3	$0.076T$
$50Hz$	$0.00017H$	0.0110Ω	4.9	$0.073T$
$150Hz$	$0.00016H$	0.0189Ω	8.1	$0.067T$
$250Hz$	$0.00016H$	0.0252Ω	10.0	$0.068T$
$350Hz$	$0.00016H$	0.0300Ω	11.5	$0.065T$
$550Hz$	$0.00015H$	0.0393Ω	13.3	$0.063T$
$800Hz$	$0.00015H$	0.0487Ω	15.1	$0.062T$

Table 3.5 P2 edge winding with no core

Frequency	Inductance	Total resistance	Quality factor	Peak flux density
$0Hz$	-	0.0048Ω	-	-
$25Hz$	$0.00007H$	0.0053Ω	1.9	$0.031T$
$50Hz$	$0.00007H$	0.0063Ω	3.3	$0.028T$
$150Hz$	$0.00006H$	0.0099Ω	5.7	$0.026T$
$250Hz$	$0.00006H$	0.0126Ω	7.3	$0.025T$
$350Hz$	$0.00006H$	0.0148Ω	8.8	$0.025T$
$550Hz$	$0.00006H$	0.0182Ω	10.9	$0.024T$
$800Hz$	$0.00006H$	0.0218Ω	13.0	$0.023T$

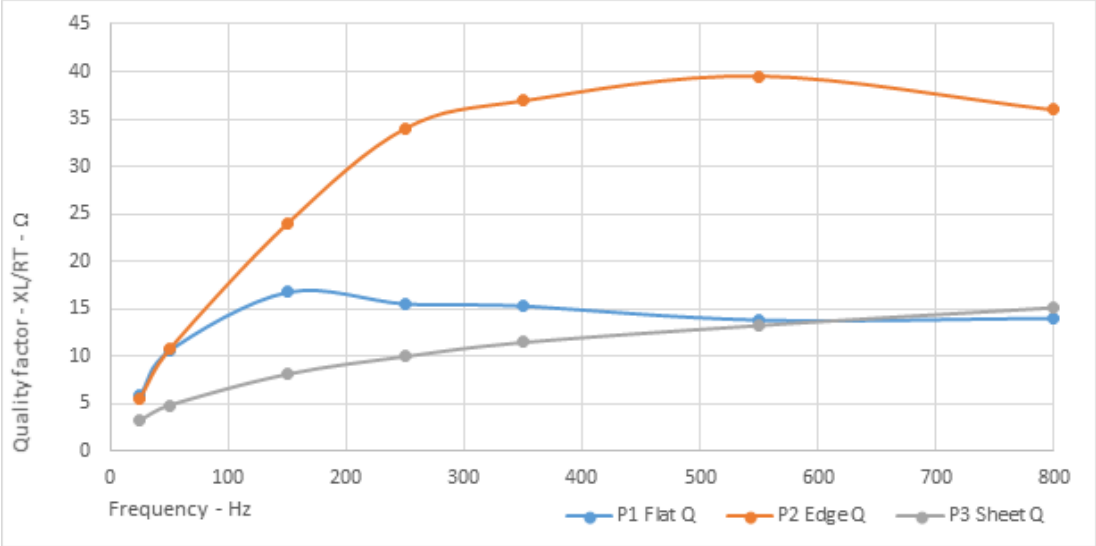

Figure 3.5 Quality factor for P1, P2 and P3

the formation of the winding and the conductor resistivity in terms of eddy current effects in the winding.

P2 (edge) has the lowest ac resistance over the frequency range tested, and a self-inductance in the order of 90% of P1 (flat).

P3 (sheet) has the lowest self-inductance at 76% of the P1 winding. The P3 total resistance falls between the P1 and P2 winding resistances however it has the poorest quality factor due to having a lower reactance for the given number of turns.

3.4.4 Discussion

The P2 edge formation winding has the best quality factor over the frequency range tested; becoming significantly better from around 100Hz when compared to the flat winding formation of P1. Flat formation is the most common winding method used in the transformer industry.

The cause of the difference in resistance between the windings is not clear. It is assumed that the core of each winding experiences a similar magnetic field effect at each given frequency and therefore core loss is approximately the same for each winding type.

As a preliminary conclusion, the difference in total resistance of each winding formation may be due to the construction of the winding under the influence of the applied magnetic field around a partial core.

Table 3.6 P2 winding with variable core length

Core length	Weight	Inductance	Total resistance 250Hz
No core	$0kg$	$0.062mH$	0.013Ω
$75mm$	$2.36kg$	$0.146mH$	0.012Ω
$100mm$	$3.15kg$	$0.187mH$	0.009Ω
$150mm$	$4.70kg$	$0.258mH$	0.010Ω
$200mm$	$6.35kg$	$0.320mH$	0.012Ω
$250mm$	$7.85kg$	$0.370mH$	0.014Ω
$300mm$	$9.40kg$	$0.423mH$	0.017Ω

3.5 EXPERIMENT 2 - PARTIAL CORE LENGTH

P2 (edge) was tested with partial cores of different length to profile a reactance and total resistance characteristic vs frequency. The P2 winding formation was chosen due to it having the lowest ac resistance across the frequency range tested. The objective for the experiment was to determine the effect of core length on the self-inductance and total series resistance.

3.5.1 Experimental method

Six core lengths of equal cross-sectional area were constructed from available steel lamination of 0.23mm thickness. Refer to Table 3.6 for core details and results.

Each core was positioned centrally in the P2 winding and was injected with an equal current to maintain a near equal flux density at each frequency of 25, 50Hz, 150, 250, 350, 550 and 800Hz. For each core length, the same terminal voltage was applied at each test frequency. In this way the core peak flux density was kept constant throughout the trial to normalise any effect caused by the magnetic field.

The frequency, voltage, current and power were measured and the total self-inductance and total resistance were calculated at each frequency. Refer to Figure 3.6 and Figure 3.7 for graphs of the self-inductance and resistance vs frequency for each core length.

3.5.2 Observations

The results show that increasing the length of the core increases the inductance of the P2 winding. In addition, the total series resistance of the inductor increases with core length. This effect becomes more prominent at higher frequencies.

Figure 3.8 shows how the quality factor of the P2 inductor is affected by partial core length.

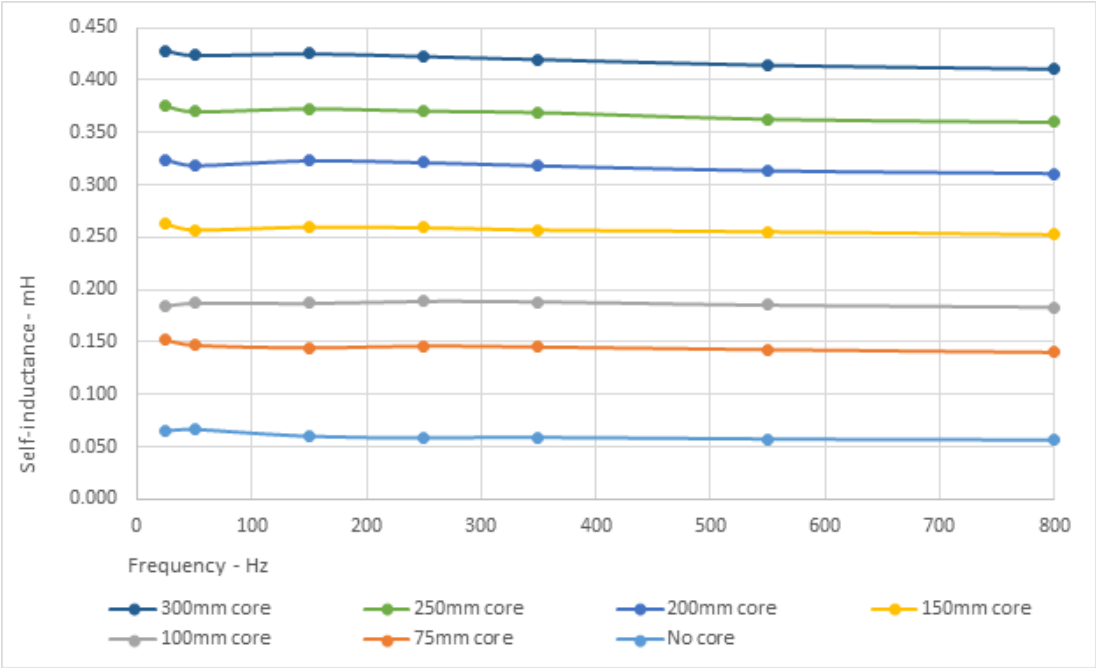

Figure 3.6 Self-inductance vs core length for P2

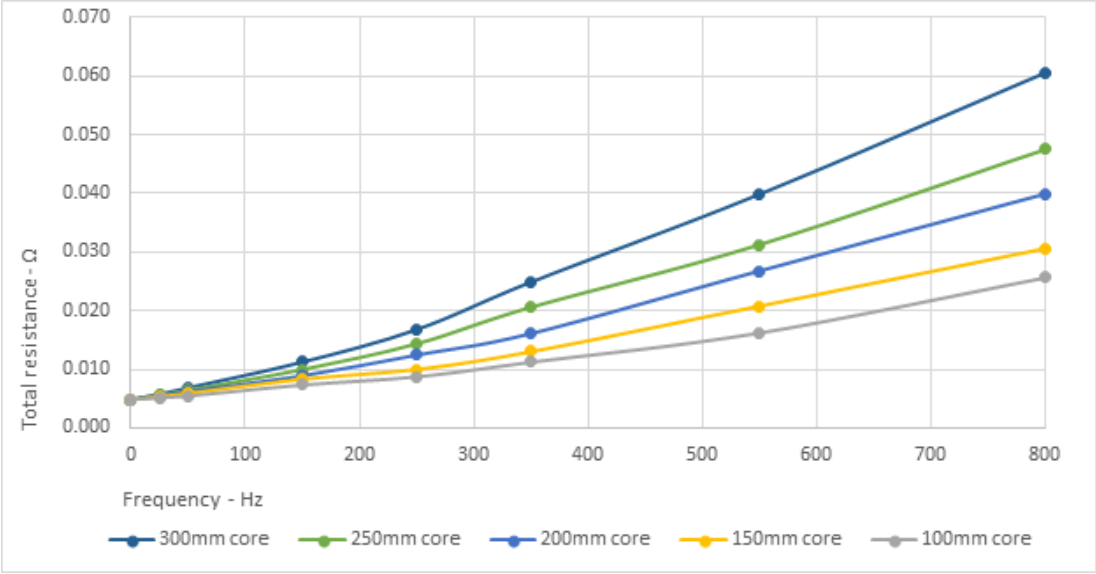

Figure 3.7 Total resistance vs core length for P2

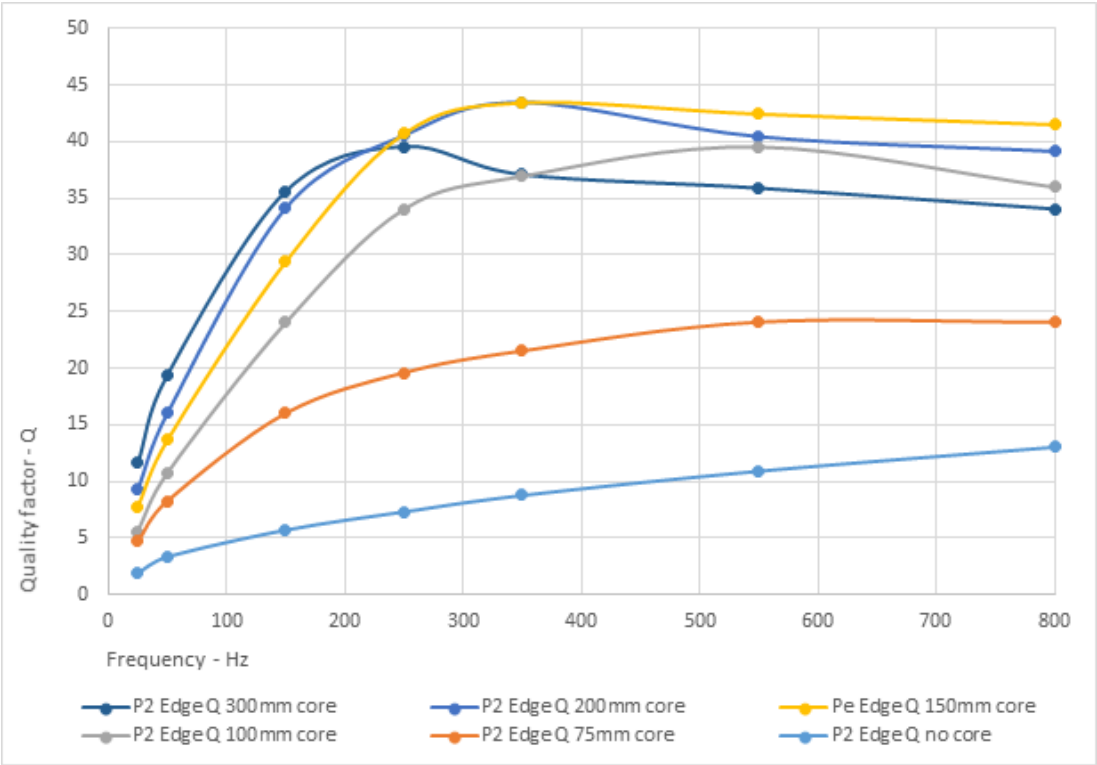

Figure 3.8 Quality factor vs core length for P2

3.5.3 Discussion

The influence of core length on P2 winding is more significant for reactance than resistance at lower frequencies and therefore larger cores produce a higher quality factor at $50Hz$ albeit at relatively low quality factor of 5 to 12. At frequencies above $250Hz$, the $300mm$ core length was less efficient than the $150mm$ and $200mm$ core.

The optimal core length appears to be around $150mm$ of the cores tested. Increasing core length in relation to the winding length by this amount may not be feasible in practice due to increased size and weight of the core. However it is possible to improve the performance of a partial core inductor by doing so.

Figure 3.8 shows a core size of $75mm$ produced a poorer quality factor due to both a smaller self-inductance and a larger *ac* resistance across the frequency spectrum tested.

The results of the P2 inductor total resistance are further compared in Figure 3.9 when the core length is less than the winding length.

Figure 3.9 shows that the resistance of the P2 inductor without a core, was higher than with a $100mm$ core at frequencies below $650Hz$.

Figure 3.9 also shows the resistance curve with no core appears to have an inverse function when compared to curves with a core.

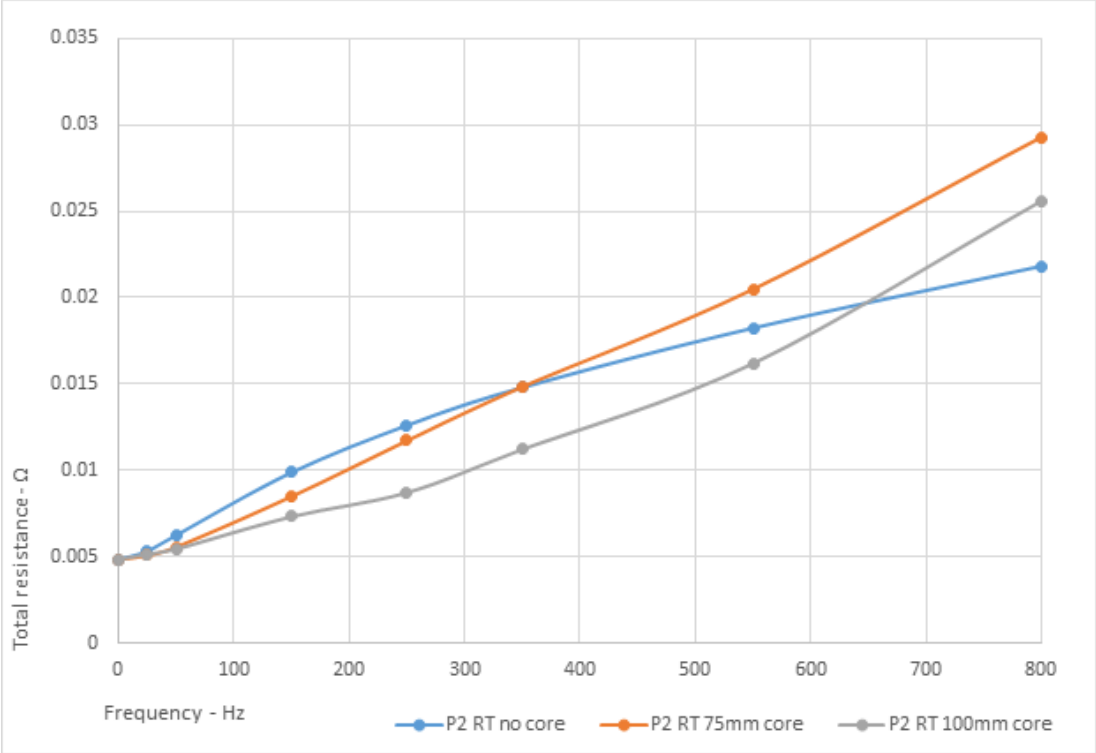

Figure 3.9 Total resistance for P2 with no core, 75mm and 100mm cores

3.5.4 Conclusion to Experiments 1 and 2

The results show that winding formation influences the resistance and reactance values in a partial core inductor and edge winding formation has better performance in terms of efficiency at higher frequencies.

In partial core work it is usual to construct a core to the length of the winding, however this may not produce the optimal result in terms of device efficiency. Increasing core length comes at the expense of device weight however, which may undermine the cost-benefit of such designs.

Due to the direct comparison of P1 and P2 windings being imperfect in terms of winding material and exact size, the experiment is repeated with new windings P4 and P5 which have a significantly larger winding aspect ratio and more comparable windings.

3.6 EXPERIMENT 3 - OPTIMAL WINDING FORMATION FOR WINDINGS OF HIGH ASPECT RATIO

3.6.1 Objective

Experiment 1 demonstrated that a winding with an edge wound formation produces an inductor with the best comparative quality factor of the three winding formations that

Table 3.7 P4 and P5 Physical construction data

Parameter	P4 Flat	P5 Edge
Conductor	Aluminium	Aluminium
Conductor dimension	5mm W x 2.5mm H	2.5mm W x 5mm H
Winding *dc* R	$32.9m\Omega$	$32.0m\Omega$
Turns	90	90
Winding layers	2	1
Former dia.	$38.6mm$	$38.6mm$
Winding thickness	$5mm$	$5mm$
Winding aspect ratio	50	50
Conductor weight	$0.47kg$	$0.47kg$
Core area	$805mm^2$	$805mm^2$
Core length	$250mm$	$250mm$
Core weight	$1.53kg$	$1.53kg$

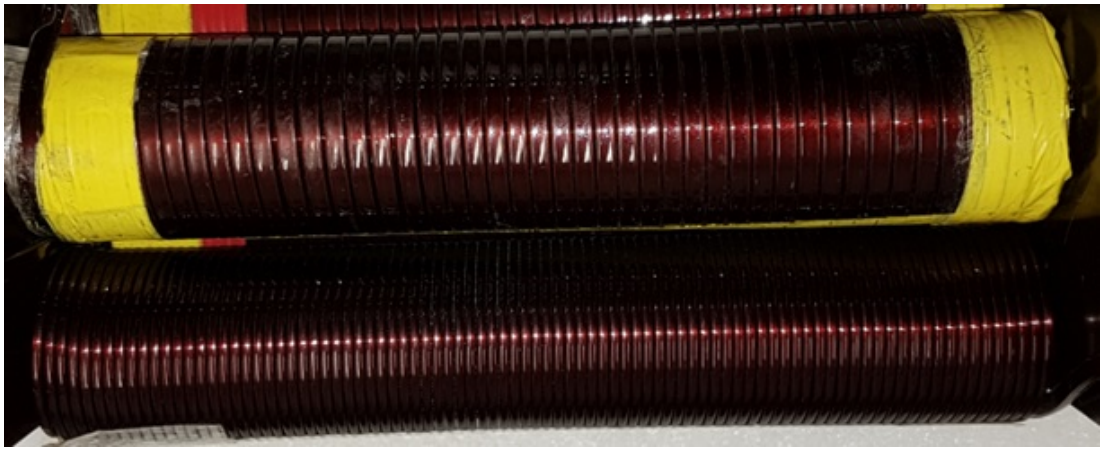

Figure 3.10 P4 flat winding formation (top) and P5 edge winding formation (below) both using the same conductor

were tested. The P1, P2 and P3 windings have a winding aspect ratio in the order of 3 which is very low for partial core inductors. The experiment is repeated with P4 flat winding and P5 edge winding which have an aspect ratio of 50. Conductor type and dimensional aspects of the P4 and P5 windings and core kept as identical as possible.

3.6.2 Experimental method

Two windings of high aspect ratio were constructed with a flat winding and an edge winding formation, as shown in Figure 3.10. The rectangular conductor used has a side dimension of 2:1 ratio. A P4 flat winding is constructed with two winding layers and a P5 edge winding with one winding layer. Thus both windings have the same number of turns, use the same amount of material and occupy a very similar spatial volume on the same sized core. Refer to Table 3.7 for physical construction details.

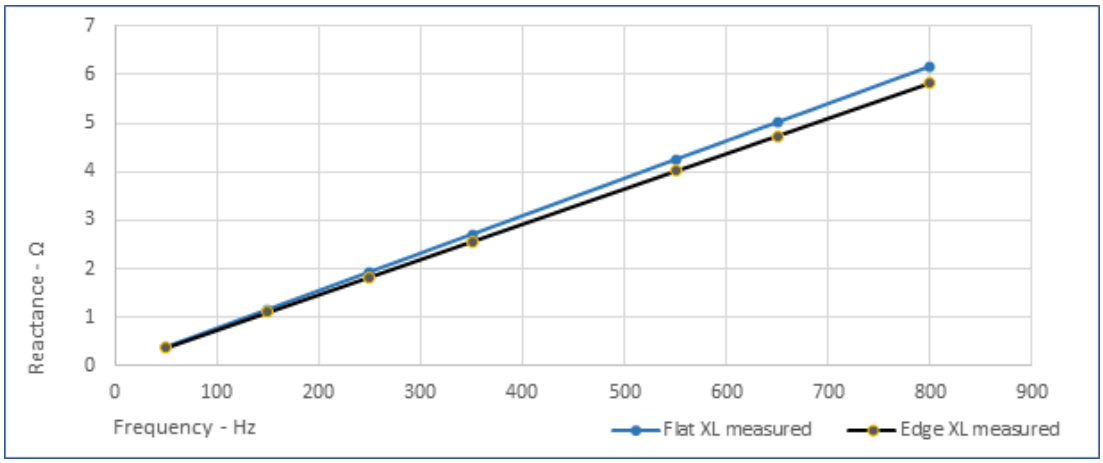

Figure 3.11 P4 flat and P5 edge reactance vs frequency

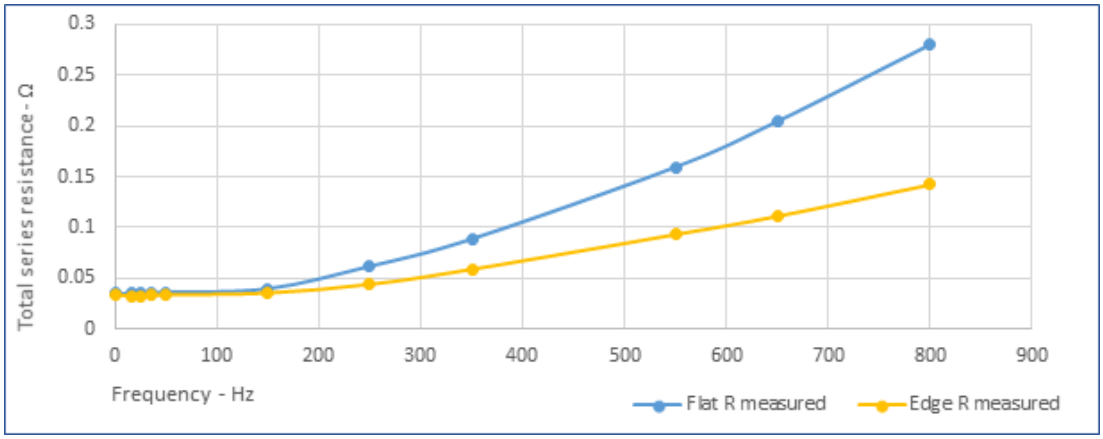

Figure 3.12 P4 flat and P5 edge total resistance vs frequency

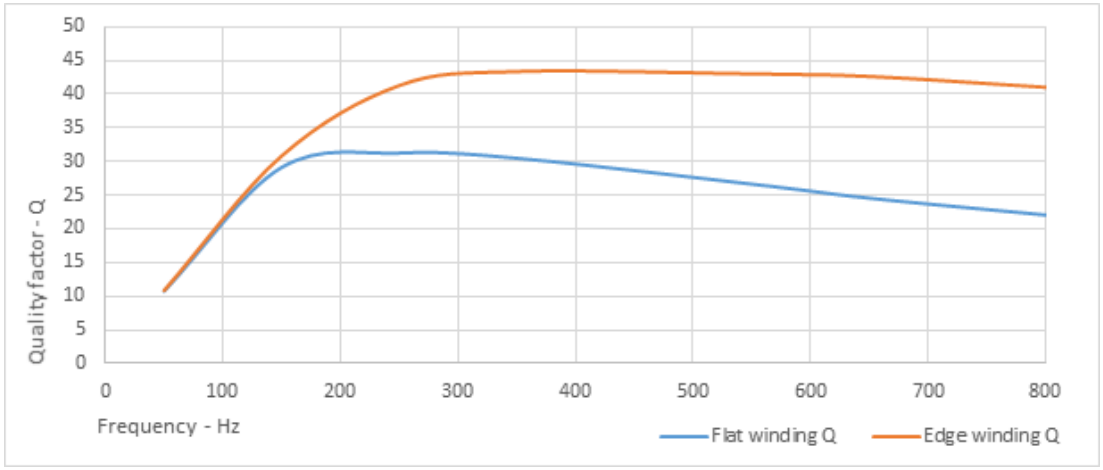

Figure 3.13 P4 flat and P5 edge quality factor vs frequency

3.6.3 Discussion

The results shown in Figure 3.11, Figure 3.12 and Figure 3.13 support the observations made in Experiment 1. A flat wound inductor has a slightly greater inductance for a given number of turns, however this is accompanied by a proportionally higher increase of series resistance, particularly as frequency increases.

Figure 3.13 compares the quality factor of the P4 flat and P5 edge wound inductors. There is a significant improvement in quality factor for P5 edge winding at higher frequencies. This would be particularly beneficial in the likes of power filter reactors where 5th, 7th and higher order harmonic current is often appreciable.

3.6.4 Conclusion

Experiment 3 shows there may be a clear benefit to consider an edge wound winding formation for partial core inductors with a high winding aspect ratio, particularly where they may encounter harmonic frequencies such as in power filtration applications.

The quality factor for P2 edge winding of low aspect ratio is lower than that of P5 edge windings of higher aspect ratio. It is therefore a preliminary conclusion that an edge-wound formation of higher aspect ratio produces the more efficient partial core inductor.

3.7 THE 3-PHASE PARTIAL CORE INDUCTOR

3.7.1 Introduction

This write-up benefits from a significant amount of experience gained through experimentation. Overall it is certainly true that edge windings produce partial core devices of better quality factor and lower power dissipation at harmonic frequencies. It will be shown that the best quality factor can be obtained with edge wound formations of only one winding layer and this is certainly true when two or more windings are brought together to form a 3-phase device.

Bringing partial core inductors in close proximity to one another increases the mutual coupling between the windings due to having a lower reluctance path which therefore increases the individual winding reactance. Refer to Figure 3.14 for a picture of a triangularly arranged 3-leg device. Refer to Figure 3.19 with defined separation distance d between the cores.

The reactance has an inverse proportional function to the distance the cores and coils are separated from one another. Closely grouping the windings may maximise the achievable reactance, however the *ac* resistance is also increased, which increases power dissipation in the device.

Figure 3.14 P4 flat winding in a triangular 3-leg arrangement

Therefore the whole design process is one of optimisation which essentially begins by choosing a conductor of adequate cross section, and as the research has shown, the optimal width.

In Experiment 4, two 3-leg, 3-phase inductors are constructed from P4 and P5 windings. The performance of the inductors is compared with the orientation of the flat steel laminations.

In Experiment 5, the three legs of P5 edge winding are separated by varying distances to compare the effect of core separation on reactance and resistance.

3.8 EXPERIMENT 4 - WINDING FORMATION AND LAMINATION ORIENTATION EFFECTS IN A 3-PHASE WINDING ARRANGEMENT

3.8.1 Introduction

Three P4 windings and three P5 windings from Experiment 3 are each grouped in a triangular arrangement to investigate which construction produces the best quality factor. A triangular arrangement was chosen due to it having symmetrical magnetic field interactions between the windings because of:

a. Equal separation between the cores and windings produce similar mutual coupling between them.
b. Reduced form factor of the device. This can be achieved because a top and bottom magnetic cross-member are not required as it is for three in-line windings in a typical 3-leg full core device.

Two constructional aspects were investigated:

1. Flat or edge winding formation in a 3-phase arrangement
2. Core lamination orientation - namely star or delta orientation - Refer to Figure 3.15

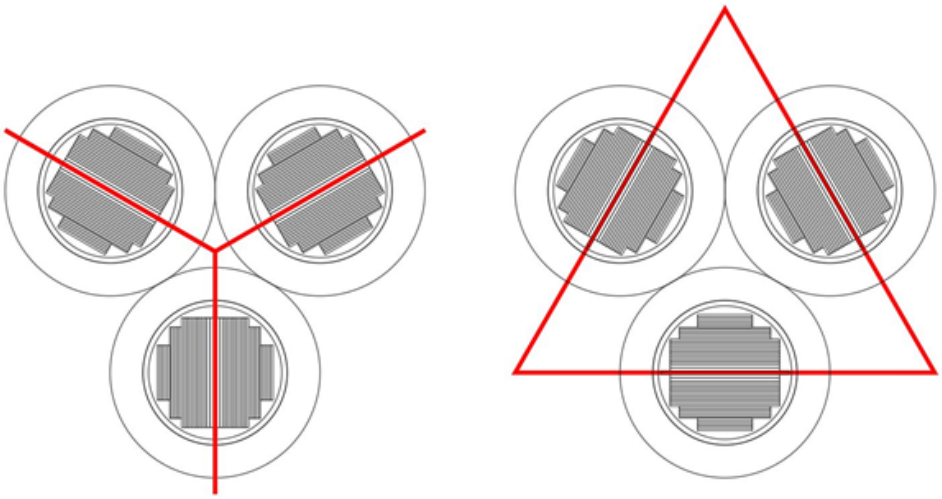

Figure 3.15 Star lamination orientation (left) and Delta orientation (right)

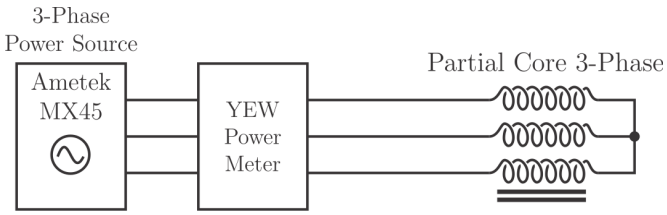

Figure 3.16 Experiment 4 connection detail

3.8.2 Experimental method

Each set of P4 and P5 windings were connected as shown in Figure 3.16 and tested at 50, 250, 550 and 850Hz at a constant current of 15 Amps for each combination of winding formation and lamination orientation:

- P4 Flat winding with delta lamination orientation
- P4 Flat winding with star lamination orientation
- P5 Edge winding with delta lamination orientation
- P5 Edge winding with star lamination orientation

3.8.3 Discussion

Figure 3.17 shows that for either flat or edge winding formation, the star lamination orientation produced a lower total resistance compared to the delta lamination orientation.

The flat winding formation gives rise to a slightly higher reactance as was also shown in Experiment 3. Experiment 5 more closely examines the effect of 3-phase arrangements in terms of total reactance.

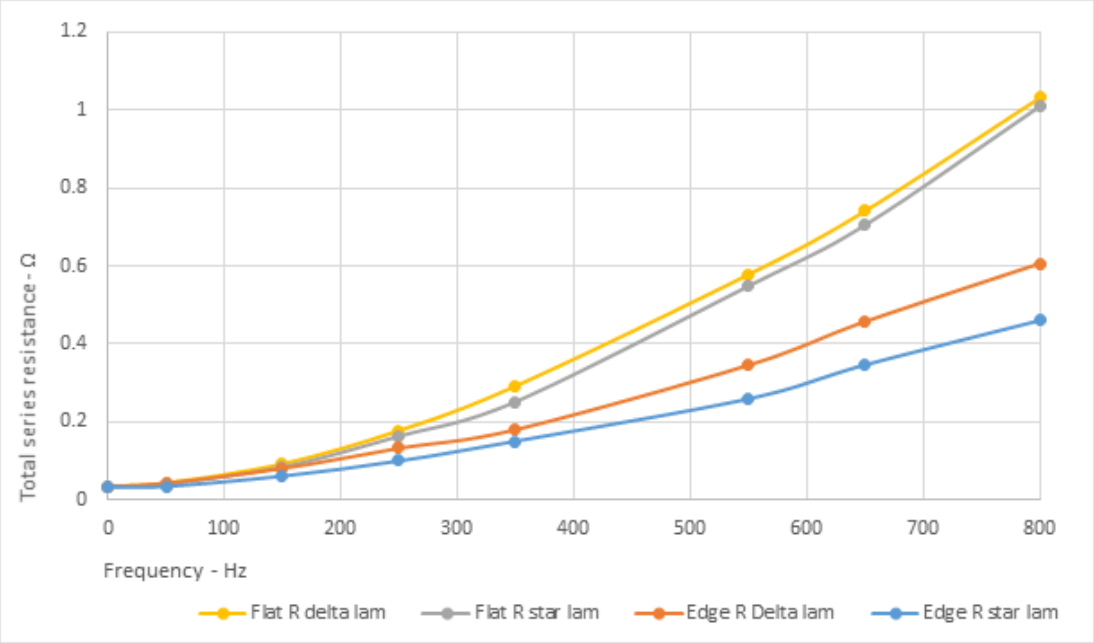

Figure 3.17 P4 and P5 total resistance vs frequency with star and delta lamination orientation

The quality factor of the star lamination orientation is compared for each winding formation in Figure 3.18. It can be seen that the edge winding with star lamination produces the best quality factor.

3.8.4 Conclusion

In a 3-leg, 3-phase arrangement, the P5 single layer edge winding formation with star core orientation produced the best quality factor compared to flat winding formation.

Given all other physical parameters were held constant, including the core, it would appear that there is a significant unaccounted for loss due to the winding formation itself, particularly at higher frequencies. The unaccounted for resistance is not due to skin effect because the conductor is the same for both P4 and P5; only the winding formation is different. The negligible influence of skin effect is confirmed later by calculation.

Star lamination orientation provides lower resistances for both flat and edge winding formations and this may be due to this lamination orientation producing lower core losses. Without knowledge of the precise loss mechanism at this stage, a star lamination orientation appears to lower losses and shall therefore be used in all future 3-leg, 3-phase arrangements.

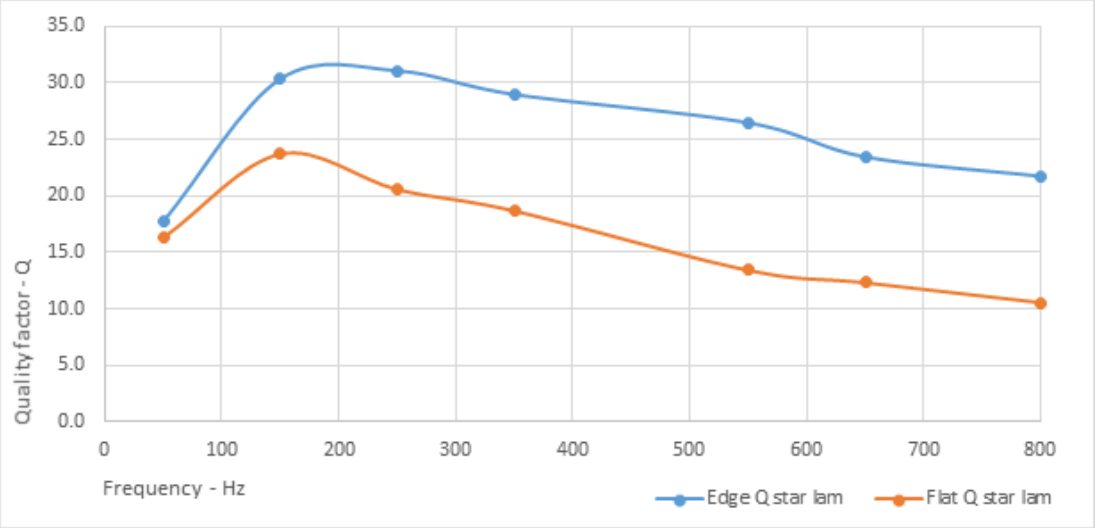

Figure 3.18 Quality factor vs frequency for P4 flat and P5 edge with star lamination orientation

3.9 EXPERIMENT 5 - EFFECT OF WINDING SEPARATION IN A 3-PHASE WINDING ARRANGEMENT

3.9.1 Objective

The 3-phase P5 edge winding with star orientated cores was tested with incremental winding separation. The reactance and resistance are compared for each separation distance along with the quality factor.

3.9.2 Experimental method

The cores were supported at the ends by a jig that holds them apart by a set distance. The inductor was connected as shown in Figure 3.16 and tested at 50, 250, 550 and $850Hz$. The core separation distance d was increased for each set of tests. The winding separation distance is defined by the shortest path between the circumferences of any two circular core sections. Refer to Figure 3.19.

The affect of core separation on quality factor, reactance and resistance is shown in Figure 3.20, Figure 3.21 and Figure 3.22 respectively.

3.9.3 Self-inductance factor

Refer to Table 3.8 for the inductance calculated by measurement at 250Hz. The inductance factor is defined as the scaling factor required to match the 1-leg inductance to the 3-phase inductance.

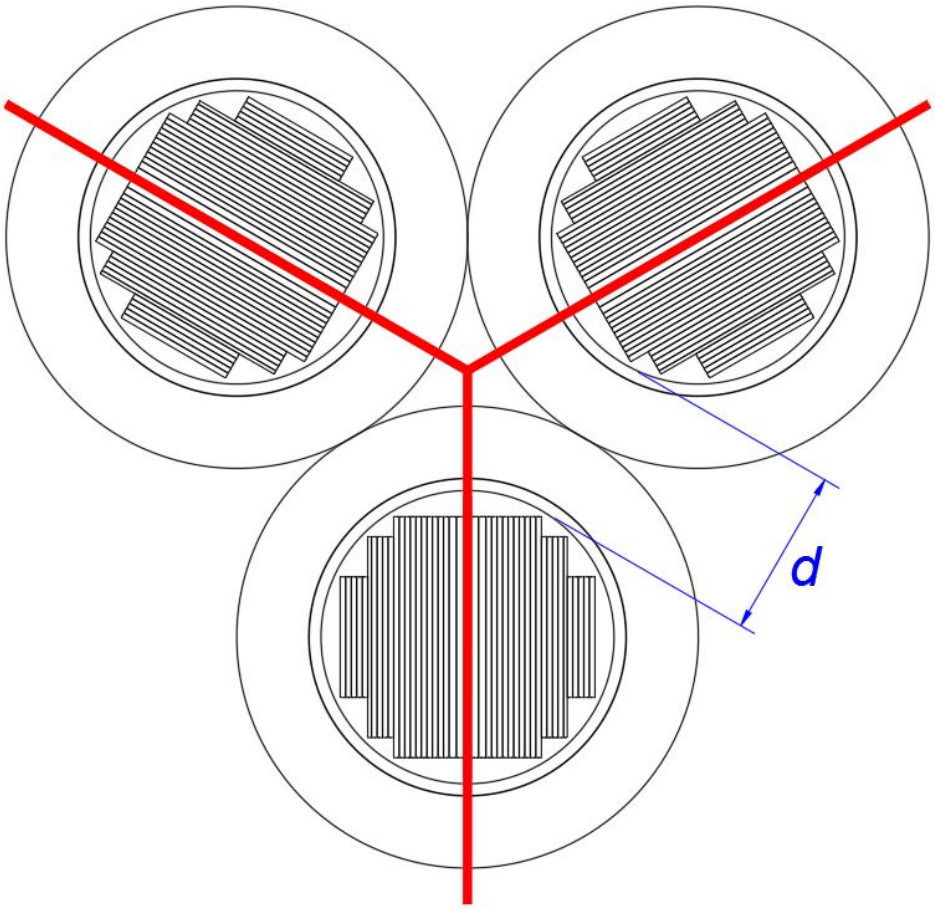

Figure 3.19 Defining the core separation distance d

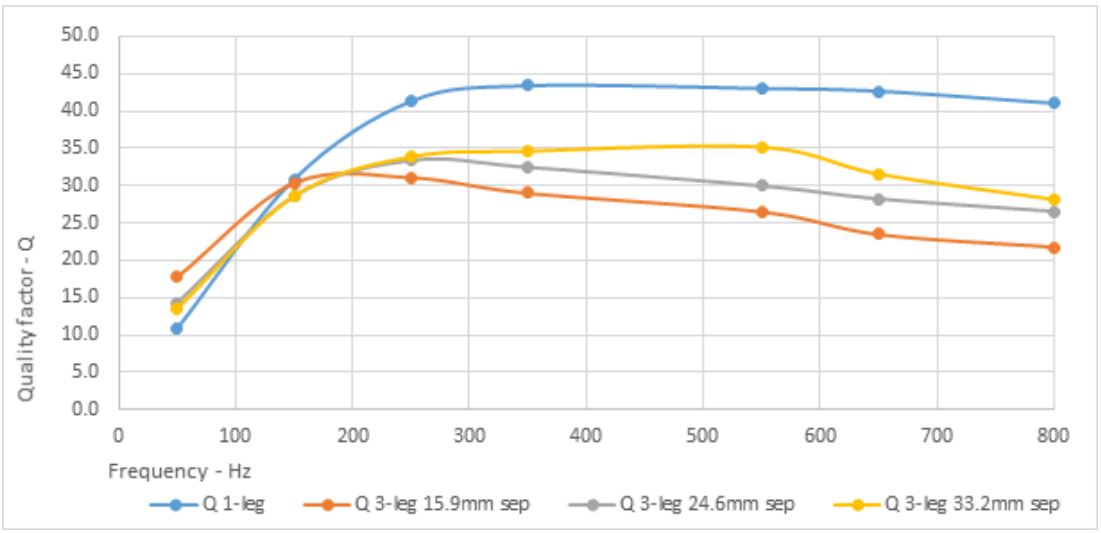

Figure 3.20 P5 quality factor vs frequency for each core separation

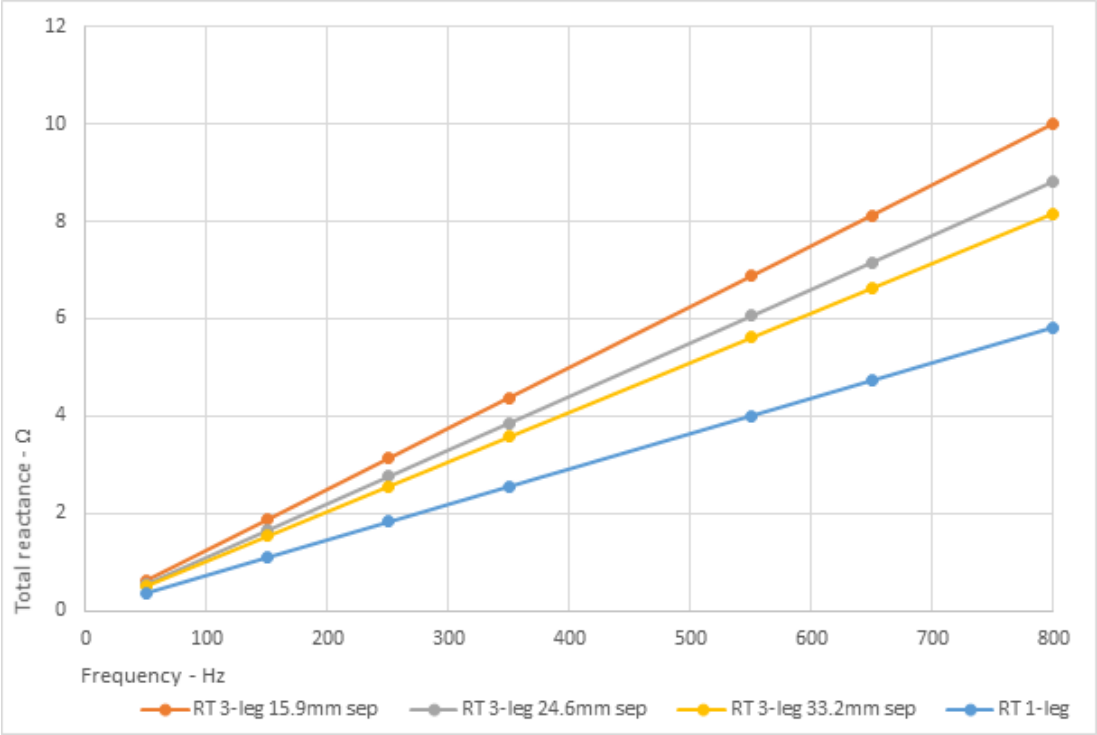

Figure 3.21 P5 reactance vs frequency for each core separation

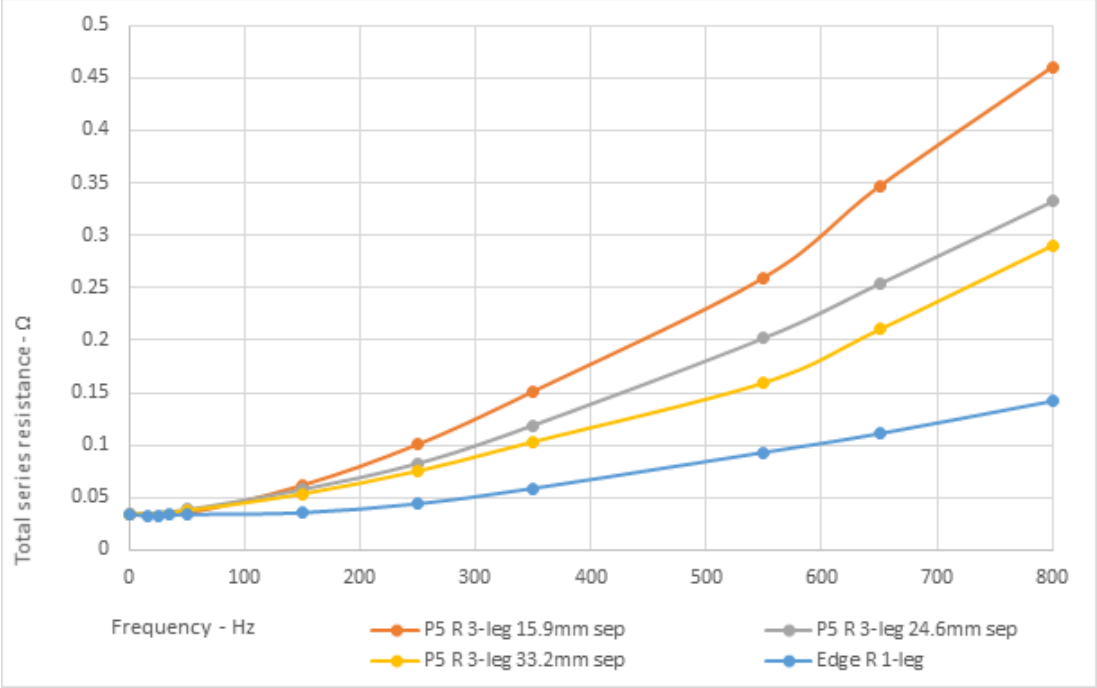

Figure 3.22 P5 total resistance vs frequency for each core separation

Table 3.8 P5 reactance factor vs core separation

Parameter	Core separation 1	Core separation 2	Core separation 3
Core separation distance	$15.9mm$	$24.6mm$	$33.2mm$
1-leg inductance	$1.83mH$	$1.83mH$	$1.83mH$
3-phase inductance	$3.13mH$	$2.76mH$	$2.55mH$
Inductance factor	1.71	1.51	1.39

3.9.4 Discussion

The closer the separation distance between the windings, the better the quality factor at low frequencies due to the higher reactance, however at higher frequencies the quality factor reduces from around 43 to 30 due to a relative increase in resistance.

Table 3.8 shows that a single factor can relate the inductance of a 3-phase device to that of a 1-leg device. This will prove useful in developing a model of 3-phase inductors based on 1-leg formulations in Chapter 4.

In Figure 3.22 the total series equivalent resistance for each P5 edge winding separation is compared to the 1-leg P5 edge winding. There is a significant increase in total resistance in a 3-phase device at higher frequencies which is also greatly affected by winding separation. Given the magnitude of increased resistance due to winding proximity, this effect must be considered in practical designs. There is no single factor to relate the resistance of a 3-phase device to a 1-leg device.

It was also observed during the P4 and P5 trials that the ends of the windings got much hotter than the central portion of the winding, particularly at higher frequencies, and particularly for P4 flat. The temperature rise was more intense as the windings were brought closer together, which is consistent with the observed increase in resistance of the inductors. This effect will also be discussed in detail in Chapter 4.

3.10 EXPERIMENT 6 - WINDING LOSSES WITH AN AIR CORE

3.10.1 Objective

A bifilar wound capacitor-coil $J5$ shown in Figure 3.23 and Figure 3.24 is used to demonstrate the effect of frequency on the winding resistance in three connection modes as shown is Figure 3.25 The aim of the experiment is to confirm the existence of an ac resistance in the winding without any core, and to confirm that the existence of the ac resistance is due to a magnetically induced effect.

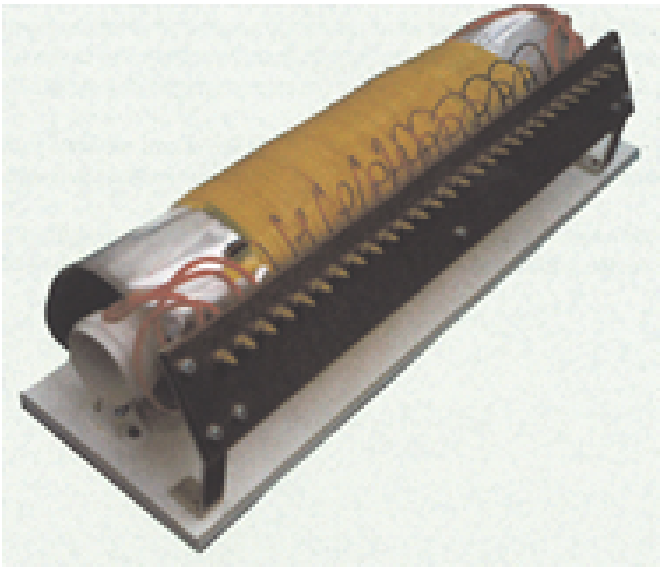

Figure 3.23 *J*5 bifilar wound capacitor-coil

Figure 3.24 J5 constructional details

Table 3.9 $J5$ bifilar wound capacitor-coil physical construction data

Parameter	Data
Foil winding material	Aluminium
Foil winding width	$0.45m$
Foil winding thickness	$0.02mm$
Foil length	$90m$
Number of foil windings	2
Dielectric thickness	$0.035mm$
Capacitance between windings	$31.5\mu F$
Inductance of each foil winding	$1.22mH$
Inductance of anti-parallel winding connection	$0.00mH$
Winding former diameter	$66.9mm$
Number of turns of each foil winding	275
Core material	Air - no magnetic core

Table 3.10 J5 dc resistance measurements

Winding	Meter scale	Trial 1	Trial 2
A-B	$100mA$	0.583Ω	0.583Ω
C-D	100mA	0.463Ω	0.465Ω
A-B//C-D	100mA	0.251Ω	0.252Ω
Calculated Resistance	-	0.258Ω	0.259Ω

3.10.2 Apparatus

Refer to Table 3.9 for details of the $J5$ construction. The natural capacitance between the foil windings is not utilized in this experiment and it does not have any influence on the results.

3.10.3 Experimental method

The *dc* resistance of the windings is measured with a Megabrass MPK 254 micro-Ohm meter and is presented in Table 3.10. Discrepancies between the winding resistances is due to old copper connections to the aluminium foil plates.

Each connection mode shown in Figure 3.25 is connected to a constant current *ac* signal of 5 Amperes at frequencies from $50Hz$ to $800Hz$.

3.10.4 Results and discussion

The results of the trial are presented in Figure 3.26 and show that resistance increases with frequency for the single winding and parallel winding connection modes. There is a constant difference between the resistances of these two modes which is the same as the *dc* resistance measured.

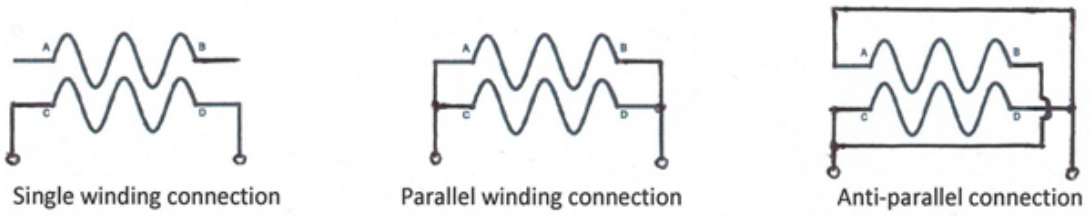

Figure 3.25 J5 experimental connection modes

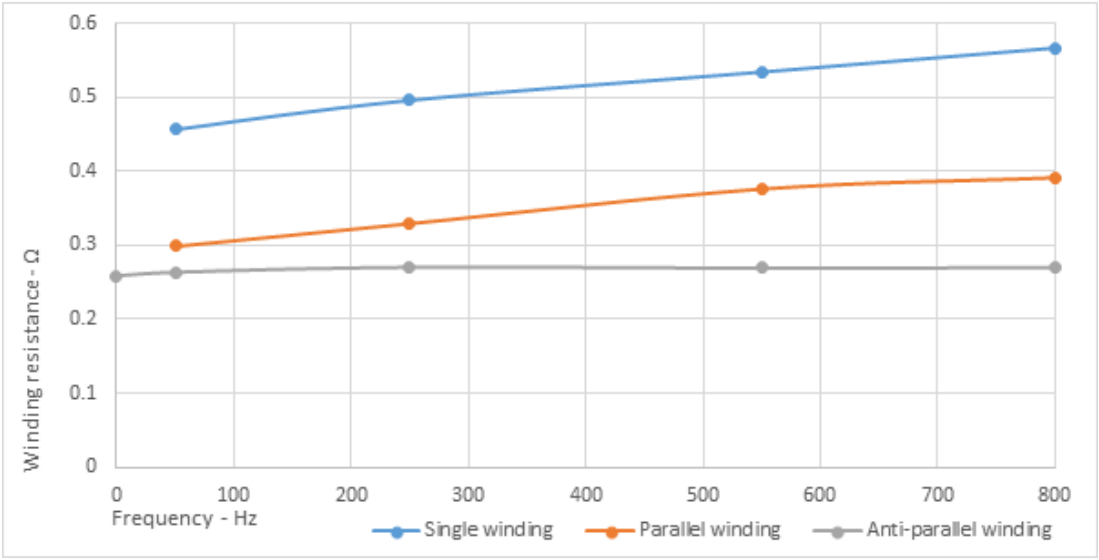

Figure 3.26 J5 total resistance vs frequency in three connection modes

The anti-parallel connection mode gives a flat line resistance measured across the frequency spectrum and is close to the measured *dc* resistance. This suggests that where the magnetic field is cancelled out by the opposing fields of each winding, there is no winding inductance and no frequency dependence on resistance is observed.

3.10.5 Conclusion

The bifilar winding formation in the $J5$ device was chosen for this experiment due to the very similar inductance of each winding sheet. In the anti-parallel connection, mode 3, the inductances of each winding are effectively nullified and the result is the complete absence of the *ac* resistance effects which were observed for both the single winding and parallel winding connection.

The winding *dc* resistance is the main contributor to winding resistance over the frequency range tested and although the effect of frequency is subtle without a core, it is apparent that there is some *ac* resistive effect in the winding due to the influence of a magnetic field. Based on previous experiments comparing the winding formation, it is believed that a partial core magnifies the effect of the *ac* resistance in the winding.

3.11 CONCLUSION CHAPTER 3

Experiments 1 to 5 show that for the purposes of project inductor design, 3-phase partial core inductors can be optimised to improve their quality factor in the power frequency spectrum by the following means.

1. Edge winding formation
2. Optimised core length
3. Higher rather than lower winding aspect ratio
4. “Star” orientation for flat stacked core lamination
5. Optimised winding separation

For the purposes of estimating useful designs in the project inductor, it will be necessary to model total resistance taking into account the influences listed above. Further investigation into the mechanisms that affect the total resistance of the device are required due to uncertainty about where these arise and how these effects may be optimised.

Based on the foregoing qualitative analysis, it is proposed that the observed effects of ac resistance may be produced by the following phenomena:

- Core losses
- ac loss in the windings particular to partial core inductors

A quantitative analysis is carried out in Chapter 4 to further understand the loss mechanisms of the partial core inductor and enable inductor optimisation. In particular, the heating effect at the winding ends is considered to be the most obvious sign that there are additional loss effects occurring in the winding because this heating effect is influenced by winding formation and proximity of the windings to one another.

To better understand the influence of each component of resistance it is necessary to isolate and quantify each effect. The following experiments are presented in Chapter 4 and attempt to separate the effects of the winding and core.

1. Experiment 7. Localization of winding ac loss in a 1-leg partial core inductor
2. Experiment 8. Localization of winding ac loss in a 3-phase partial core inductor
3. Experiment 9. Calorimetric analysis of core and winding losses in a 3-phase partial core inductor
4. Experiment 10. Flux emanations about a partial core inductor

Chapter 4

THE 3-PHASE PARTIAL CORE INDUCTOR

4.1 OVERVIEW

Following on from the experiments of Chapter 3, this chapter begins by quantifying the winding *ac* resistance of partial core inductors through experiments designed to separate out winding losses from core losses by means of split windings and calorimetric measurements. The results of the experiments identify eddy current loss in the winding, and the magnitude of orthogonal eddy current loss in the core. The chapter concludes by developing expressions to quantify inductance and orthogonal components of resistance in 3-phase partial core inductors based on core separation between the three limbs.

4.1.1 Quantifying partial core winding ac resistance

In this chapter, a series of experiments have been conducted to verify and quantify the existence of low frequency winding *ac* resistance in partial core inductors. Observations have shown three main features of partial core winding loss that give rise to this enquiry:

1. Increased temperature rise at the winding ends
2. Temperature rise increases with frequency of excitation
3. Temperature rise increases with proximity of neighbouring windings in 3-phase inductors

Figure 4.1 demonstrates some of these effects in the P6 3-phase test inductor.

The test in Figure 4.1 was conducted over the first two minutes of each frequency test with a cool down period between each test of at least one day. The results show that the rate of temperature rise increases significantly 1) towards the ends of the winding, and 2) with increased frequency.

The details of the 3-phase test winding P6 will be will be discussed further in this section along with a quantitative analysis.

The increase in winding temperature is thought to be due to radial flux emanation from the core which increases toward the winding ends. A measurement of the orthogonal

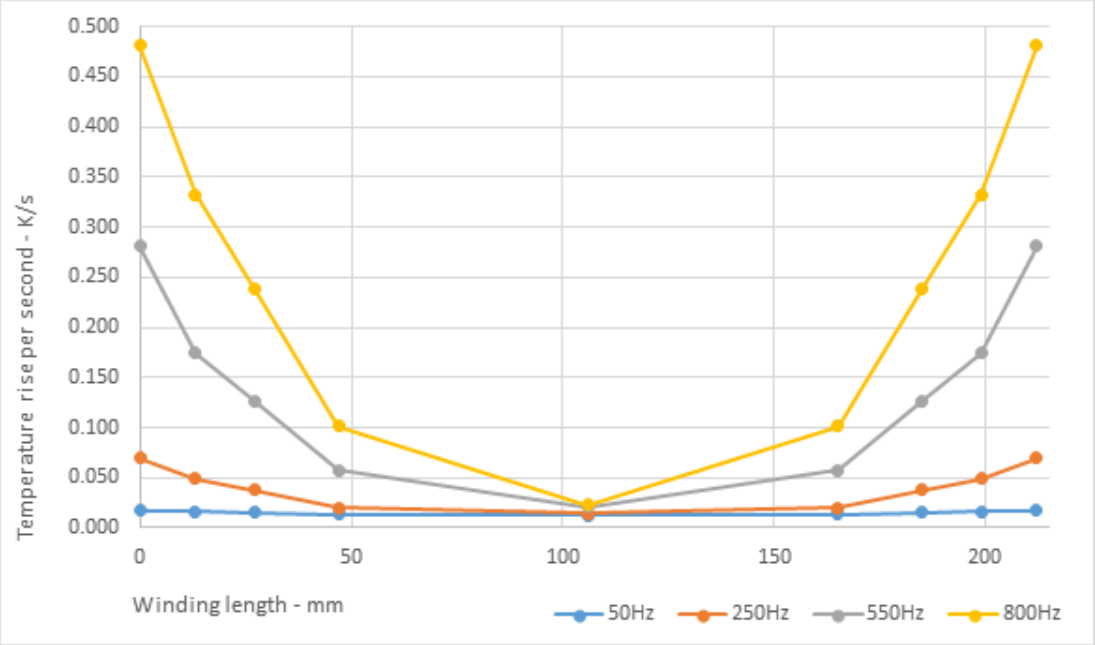

Figure 4.1 P6 temperature rise per second vs winding length for each test frequency

(radial) flux component along the length of the winding was taken and the results are presented in Figure 4.2.

4.1.2 Measurement of orthogonal flux

A search coil was constructed to measure the magnetic flux distribution along the length of the P6 winding. The search coil comprises 100 turns of fine enamelled copper wound on a plastic former of 10mm diameter. The peak flux density through the search coil winding is calculated by the transformer equation. Refer to Figure 4.3 for a picture of the search coil held perpendicular to the P6 winding.

As the results of the measurements were used to provide comparative measurements to observe general behaviour of the magnetic field, no attempt was made to benchmark the results to a known standard.

The measurement of the orthogonal flux was completed via the use of a small search coil positioned at increments along the test winding P6. The results show a V-shaped characteristic.

The results of Figure 4.2 suggest that the orthogonal flux density is proportional to the distance from the centre of the winding. This result is compared to that obtained for the same winding without any steel core in Figure 4.4.

The presence of a partial core reduces the average orthogonal flux significantly and is consistent with increased resistance of an air core winding as shown in Figure 3.9 of Experiment 2. All tests were conducted with a near equal calculated peak flux density as will be shown in the accompanying quantitative analysis.

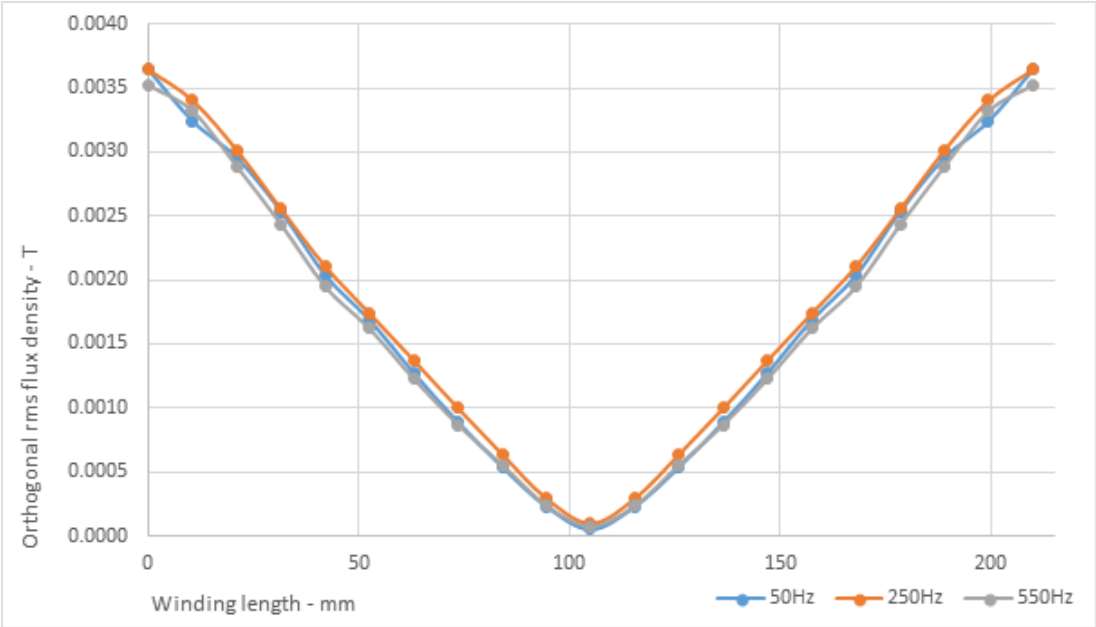

Figure 4.2 P6 1-leg (with core) orthogonal flux density vs winding length for each frequency

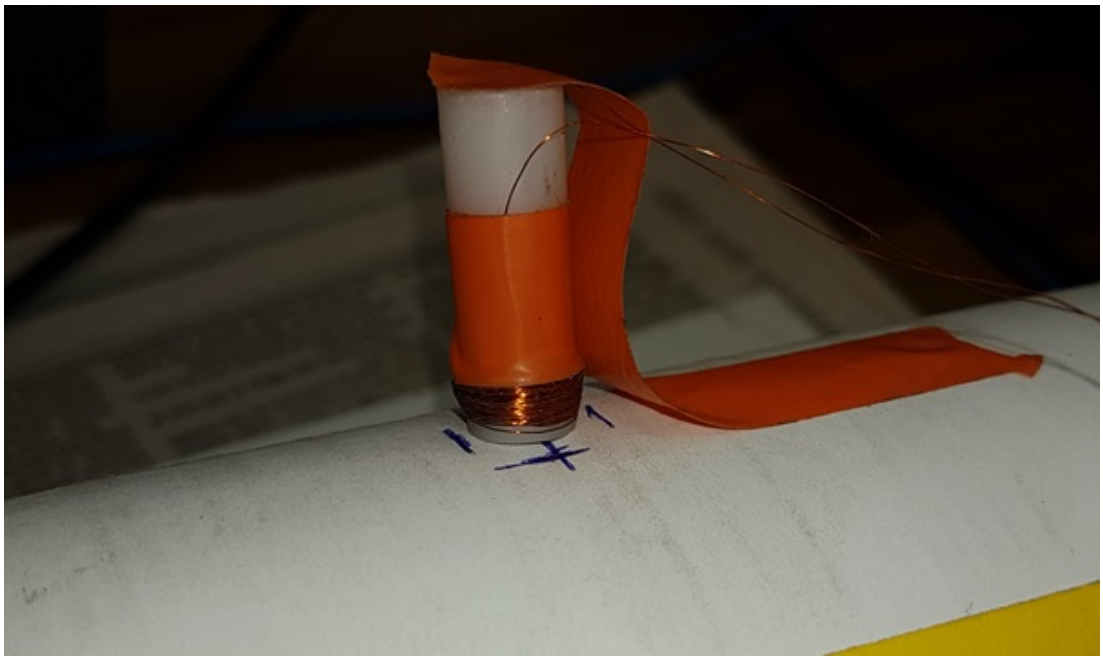

Figure 4.3 Orthogonal flux search coil held perpendicular to P6 winding

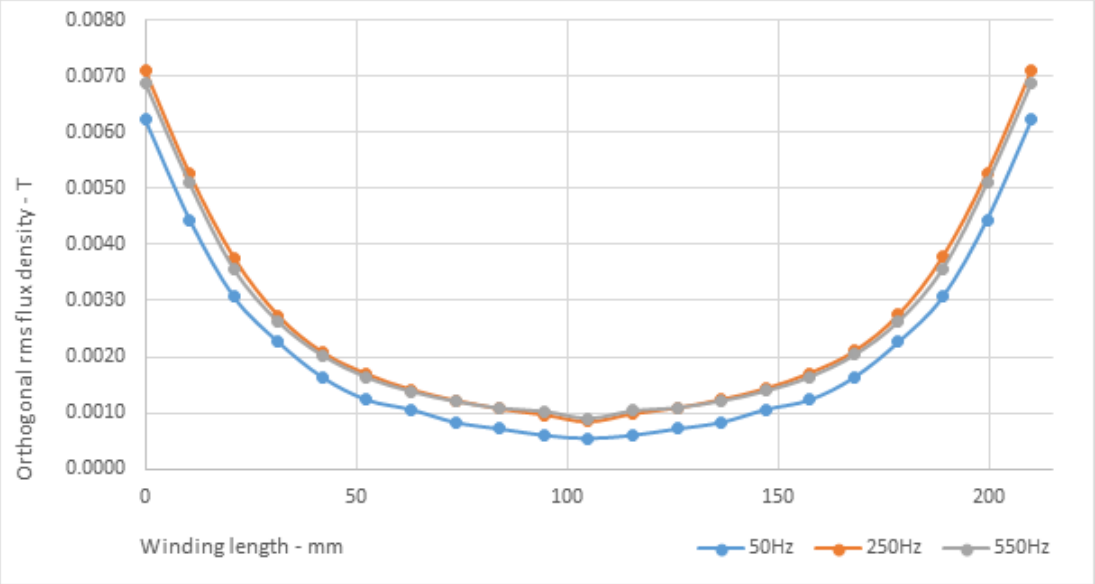

Figure 4.4 P6 1-leg (no core) orthogonal flux density vs winding length for each frequency

The objective of this work therefore is to link the presence of orthogonal flux though the winding, to the observed increased temperature rise behaviour in the winding.

4.2 EXPERIMENT 7 - LOCALIZATION OF WINDING AC LOSS IN A 1-LEG PARTIAL CORE INDUCTOR

4.2.1 Objective

To confirm the nature of the partial core winding ac resistance in a 1-leg device, and if it may be attributed to conduction losses or induction losses.

4.2.2 Introduction

Increased power dissipation at the winding ends may be due to either conduction losses or induction losses in the winding itself. Conduction losses would imply that the resistance per turn of the winding increases toward the ends. Examples of electromagnetic effects on conduction losses include skin effect and proximity effect.

Electromagnetic effects may also give rise to induction losses in non-permeable materials caused by eddy currents. Eddy currents generate power loss, or heating, at the location where they occur. However, the effective resistance of the loss is coupled by induction to the whole winding. Therefore the equivalent resistance of the eddy current loss is not necessarily localised to where the power loss, or heating, occurs.

Experiment 7 was conducted to examine the localization of power loss in 1-leg test winding P6. The experiment was devised so that power loss may be measured in the winding's central or outer regions by means of a split winding, as shown in Figure 4.5

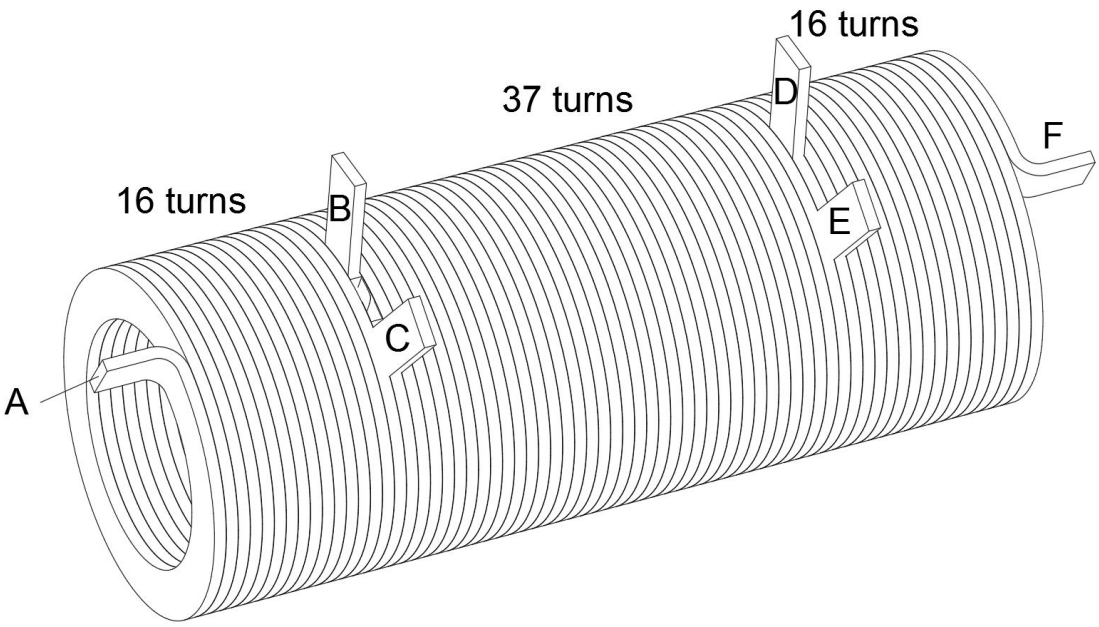

Figure 4.5 P6 split winding arrangement

and Figure 4.6. The power loss is measured in each winding portion depending on the connection mode shown in Figure 4.7.

It is reasoned that if the outer portions of the winding have a greater resistance per turn than the central portion, the temperature rise may be linked to conduction losses brought about by some electromagnetic effect. (Similar to superconducting winding ac losses - Lapthorn 2012)

4.2.3 Apparatus

The full winding contains 69 turns; 37 in the central portion, and 16 turns at each end.

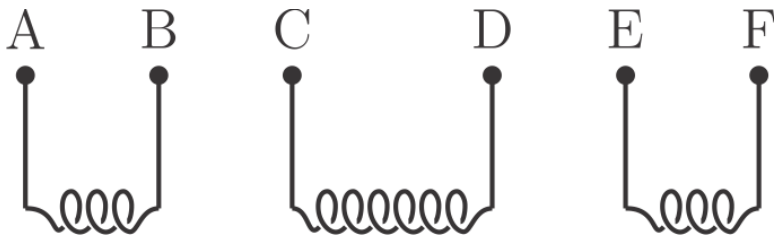

Figure 4.6 P6 split winding connections

4.2.4 Experimental method

Three connection modes shown in Figure 4.7 enable power measurements of each portion while maintaining equal current flow through the total winding. In this way

Table 4.1 P6 Split winding physical parameters

Parameter	Data
Conductor material	Aluminium
Conductor dimension	$2.5mm$ W x $12.5mm$ H
Conductor formation	Edge
Number of turns in total	69
Winding length	$212mm$
Winding internal diameter	$53.8mm$
Winding dc resistance (full 69 turns)	$R_{dc} = 0.0140\Omega$
Air core CSA	$0.00227mm^2$
Steel core CSA (when used)	$0.00159mm^2$
Steel core length (where used)	$215mm$

the reactance of the winding remains unaltered in each connection mode, but the power loss occurring at the ends or in the central portion can be electrically measured.

The power loss in each connection mode was measured at frequencies of 50, 150, 250 and $800Hz$.

To enable a direct comparison of the power dissipation, all measurements were made with an equal peak flux density as calculated by the transformer equation 4.1

$$B = \frac{V}{4.44fNA_c} \tag{4.1}$$

where B is the peak flux density
V is the applied voltage
F is the frequency
N is the number if winding turns
A_c is the cross sectional area of the core

Refer to Table 4.2 for the results of each connection mode.

As the turns and core cross sectional area are fixed, the flux density is proportional to the winding voltage at each test frequency. The peak flux density chosen for the tests was set by P6 with air core due to the magnitude of the current required ($45A$) to achieve $0.04T$.

4.2.5 Results

In Figure 4.8 the total measured resistance is compared to the summation of the central and outer portions. It can be seen that the summation values are all within 5% the total resistance values at each frequency, confirming the validity of the measurement technique.

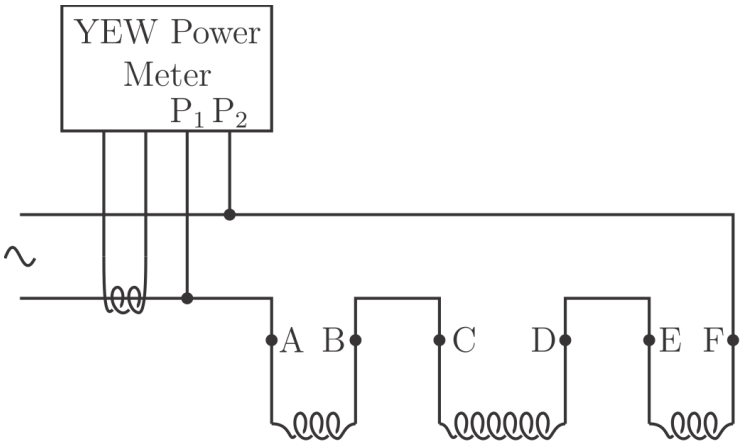

Total Winding Power

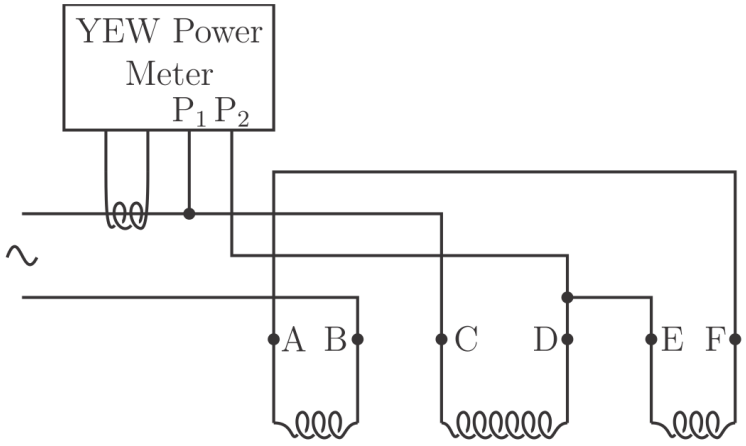

Centre Winding Power

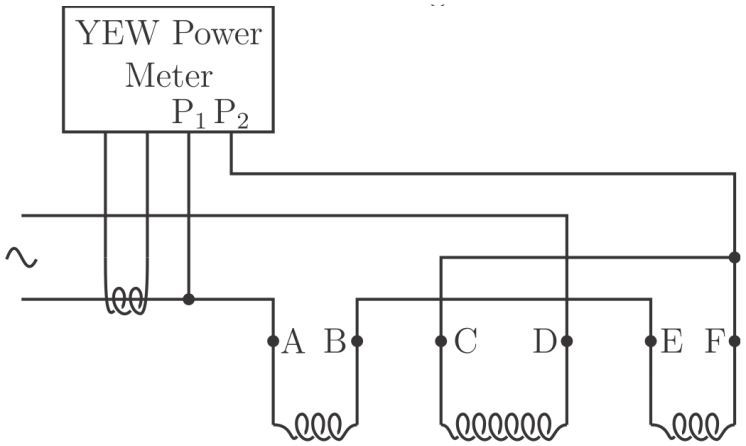

Outer Winding Power

Figure 4.7 P6 1 leg split winding connection modes

Table 4.2 P6 1-leg power dissipation in each winding portion

Frequency Hz	Current A	Power W	RT/turn Ohm	B T
Total winding				
50	3.29	0.17	0.00023	0.043
150	3.80	0.3	0.00030	0.040
250	3.92	0.45	0.00042	0.041
550	3.95	0.85	0.00079	0.041
800	4.03	1.5	0.00134	0.041
Central winding				
50	3.32	0.09	0.00022	0.027
150	3.82	0.17	0.00031	0.026
250	3.94	0.27	0.00047	0.026
550	3.96	0.50	0.00086	0.026
800	4.04	0.9	0.00149	0.026
Outer winding				
50	3.30	0.08	0.00023	0.016
150	3.81	0.03	0.00028	0.015
250	3.93	0.18	0.00036	0.015
550	3.95	0.30	0.00060	0.015
800	4.03	0.54	0.00104	0.015

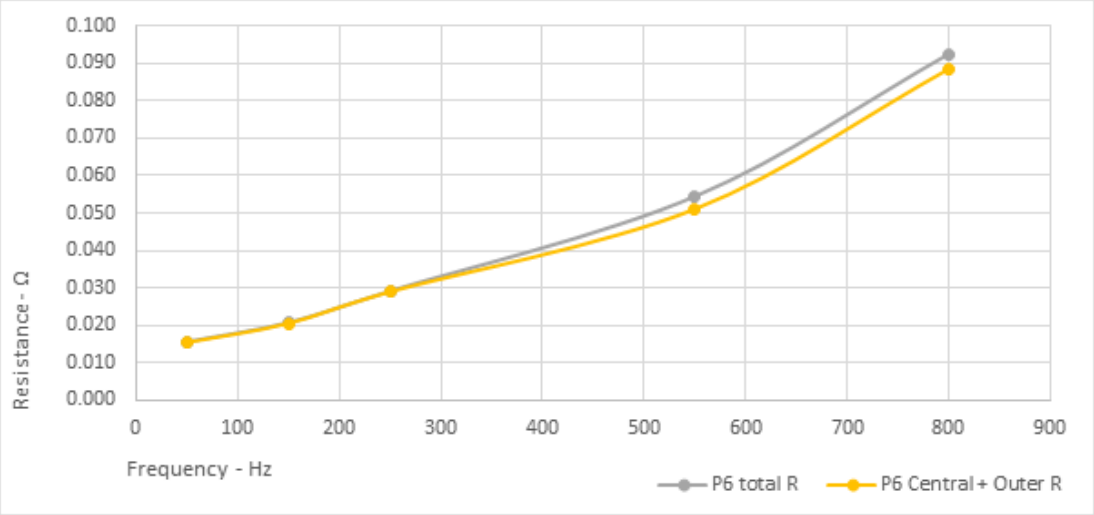

Figure 4.8 P6 1 leg total resistance vs frequency for full winding and summation of winding portions

The resistance values shown in Table 4.2 include winding *dc* resistance and *ac* losses coupled by induction.

To better visualize the significance of the data, the resistance per turn measurements for total, central and outer portions of the winding are compared in Figure 4.9.

4.2.6 Discussion

For the 1-leg P6 with partial core, the average resistance per turn of the central winding portion is higher than for the outer winding portion, and the resistances per turn each increase with frequency. The average resistance per turn of the total winding falls between the central and outer portion values. The winding portions have approximately equal turns and the winding total resistance per turn result suggests it is an average value of the central and outer portion resistances.

The resistance per turn of the winding outer portions is significantly less than that of the central portion, ruling out increased conductive losses at the ends of the winding being the cause of greater heating.

To account for the winding central portion having a greater resistance per turn, the *ac* resistances and the inductances of each portion are compared and given in Table 4.3 The results show that the proportions of *ac* resistance and inductance of each winding are similar; suggesting that the *ac* resistance for each winding portion is coupled by the proportion of inductance for that portion.

The *ac* resistance is obtained by subtracting the winding *dc* resistance from the total measured resistance at each frequency. For example, at $150Hz$, and at each frequency:

$$R_{ac} = R_T - R_{dc} \tag{4.2}$$

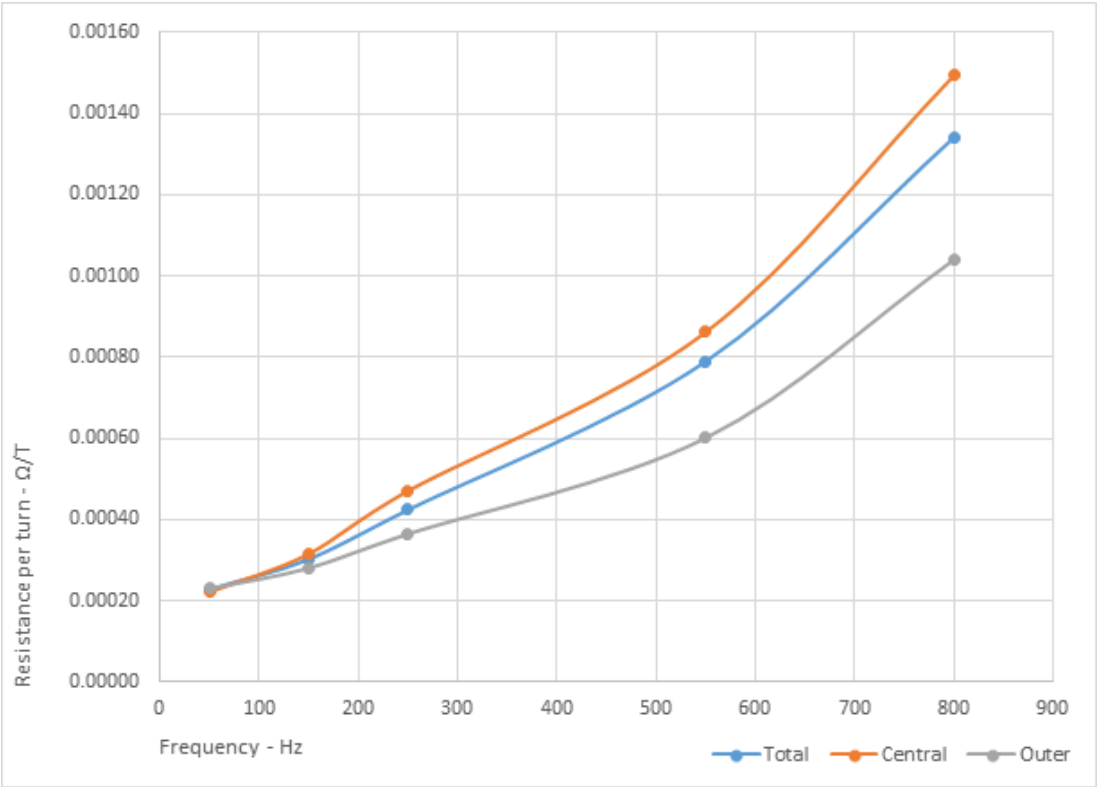

Figure 4.9 P6 1 leg resistance per turn vs frequency for full, central and outer winding portions

where R_{ac} is the winding ac resistance at each frequency
R_T is the winding total resistance measured at each frequency
R_{dc} is the winding dc resistance

The *ac* resistance of each portion of winding is taken as a percentage of the respective total winding *ac* resistance at each frequency. For example, the percentage resistance of the central portion at $150Hz$ is,

$$\%R_{C150} = \frac{R_{C150}}{R_{T150}} \times 100 \tag{4.3}$$

where $\%R_{C150}$ is the percentage resistance in the central portion to total resistance at $150Hz$
R_{C150} is the ac resistance of the central winding portion at $150Hz$
R_{T150} is the ac resistance of the total winding at $150Hz$

Finally, an average of each resistance percentage at each frequency is taken for each winding portion. For example, the average percentage resistance of the central winding

Table 4.3 P6 Split winding comparison of winding portion inductance and resistance

Winding portion	Inductance LT-mH	%L of LT %	% R of RT %
1-leg no core			
Total	0.076	99.6	88.9
Central	0.044	57.7	51.3
Outer	0.032	41.9	37.6
1-leg with core			
Total	0.845	100.0	95.6
Central	0.537	63.6	61.7
Outer	0.308	36.4	33.9

portion is,

$$\%R_{Cac} = \frac{\%R_{C150} + \%R_{C250} + \%R_{C550} + \%R_{C800}}{4} \tag{4.4}$$

where $\%R_{Cac}$ is the percentage of ac resistance in the central portion of the winding

Note that the results for $50Hz$ measurements were not included as they were too close to the *dc* resistance values and were subject to too large an error to give a meaningful comparison. Therefore the $\%R_{Cac}$ total values shown do not equate to 100%.

The Results in Table 4.3 show a correlation of percentage *ac* resistance ($R^2_{value} = 0.89$) to the percentage inductance of each of the central and outer winding portions. The *ac* resistance includes the effects of both core and winding losses but demonstrates that they are somewhat related to the inductance of the winding portion measured.

This observation further supports the proposition that the *ac* resistance effects are induced losses and not conduction losses because a loss coupled by induction would be in proportion to the inductance of the turns in which it was measured. The results also show that the inductance of a given number of turns is determined by their relative location along a partial core. The measured ac loss resistance per turn increases towards the centre of the winding along with the measured inductance per turn. The heating effect behaves in an opposite manner, increasing towards the ends of the winding.

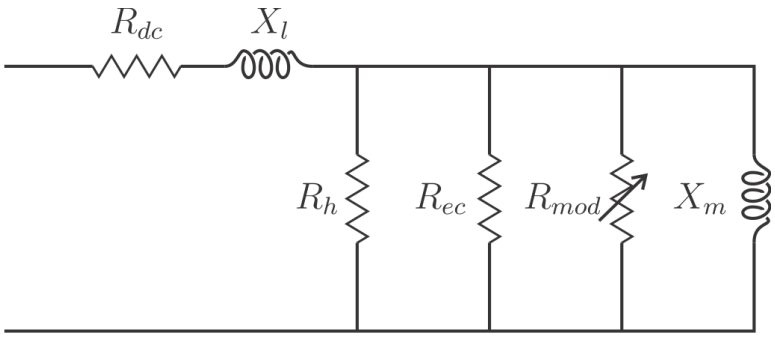

Figure 4.10 Steinmetz equivalent circuit with the inclusion of additional loss resistance R_{mod}

4.3 QUANTITATIVE ANALYSIS OF THE AC RESISTANCE

The transformer equivalent circuit was modified to analyse the measured *ac* resistance in the P6 1-leg inductor with partial core as shown in Figure 4.10.

A variable component of resistance R_{mod} is included to account for induced loss resistance not calculated by the current formulations. R_{mod} may therefore include orthogonal flux components of the core and winding losses.

4.3.1 Core Hysteresis loss resistance

A general formulation for hysteresis power loss can be empirically derived using Nasar and Boldera [1989],

$$P_h = k_{hc} f B_c^{S_{Fc}} W_{Tc} \tag{4.5}$$

where k_{hc} is the hysteresis loss constant that depends on the material
S_{Fc} is the Steinmetz factor
W_{Tc} is the weight of the core

Research has shown that the S_{Fc} factor is very close to 1.84 for a wide variety of partial core transformers tested at University of Canterbury Liew [2001]. However the k_{hc} constant does not generally agree between differing designs and a new constant was found for partial core transformers. A new general solution for partial core hysteresis real power loss is given in equation 4.6.

$$P_{hpc} = \nu_{core}^{1+\alpha hpc} \gamma_{core} k_{hpc}^{\alpha hpc} f B_{core}^{1.84} \tag{4.6}$$

where αhpc is the partial core factor found to be -2.5
k_{hpc} is the partial core hysteresis loss constant found to be 3.5×10^3

For the particular core steel used in the research concerned, the general solution becomes Liew [2001],

$$P_{hpc} = 1.38 \times 10^{-9} v_{core}^{-1.5} \gamma_{core} f B_{core}^{1.84} \tag{4.7}$$

where v_{core} is the core volume
γ_{core} is the core material density

The hysteresis resistance is therefore,

$$R_h = \frac{e_1^2}{P_{hpc}} \tag{4.8}$$

where e_1 is the emf across the magnetising reactance

Equation 4.7 relates only to the core steel used in that research and will be applied to the results in this work as well. Further, the formulation relies on equal and uniform axial flux density in the core.

Though not justified at this point, it is assumed that the average axial flux density is uniform in the core material, and therefore the formulation for hysteresis loss resistance shall be applied in its present form.

4.3.2 Core eddy current loss resistance

The method presented for calculating core eddy current loss is the same as that used for full core transformers and assumes that all of the core flux flows uniformly through the entire core and is not affected by frequency as long as the skin depth of the lamination is greater than half the lamination thickness.

It has been shown that radially stacked laminations significantly reduce core losses, and this has been attributed to reducing eddy current effects where the flux bends through the core steel towards the ends. Therefore the standard formulation for eddy current loss resistance does not account for additional eddy current loss in partial core inductors Bodger [2014 lecture notes].

Temperature affects the resistivity of core steel and is taken into account by

$$\rho_c = \rho_{c20C} \left(1 + \Delta\rho_c \left(T_c - 20\right)\right) \tag{4.9}$$

where $\Delta\rho_c$ is the thermal resistivity coefficient of the core material
ρ_{c20C} is the core material resistivity at 20°C in $m\Omega$

The skin depth of eddy currents in the core steel is also affected by the change in resistivity of the core material with temperature.

$$\delta_{ec} = \sqrt{\frac{2\rho_c}{\mu_0 \mu_{rc} \omega}} \tag{4.10}$$

where μ_{rc} is the relative permeability of the core material.

The eddy current real power loss can be expressed as

$$P_{ec} = \frac{c_{lam}^2 l_{fc}}{12\rho_c N^2 A_c} \cdot e_1^2 \tag{4.11}$$

where
- C_{lam} is the thickness of one lamination $= w_{core}/n$
- n is the number of laminations
- l_{fc} is the length of the flux path through the core (core length)
- A_c is the cross sectional area of the core
- N is the number of turns of the winding

The eddy current resistance for the transformer equivalent circuit is

$$R_{ec} = \frac{e_1^2}{P_{ec}} = \frac{N^2 A_c 12\rho_c}{l_{fc} c_{lam}^2} \tag{4.12}$$

4.3.3 Conduction losses in the winding

The winding *dc* resistance is calculated from the winding conductor parameters as follows,

$$R_{dc} = \frac{\rho l}{A} \tag{4.13}$$

where
- ρ is the resistivity of the conductor
- l is the length of the conductor
- A is the cross sectional area of the conductor

The resistivity of a conductor is temperature dependent

$$\rho_w = \rho_{w20C} \left(1 + \Delta\rho_w \left(T_c - 20\right)\right) \tag{4.14}$$

where
- $\Delta\rho_w$ is the thermal resistivity coefficient of the winding material
- ρ_{w20C} is the winding material resistivity at 20°C in $m\Omega$

The influence of skin effect is not considered in this analysis as it can be shown by calculation that it has a negligible effect.

The skin depth for a conductor is given as,

$$\delta = \sqrt{\frac{2\rho}{\mu_0 \mu_r \omega}} = \sqrt{\frac{\rho}{\pi \mu_0 \mu_r f}} \tag{4.15}$$

where	δ	is the skin depth
	ρ	is the resistivity of the conductor
	f	is the frequency of a sinusoidal wave
	$\mu_0\mu_r$	is the permeability of the conductor

For aluminium the skin depth is $4.6mm$ at $800Hz$ which is greater than half the thickness of conductors used in this work by a factor of 2.6. For the lamination steel the skin depth at $800Hz$ is $0.4mm$. The laminations used in this work are $0.23mm$ thick and therefore the skin depth is greater than half of this thickness by a factor of 3.5.

4.3.4 Results

The results are presented in graphical form in Figure 4.11. The addition of R_{mod} provides a satisfactory alignment to the measured values over the frequency range tested. The addition of a single value resistance to correct the departure in resistance over a range of frequencies is consistent with effects produced by an inductively coupled loss component. Therefore loss component R_{mod} may be occurring in both the winding and core as additional losses coupled by induction.

There also appears to be a reduction in the measured magnetising reactance of the test winding P6. This is not accounted for here as the influence on resistance results is not significant.

Table 4.4 provides a comparison of the model with the inclusion of R_{mod} in the modified model.

4.3.5 Conclusion

Experiment 7 has shown that the total resistance of a partial core inductor is frequency dependent and can be modelled by the inclusion of a single resistance value to the standard Steinmetz equivalent circuit.

The measured *ac* resistance per turn decreases towards the winding ends, suggesting the end heating effect is not due primarily to increased conduction losses.

The standard Steinmetz transformer equivalent circuit produces low series equivalent resistance values at higher frequencies which can be corrected by the inclusion of an additional resistance, R_{mod}, across the magnetising reactance. This additional resistance

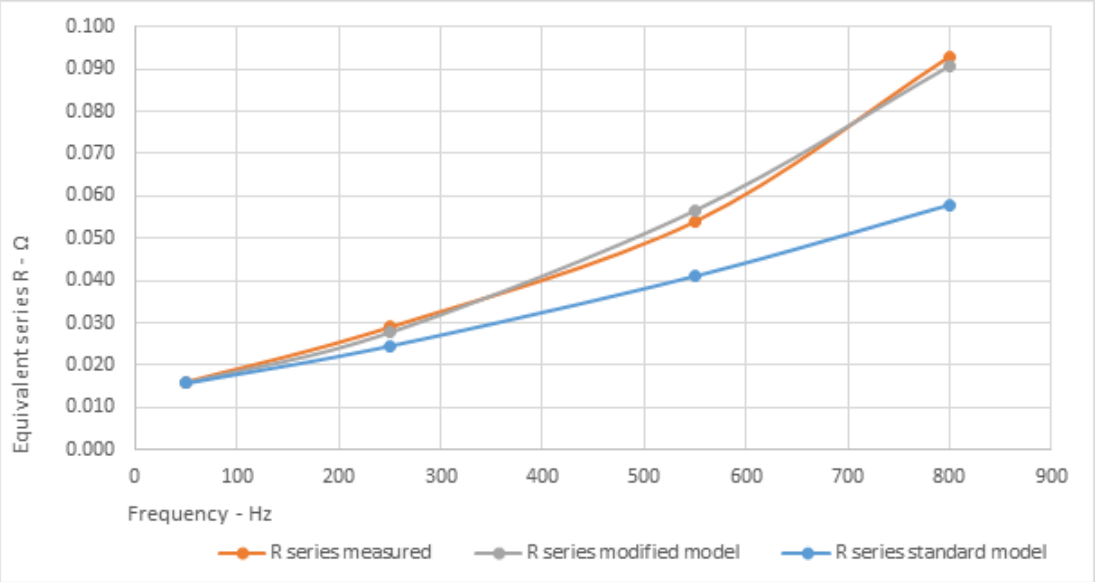

Figure 4.11 P6 1 leg series equivalent resistance vs frequency with the inclusion of additional loss resistance R_{mod}

Table 4.4 P6 Comparison of model resistance with R_{mod}

Frequency	50Hz	250Hz	550Hz	800Hz
P6 Standard model				
X_m	0.30Ω	1.5Ω	3.3Ω	4.80Ω
R_h	49.4Ω	241.9Ω	531.1Ω	772.2Ω
R_{ec}	1608.9Ω	1608.9Ω	1608.9Ω	1608.9Ω
R_{mod}	α	α	α	α
R_c total	47.9Ω	210.3Ω	399.3Ω	521.7Ω
R_T series	0.016Ω	0.025Ω	0.041Ω	0.058Ω
P6 Modified model with R_{mod}				
X_m	0.30Ω	1.5Ω	3.3Ω	4.80Ω
R_h	49.4Ω	241.9Ω	531.1Ω	772.2Ω
R_{ec}	1608.9Ω	1608.9Ω	1608.9Ω	1608.9Ω
R_{mod}	700Ω	700Ω	700Ω	700Ω
R_c total	44.9Ω	161.7Ω	254.3Ω	298.9Ω
R_T series	0.016Ω	0.028Ω	0.057Ω	0.091Ω
P6 Measured				
X_m	0.308Ω	1.23Ω	2.67Ω	3.86Ω
R_T series	0.016Ω	0.029Ω	0.054Ω	0.093Ω

simulates the effect of losses coupled by induction and would be typical of the effect that eddy current losses might have.

The induced ac resistance component R_{mod} may therefore simulate eddy current losses in both the core and winding.

4.4 EXPERIMENT 8 - THE NATURE OF WINDING AC LOSS IN A 3-PHASE PARTIAL CORE INDUCTOR

4.4.1 Objective

As the design application of this work is a 3-leg, 3-phase reactor (project inductor), Experiment 7 was repeated on a 3-leg device constructed from three P6 windings to determine if the same effects could be observed, along with the relative magnitude of the effects. Additional testing was carried out to enable the equivalent circuit model for a 1-leg device to be extended to model a 3-phase device.

4.4.2 Experimental method

A 3-phase partial core inductor was constructed from three P6 windings with one of them being the split winding used in Experiment 7. Testing was carried out with a 3-phase supply at test frequencies, 5, 150, 250, 550 and $800Hz$. The arrangement was connected as shown in Figure 4.12. Once again, three connection modes enable the power dissipation to be measured in each portion of the split winding. The applied voltage was chosen to maintain the same calculated peak flux density at each frequency as for Experiment 7.

4.4.3 Results

Figure 4.13 shows a comparison between the total resistance obtained for the split winding compared to the summation of the central and outer portions. The error between the two results is less than 5.5% and is therefore regarded as a reliable data source.

Figure 4.14 displays the data of Table 4.5 resistances per turn of the P6, 3-phase inductor with partial cores.

The results of Table 4.5 show a significant increase in total series resistance in each of the measured portions when compared to the P6, 1-leg inductor. Table 4.6 compares the 1-leg and 3-phase test results.

The results in Table 4.6 show that the total series resistance percentage increases in the 3-phase inductor compared with the 1-leg inductor at each frequency.

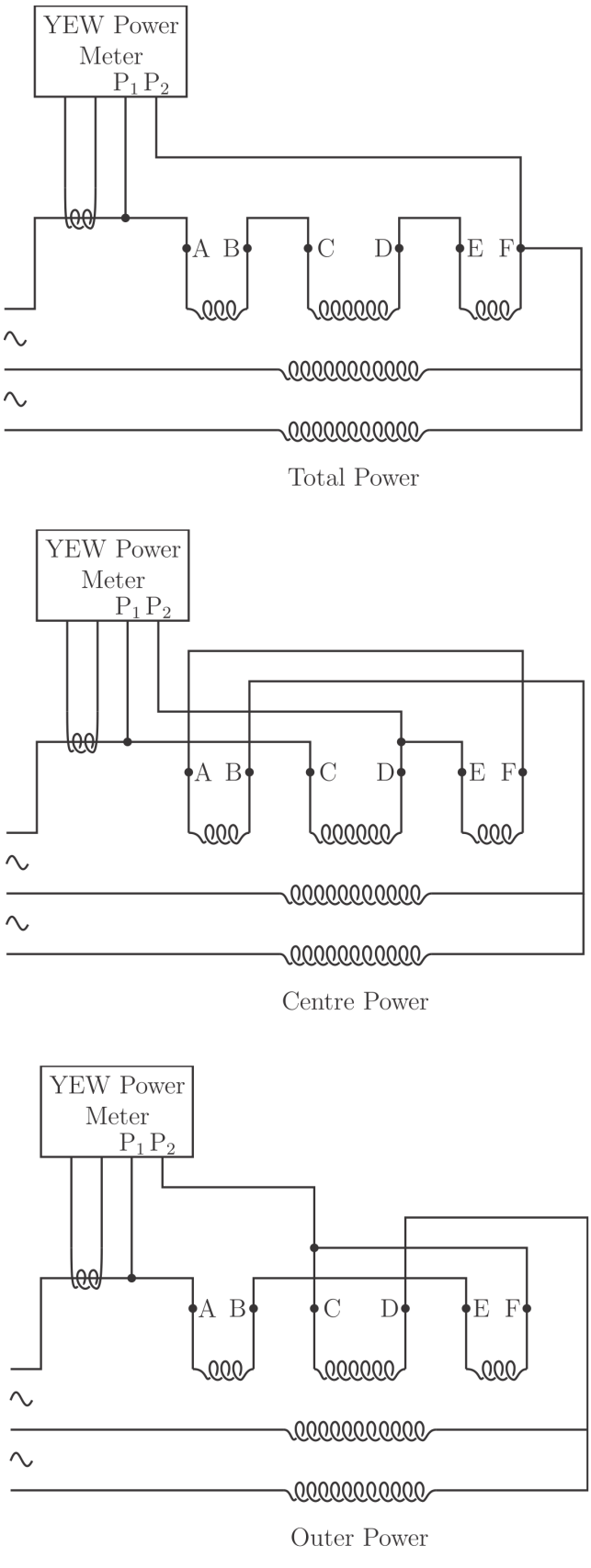

Figure 4.12 P6 3-phase split winding connection modes

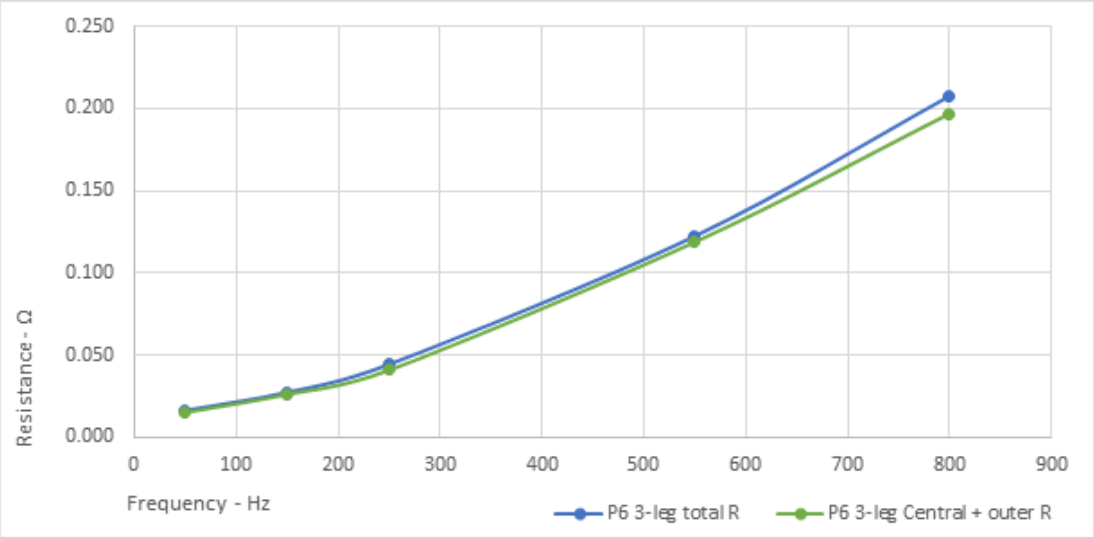

Figure 4.13 P6 3-phase total resistance vs frequency for full winding and summation of winding portions

Table 4.5 P6 3-phase power dissipation in each winding portion

Frequency Hz	Current A	Power W	RT/turn Ohm	B T
Total winding				
50	2.81	0.13	0.00024	0.043
150	2.83	0.22	0.00040	0.040
250	2.88	0.37	0.00065	0.041
550	2.89	1.02	0.00079	0.041
800	2.94	1.5	0.00178	0.041
Central winding				
50	2.81	0.07	0.00024	0.027
150	2.83	0.13	0.00044	0.026
250	2.88	0.23	0.00075	0.027
550	2.89	0.70	0.00227	0.026
800	2.96	1.2	0.00370	0.027
Outer winding				
50	2.81	0.05	0.00020	0.015
150	2.83	0.08	0.00031	0.014
250	2.88	0.11	0.00041	0.014
550	2.89	0.29	0.00109	0.014
800	2.94	0.52	0.00187	0.014

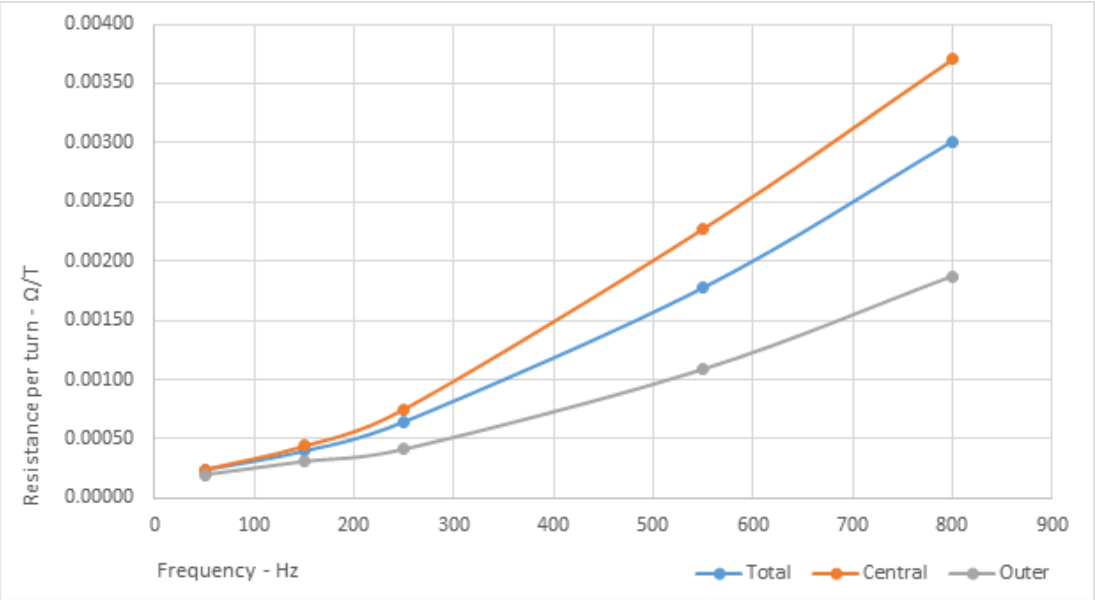

Figure 4.14 P6 3-phase resistance per turn vs frequency for full, central and outer winding portions

Table 4.6 P6 comparison of 1-leg and 3-phase results

	1-leg (Exp. 7)	3-phase (Exp. 8)	3-phase % increase
Peak flux density	0.041T	0.041T	0.1%
$RT50Hz$	0.016Ω	0.17Ω	5.1%
$RT150Hz$	0.021Ω	0.027Ω	32.0%
$RT250Hz$	0.029Ω	0.045Ω	52.3%
$RT550Hz$	0.054Ω	0.123Ω	124.9%
$RT800Hz$	0.093Ω	0.208Ω	124.4%
Inductance Total (LT)	$0.845mH$	$1.113mH$	31.7%
Inductance Central	$0.537mH$	$0.720mH$	34.0%
Inductance Outer	$0.308mH$	$0.390mH$	26.7%
Central %L of LT	63.6%	64.7%	1.7%
Central %R of RT	61.7%	67.1%	8.7%
Outer %L of LT	36.4%	35.0%	−3.7%
Outer %R of RT	33.9%	25.4%	−25.1%

Table 4.6 shows the 3-phase central portion inductance increases and outer portion inductance reduces. The ratios of central and outer portion resistances to total resistances follow a similar trend.

It is therefore concluded that the the 3-phase inductor behaves in a similar manner to the 1-leg inductor except for the increase of inductance and resistance in the 3-phase device.

4.4.4 Conclusion

The significant increase of P6, 3-phase *ac* resistance at higher frequencies can be accommodated in the Steinmetz equivalent circuit by the inclusion of an additional resistive burden across the magnetising reactance in the same way as for the 1-leg inductor shown in Experiment 7. The results of adding R_{mod} to the 3-phase inductor will be presented in Experiment 9.

Although the addition of resistance across the magnetising reactance produces calculated results to closely match the measured results, it does not explain where the actual loss is occurring. In Experiment 9, a calorimetric analysis is conducted to establish the relative power loss that occurs in the core and in the winding.

4.5 EXPERIMENT 9 - CALORIMETRIC ANALYSIS OF CORE AND WINDING LOSSES

4.5.1 Objective

Calorimetric analysis enables the measurement of energy flow into the winding and core to determine what proportion of the total electrical power is dissipated in the core or winding.

4.5.2 Apparatus

The 3-phase test winding P6 of Experiment 8 was used in this experiment. A 3-leg, 3-phase configuration was chosen to maximise resistive losses in both the core and winding thus providing a clearer indication of where they arise and also to aid in the development of a 3-phase model.

The test winding was fitted with 6× K-type thermocouples connected to a YEW MX100 data acquisition unit to monitor each temperature against time. The thermocouples were attached to the winding as shown in Figure 4.15. Note the placement of thermocouple X at the far left, inserted directly into a small hole in the side of the winding.

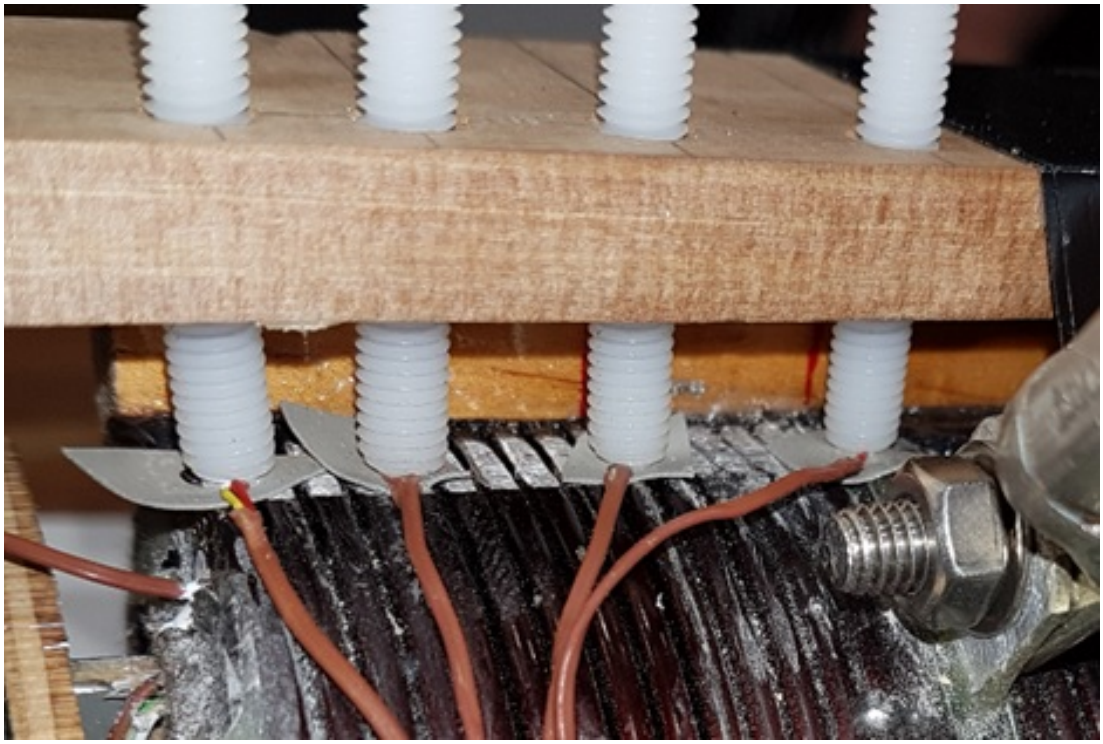

Figure 4.15 Placement of thermocouples on the P6 winding

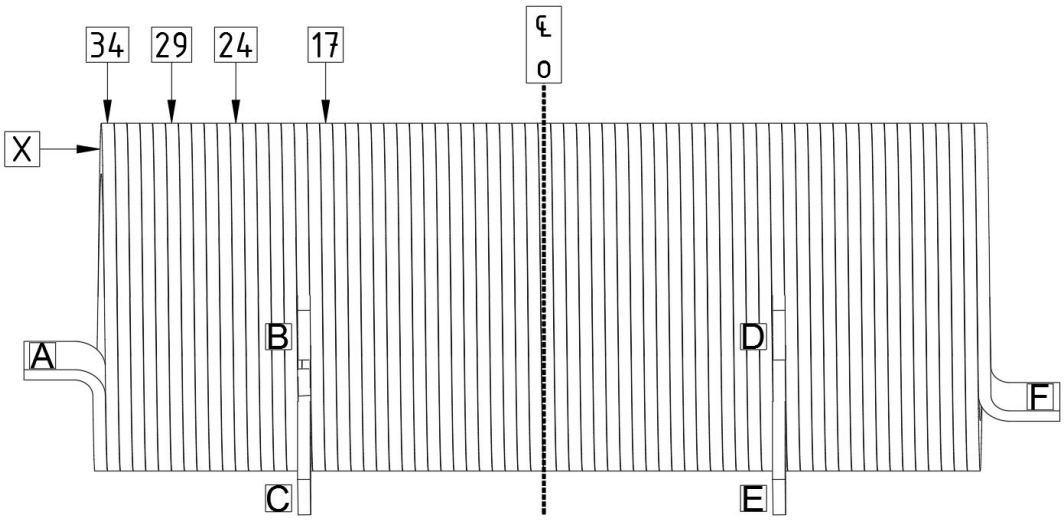

Figure 4.16 Placement of thermocouples on the P6 winding at windings 17, 24, 29 & 34 from the centre

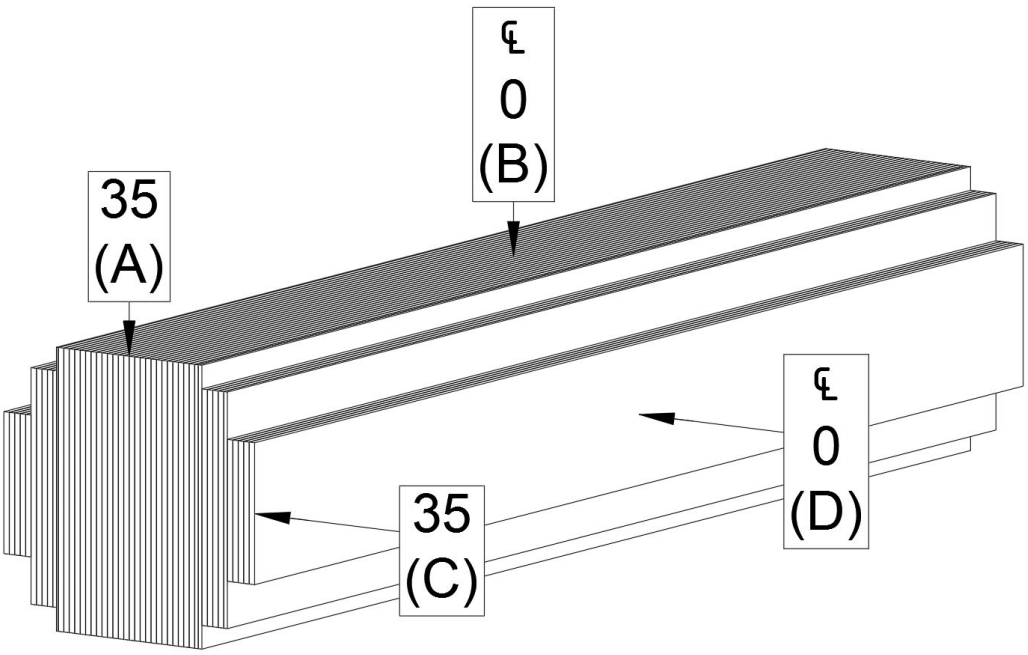

Figure 4.17 Placement of thermocouples on the P6 core

4.5.3 Experimental method

Thermocouples were attached to one P6 winding as shown in Figure 4.16. by the following method so as maximise the thermal contact with the winding.

- Winding cleaned of varnish at the outer surface
- Small rubber heat conductive compound inserted between winding and thermocouple for electrical isolation
- Thermocouple clamped tightly by means of nylon screw
- One thermocouple X was inserted into a small drilled hole at the winding end with heatsink paste. This thermocouple was used to serve a reference to confirm the other probes give time synchronised results.

The end reference thermocouple X temperature trace matches very closely to the end thermocouple "34" fitted by the above technique; therefore validating the method of attaching thermocouples. Thermocouples were also inserted into the core at locations shown in Figure 4.17. Probes (A) and (B) are located on the lamination edge, while probes (C) and (D) are located on the outer lamination flat surface.

The device was then energised by a 3-phase supply at each frequency of 50, 250, and $800Hz$ and a recording of temperature was made at one-second intervals. A cool down period of at least one day was provided between each frequency trial.

The power in the test leg is estimated based on the total power measured for the 3-phase device divided by three as the windings are very similar. Voltage and current

were also recorded with current being kept constant at each frequency to maintain near equal peak flux density between each frequency trial.

The data were then analysed to produce the average temperature rise for each portion of windings between the thermocouples. Based on the temperate rise and the mass specific heat for winding and core materials, an estimate of the energy delivered to each portion of winding and core was calculated.

To obtain the power delivered to each portion of the core, a suitable time span was chosen where the temperature rise was reasonably constant with time from the start of the trial. For the $50Hz$ and $250Hz$ trials, 2 minutes was chosen. For the $800Hz$ trial, 74 seconds was chosen.

No particular care was taken to insulate the device windings during the trials but it may have been preferable to do so. A lack of insulation may have resulted in lower winding temperatures, and therefore a lower calorimetric winding loss estimate as can be seen in the results.

The influence of the core on the winding as a heatsink was also not thought to be very significant, but may also tend to under-represent the magnitude of true loss in the winding by a small amount.

4.5.4 Results

Calorimetric data is presented in Figure 4.18. Each column represents the temperature rise recorded at each location on one winding and core. Based on the temperature difference over the time taken, and the weight of that section of the winding or core, the average power delivered over the time span is calculated for that section.

The power per turn is calculated to enable direct comparison of each winding segment, and between results obtained for the winding and core. The data is graphed in Figures 4.19, Figure 4.20 and Figure 4.21. Table 4.7 compares the raw results of the losses measured by the Yew power meter and the calorimetric method described above.

A significant margin of error exists at $50Hz$ and $250Hz$ and it can be seen that the total calorimetric power loss is lower than the total electrical power loss measured, and at $50Hz$, the calorimetric estimate is less than the calculated loss for the winding *dc* resistance alone.

A correction* is therefore applied to bring the total calorimetric loss up to that of the measured electrical power loss in Table 4.8. It is a small and proportionate correction at each frequency to enable a useful comparison. Naturally there is a margin of error associated with this method, however the results provide a good indication of the observed relative flow of energy into the core and winding.

It is now possible to compare the calorimetric loss of the core and winding with that of the model for hysteresis and eddy current core losses and the observed additional

		CORE					WINDING				
		Core Edge		Core Flat							
T/C placement	Turns	0	35	0	35		0	17	24	29	34
		(B)	(A)	(D)	(C)						
50Hz											
Start temp	°c	23.5	23.5	23.5	23.5		23.6	23.5	23.5	23.6	23.6
Finish temp	°c	23.5	23.6	24	24		25.1	25.1	25.3	25.5	25.7
ΔT	°c	0	0.1	0.5	0.5			1.6	1.7	1.9	2.0
Weight	kg	1.15	1.15	0.15	0.15			0.332	0.137	0.098	0.098
Time	sec	120	120	120	120			120	120	120	120
Energy	J	0.0	93.4	60.9	60.9			468.1	211.4	164.3	177.7
Power ave	W	0.0	0.8	0.5	0.5			7.8	3.5	2.7	3.0
W/turn	W/turn	0.00	0.01	0.01	0.01			0.23	0.25	0.27	0.30
Core total	W/turn	0.01	0.02								
250Hz											
Start temp	°c	23.8	23.8	23.9	23.9		24.8	24.2	24.2	24.2	24.2
Finish temp	°c	24.2	24.4	28.0	28.8		26.5	26.6	28.7	30.1	32.5
ΔT	°c	0.4	0.6	4.1	4.9			2.1	3.5	5.2	7.1
Weight	kg	1.15	1.15	0.15	0.15			0.332	0.137	0.098	0.098
Time	sec	120	120	120	120			120	120	120	120
Energy	J	373.5	560.3	499.4	596.8			619.2	429.1	461.9	630.7
Power ave	W	3.1	4.7	4.2	5.0			10.3	7.2	7.7	10.5
W/turn	W/turn	0.05	0.07	0.06	0.07			0.30	0.51	0.77	1.05
Core total	W/turn	0.11	0.14								
800Hz											
Start temp	°c	23.2	23.2	23.3	23.2		23.8	23.5	23.4	23.5	23.4
Finish temp	°c	25.2	25.0	42.8	48.2		25.5	31.0	41.1	48.1	59.0
ΔT	°c	2	1.8	19.5	25			4.6	12.6	21.2	30.1
Weight	kg	1.15	1.15	0.15	0.15			0.332	0.137	0.098	0.098
Time	sec	74	74	74	74			74	74	74	74
Energy	J	1867.6	1680.8	2375.1	3045.0			1389.3	1567.0	1878.8	2673.8
Power ave	W	25.2	22.7	32.1	41.1			37.5	42.4	50.8	72.3
W/turn	W/turn	0.37	0.33	0.47	0.61			1.10	3.03	5.08	7.23
Core total	W/turn	0.84	0.94								

Figure 4.18 Calorimetric data at each frequency

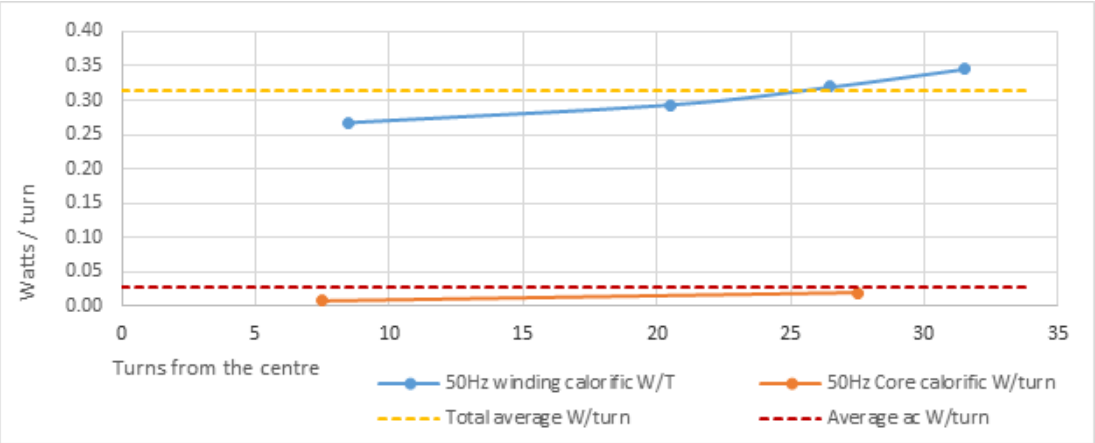

Figure 4.19 Calorimetric Watts per turn vs turns from winding centre at 50Hz

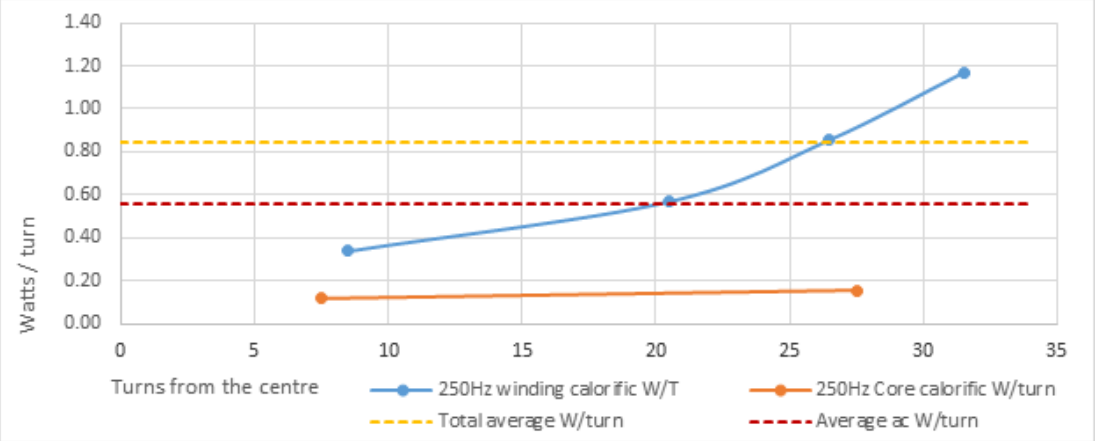

Figure 4.20 Calorimetric Watts per turn vs turns from winding centre at 250Hz

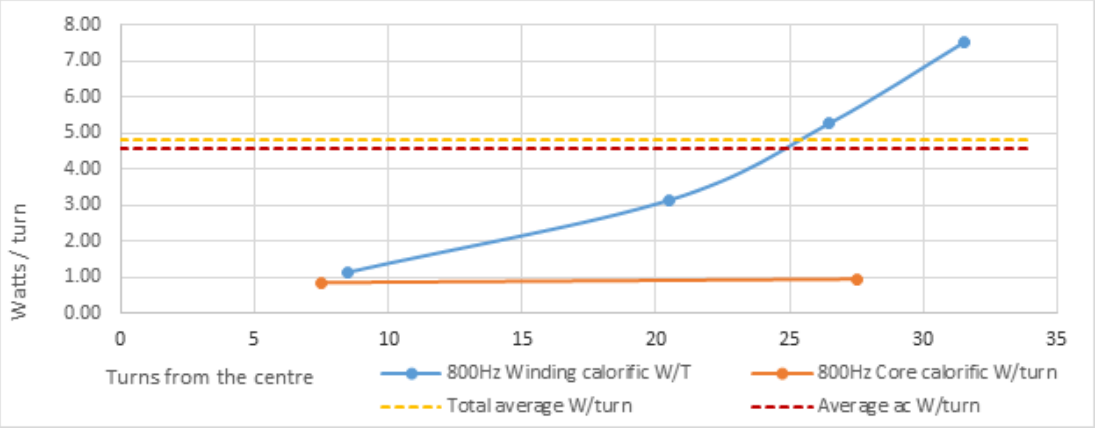

Figure 4.21 Calorimetric Watts per turn vs turns from winding centre at 800Hz

Table 4.7 P6 3-phase calorimetric power and measured electrical power

Frequency	50Hz	250Hz	800Hz
Calorimetric results			
Winding	17.0W	35.7W	202.9W
Core	1.8W	16.9W	121.2W
Total	18.8W	52.6W	324.1W
Electrical measurement (YEW)			
Total	21.7W	58.3W	334.0W
Error % calorimetric to electrical	87%	90%	97%
Calculated winding dc power			
Total	19.8W	19.9W	19.9W

Table 4.8 P6 3-phase adjusted calorimetric power and measured electrical power

Frequency	50Hz	250Hz	800Hz
Calorimetric results			
Winding	17.0+2.8*W	35.7+4*W	202.9+8*W
Core	1.8+0.1*W	16.9+1.7*W	121.2+2*W
Total	21.7W	58.3W	334.1W
Electrical measurement (YEW)			
Total	21.7W	58.3W	334.0W
Error % calorimetric to electrical	100%	100%	100%
Calculated winding dc power			
Total	19.8W	19.9W	19.9W

losses coupled by induction.

4.5.5 Further discussion of Figure 4.19 50Hz, Figure 4.20 250Hz and Figure 4.21 800Hz

The yellow dotted line represents the total average electrically measured power per turn delivered to one inductor leg.

The red dotted line represents the average *ac* power delivered to one inductor leg. This is calculated from the total power, less the power developed by the *dc* resistance of the winding. This power is therefore dissipated in the core and winding by effects other than by the *dc* resistance.

The blue line shows the average power dissipated per turn in one winding as measured by the calorimetric method. Each dot on the line denotes the point along the winding at which the average power is calculated for that winding segment. The trend shows that the winding progressively dissipates more power per turn as the winding approaches the end at 34 turns from the winding centre. The end heating effect is much greater at $800Hz$ ($7.5W/turn$) than it is at $50Hz$ ($0.35W/turn$).

The orange line shows the average power in the core in the location denoted by the dots on the line. This trend also suggests that the power dissipated increases towards the ends but the increase is not as dramatic as for the winding.

At $50Hz$ it can be seen that most of the loss not accounted for by the winding *dc* resistance losses is due to the core, with only a little due to *ac* winding loss. Overall the core accounts for around 7% of the total loss with the rest being approximately due to winding *dc* resistance.

At $250Hz$ the core loss is around 19%, winding dc resistance loss is 34% and the balance, 47%, is due to loss in the winding due to *ac* resistance effects.

At $800Hz$ the core loss is around 21%, winding *dc* resistance loss is 6% and the balance, 73%, is due to loss in the winding due to *ac* resistance effects.

It can be seen that the unaccounted for loss in the winding becomes progressively more dominant as frequency increases. Core losses also increase with frequency.

4.5.6 Quantitative analysis of the calorimetric method

To establish the origin of the observed loss effects in the core and winding, the calorimetric results are compared with the theory for winding dc resistance losses, hysteresis loss and eddy current loss in the core.

Hypothesis - there are two unaccounted for eddy current loss components in the standard Steinmetz model.

1. Eddy current losses in the core due to orthogonal flux effects, and

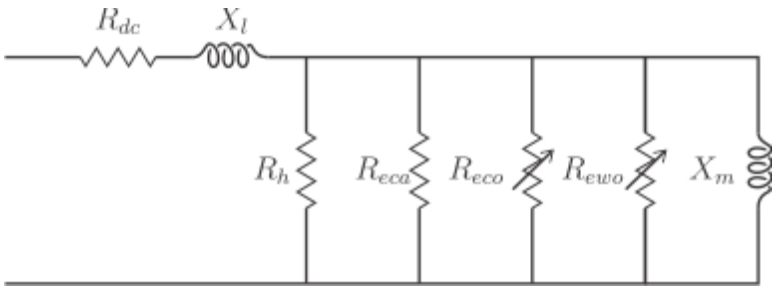

Figure 4.22 Modified inductor equivalent circuit to include orthogonal eddy current loss components

2. Eddy current losses in the winding

The proposed losses may be represented by additional resistive components in the Steinmetz equivalent circuit as shown in Figure 4.22. In this equivalent circuit representation, the core eddy current resistance R_{ec} shown in Figure 4.10, is redefined in Figure 4.22 as the axial component of core eddy current loss R_{eca} and core orthogonal loss is represented as R_{eco}. Winding eddy current losses are represented as R_{ewo}. R_{eco} and R_{ewo} are shown as variable resistances which were adjusted to find a single value that makes the core loss resistance, winding loss resistance and total resistance match the calorimetric loss resistances estimated at each frequency.

Referring to Table 4.9, the total core losses are represented by R_c and total series equivalent resistive losses are represented by R_T for each winding.

The results of Table 4.9 are displayed in Figure 4.23.

4.5.7 Discussion

Figure 4.23 illustrates a good fit is obtained for unaccounted loss due to heating effects in the core and in the winding.

From Table 4.9 the added resistance R_{eco} of 790Ω in parallel with the model estimate for core eddy current loss resistance of 1732.2Ω, produces a close fit to the calorimetric loss value of the core across the frequency range. Figure 4.23 light blue and black traces closely match.

By adding a further resistance R_{ew} of 238Ω in parallel with the core losses, the total loss resistance is a very close match to the total calorimetric loss value. The blue and orange traces overlap. This suggests that the unaccounted for calorimetric loss in the winding may be represented by a resistance of 238Ω.

The total calorimetric power is the summation of the individually measured core and winding power losses and is in close agreement to the measured electrical power.

Table 4.10 shows the new loss resistances for each loss component compared to the values obtained by the standard formulations. While it is true that this exercise

Table 4.9 P6 3-phase modelled inclusion of orthogonal loss components

Frequency	$50Hz$	$250Hz$	$550Hz$	$800Hz$
Standard model				
Winding dc R_{dc}	0.0138Ω	0.0138Ω	0.0138Ω	0.0138Ω
Core hysteresis R_h	74.5Ω	371.1Ω	816.5Ω	1187.7Ω
Core axial eddy current R_{eca}	1732.2Ω	1732.2Ω	1732.2Ω	1732.2Ω
Standard model result				
Core loss resistance (series equiv.) R_c	0.0018Ω	0.0107Ω	0.029Ω	0.049Ω
Total resistance (series equiv.) R_T	0.0156Ω	0.025Ω	0.043Ω	0.063Ω
Modified model with orthogonal core loss R_{eco}				
Core orthogonal eddy current R_{eco}	790Ω	790Ω	790Ω	790Ω
Core loss resistance (series equiv.) R_c	0.002Ω	0.0148Ω	0.0487Ω	0.090Ω
Calorimetric estimate of R_c				
Core loss resistance (series equiv.) R_c	0.0014Ω	0.013Ω	0.047Ω	0.086Ω
Modified model with winding orthogonal loss R_{ewo}				
Winding orthogonal eddy current R_{ewo}	238Ω	238Ω	238Ω	238Ω
Calorimetric estimate of R_{ewo}				
Winding orthogonal resistance (series equiv.) R_{ewo}	0.00139Ω	0.028Ω	0.083Ω	0.148Ω
Modified model total loss resistance R_T				
Total resistance (series equiv.) R_T	0.0164Ω	0.042Ω	0.128Ω	0.243Ω
Measured total loss resistance R_T				
Total resistance (series equiv.) R_T	0.0153Ω	0.041Ω	0.130Ω	0.243Ω

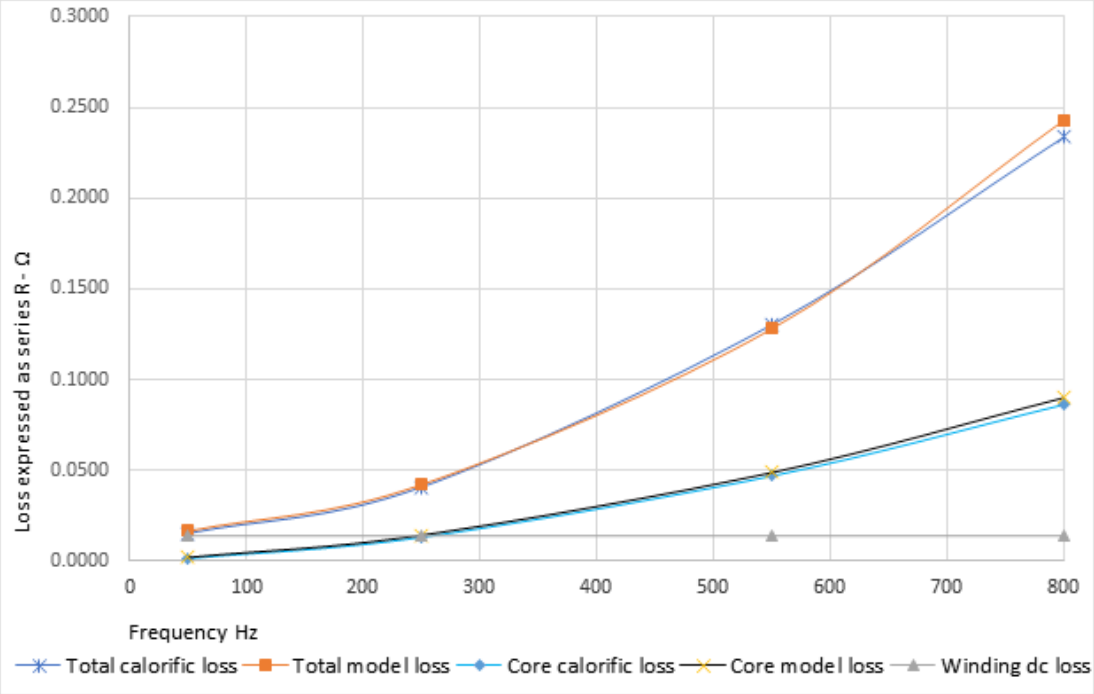

Figure 4.23 P6 3-phase total series equivalent resistance vs frequency for modelled, calorimetric and measured values

has been one of *curve fitting*, it has shown that the unaccounted for losses may be represented by additional burdens reflected across the magnetising reactance.

This method has also shown that it may be reasonable to use the hysteresis loss resistance as calculated by the standard formulation (4.8). Hysteresis loss resistance is proportional to frequency whereas eddy current loss resistance has a negligible frequency dependence under the condition that the flux is uniform throughout the lamination. The combined effect of the hysteresis and eddy current losses produces a satisfactory fit with the measured resistance which suggests that the standard formulation for hysteresis loss resistance is a useful first order approximation.

4.5.8 Conclusion

A close fit has been obtained between calorimetric measurements of heating effects in the core and winding and electrical power measurements. These effects can be simulated in the model by adding further burdens to the inductor equivalent circuit to represent the additional core eddy current loss and a proposed winding eddy current loss.

As these burdens may be individually represented by a resistance that is not dependent upon frequency or flux density over the range tested, it is proposed that these burdens represent eddy current heating effects. Therefore there are additional eddy current losses in the core, and also eddy current losses produced in the winding material in agreement with the hypothesis.

Table 4.10 P6 3-phase standard model compared to revised model

Frequency	50Hz	250Hz	550Hz	800Hz
Standard model				
Winding *dc* resistance R_{dc}	0.0138Ω	0.0138Ω	0.0138Ω	0.0138Ω
Core hysteresis resistance R_h	74.5Ω	371.1Ω	816.5Ω	1187.7Ω
Core orthogonal eddy current resistance R_{eco}	1732.2Ω	1732.2Ω	1732.2Ω	1732.2Ω
Winding orthogonal eddy current resistance R_{ewo}	α	α	α	α
Leakage reactance X_{leak}	0.009Ω	0.044Ω	0.095Ω	0.142Ω
Magnetising reactance X_{mag}	0.354Ω	1.769Ω	3.974Ω	5.659Ω
Modified model				
Winding *dc* resistance R_{dc}	0.0139Ω	0.0139Ω	0.0139Ω	0.0139Ω
Core hysteresis resistance R_h	74.5Ω	371.1Ω	816.5Ω	1187.7Ω
Core orthogonal eddy current resistance R_{eco}	542.6Ω	542.6Ω	542.6Ω	542.6Ω
Winding orthogonal eddy current resistance R_{ewo}	238Ω	238Ω	238Ω	238Ω
Leakage reactance X_{leak}	0.009Ω	0.044Ω	0.095Ω	0.142Ω
Magnetising reactance X_{mag}	0.354Ω	1.769Ω	3.974Ω	5.659Ω

It was assumed that the core hysteresis loss resistance was not significantly altered by a partial core configuration due to the loss being proportional to the weight of the core. The formulation of hysteresis loss resistance assumes that the magnetic flux is uniform throughout the core, and while it will been shown this is not strictly true, the average effect is deemed to be close enough for the purposes of the present work.

Now that the magnitude of the core loss and winding losses has been quantified, a formulation for the new loss components is sought. It appears to be a reasonable proposition that these losses are due to an orthogonal magnetic flux component emanating through the core and winding. An investigation of orthogonal flux emanation is conducted in Experiment 10 which leads to the development of empirical formulation of 3-phase inductor reactance and resistance values.

4.6 EXPERIMENT 10 - FLUX DISTRIBUTION ABOUT A PARTIAL CORE INDUCTOR

4.6.1 Objective

In this experiment, the flux profiles of a 3-phase inductor are examined. The purpose is to show the measurable difference that exists between a 1-leg partial core winding and multiple windings when grouped together. The work provides a backdrop to the formulations that follow for inductance and *ac* resistance in a 3-phase partial core inductor.

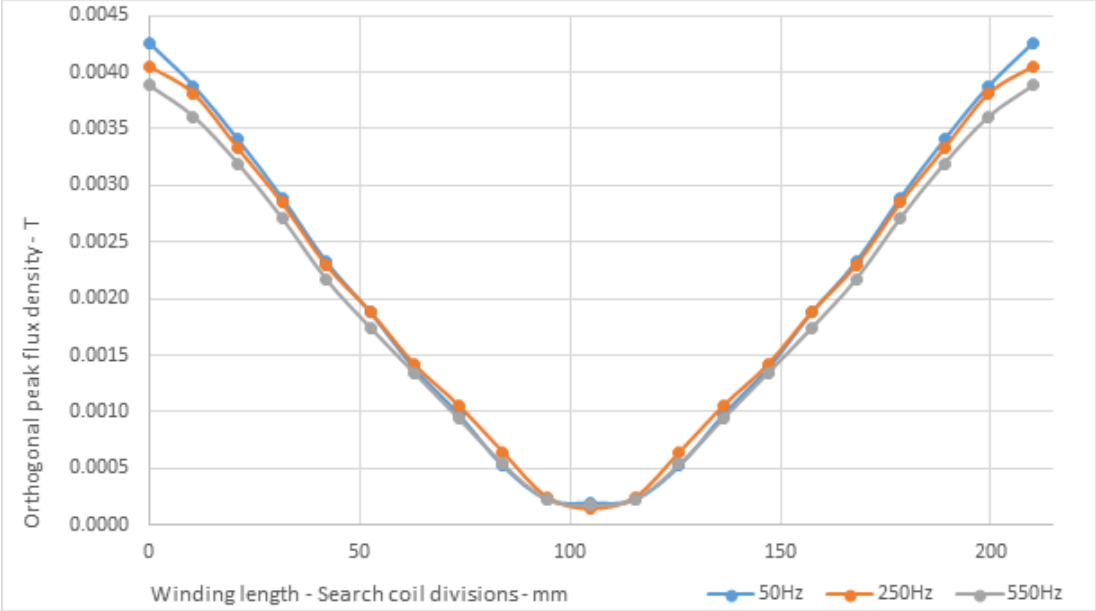

Figure 4.24 P6 3-phase orthogonal flux profile for one leg at position 1

4.6.2 Experimental method

Figure 4.24 depicts the orthogonal flux profiles for one leg of a 3-phase winding constructed from three P6 windings. The profile shown in Figure 4.24 was taken at flux measurement position 1 as shown in Figure 4.25 and has a more rounded profile in the middle of the winding compared to the "V" shaped profile of the P6 1-leg with partial core in Figure 4.2 at the start of this chapter. The orthogonal flux density is greater at the middle of the P6 3-phase winding length than for the 1-leg device, which suggests there is a greater magnitude of orthogonal flux between adjacent windings.

To obtain a more accurate picture of the flux distribution around a given winding in a 3-phase arrangement, the orthogonal flux was measured around the end of one winding. A profile of the circumferential orthogonal peak flux density is presented in Figure 4.26.

By taking the average of the circumferential peak flux density results, the average orthogonal flux density for the end band is obtained. The average value obtained for the end band was $0.0043T$.

Assuming (due to difficulty of measurement) that the proportionality between the average circumferential band flux density and that obtained at position 1 remains the same for each band along the length of the winding, a factor is found to match the position 1 measurement to the average orthogonal circumferential flux result. Therefore the flux density results obtained at position 1 along the length of the winding are each multiplied by the same factor obtained for the end band.

The orthogonal flux density results for the 1-leg and 3-phase inductors are compared

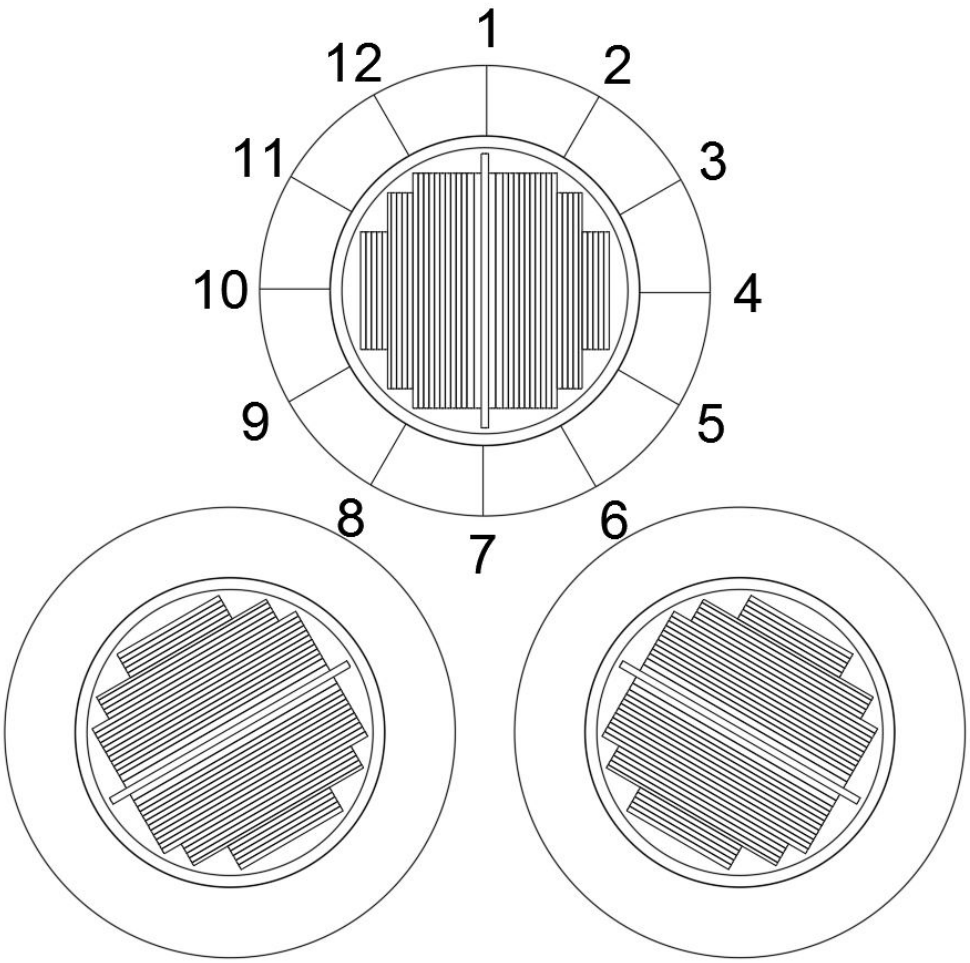

Figure 4.25 P6 3-phase orthogonal flux measurement positions at one end of one winding

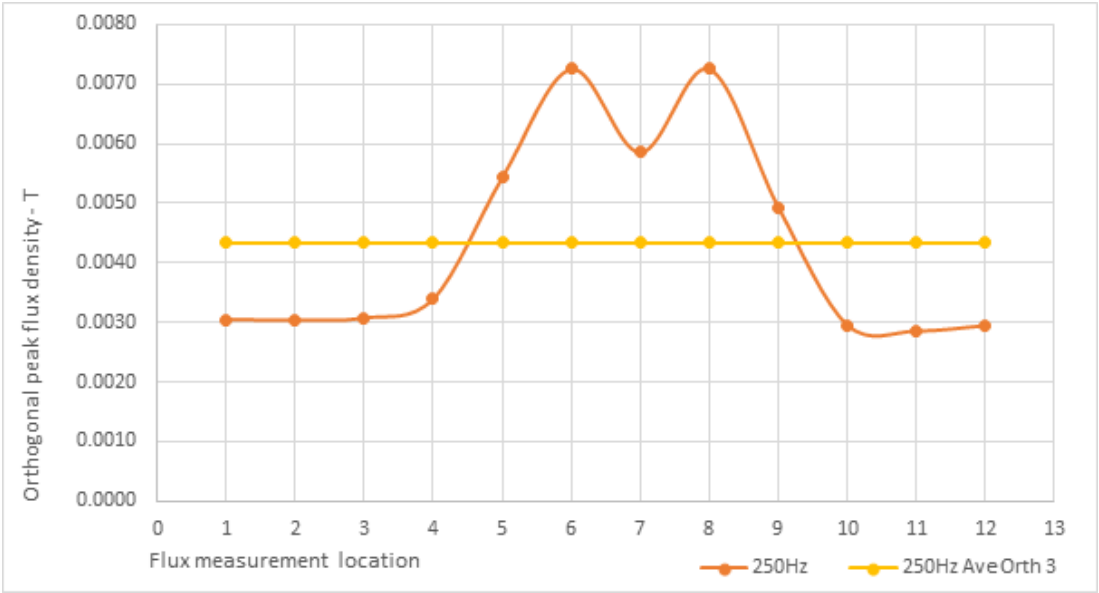

Figure 4.26 P6 3-phase circumferential orthogonal flux measurements of one winding end at $250Hz$

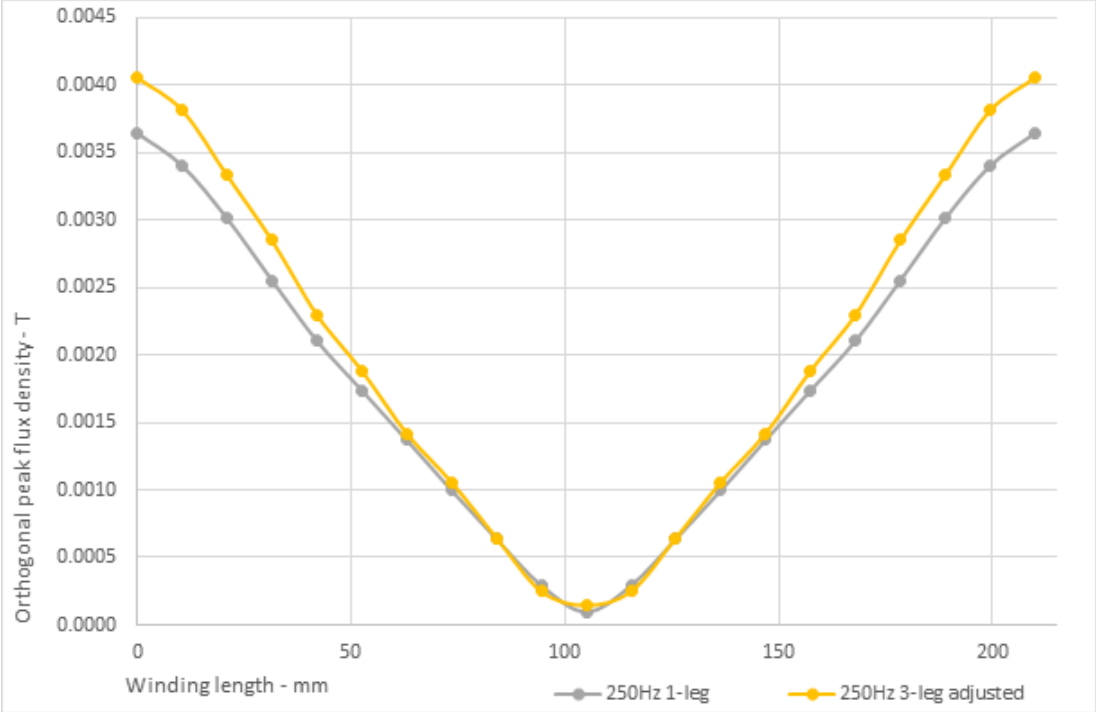

Figure 4.27 P6 1-leg and 3-phase orthogonal flux profile vs winding length at $250Hz$

at $250Hz$ in Figure 4.27 It can be seen that there is an increase in the average orthogonal flux in the 3-phase inductor, although when compared to the axial flux density the effect is subtle. In Figure 4.28, the orthogonal results shown in Figure 4.27 are contrasted with axial flux measurements made at the same positions along the winding. The axial search coil measurements for both the 1-leg inductor and the 3-phase inductor were made with the same voltage across the winding. There is a difference between the profiles of the orthogonal flux densities due to the proximity of the windings to one another. It is proposed that these different flux profiles give rise to changes in the inductance and *ac* resistance of the windings and core.

Modelling of the reactive and resistive elements coupled with experimental observation and the physical geometric relationships of the cores and windings enable formulations of the 3-phase characteristic to be made.

4.7 FORMULATION OF 1-LEG PARTIAL CORE INDUCTANCE REVISITED

4.7.1 Equivalent circuit model for a partial core inductor

To recap, the 1-leg partial core inductor model is developed based on the primary winding of a partial core transformer using the transformer equivalent circuit Paul et al. [1986]. The inductor may be modelled as a 2-terminal device as shown in Figure 4.29

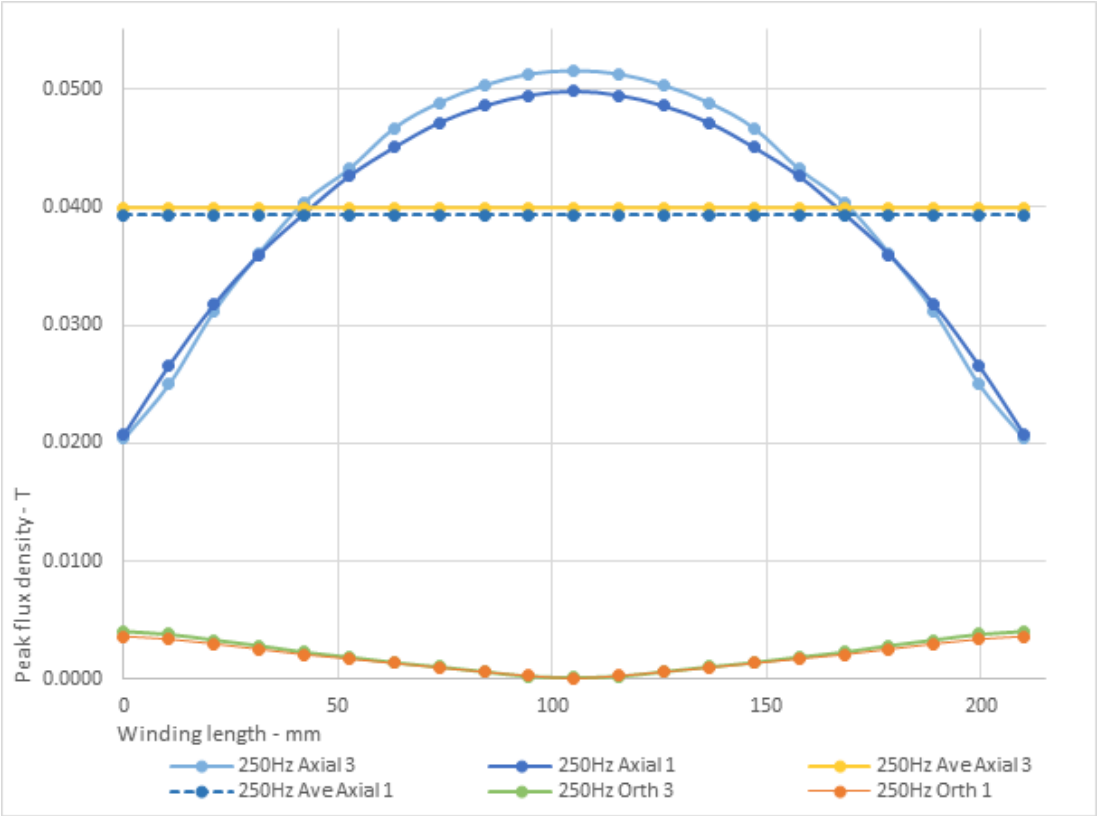

Figure 4.28 P6 1-leg and 3-phase axial orthogonal flux profile vs winding length at $250Hz$

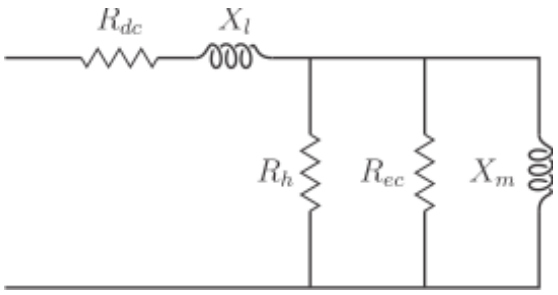

Figure 4.29 Transformer equivalent circuit adapted for a partial core inductor

The model is used to estimate the reactance and resistance of the device at fundamental and harmonic frequencies.

The parameters of the model are:

1. Magnetising reactance - X_m
2. Leakage reactance - X_l
3. Winding dc resistance - R_{dc}
4. Core hysteresis losses - R_h
5. Core and winding eddy current losses - R_{ec}

The model components are linked to the physical parameters of the inductor to calculate performance of any given design. The design approach is based on the reverse design transformer modelling technique which enables designs to be based on available materials.

4.7.2 Magnetising reactance for 1-leg partial core inductor

The general expression for the magnetising reactance is

$$X_m = \frac{\omega N^2 \mu_0 \mu_{rT} A_c}{l_c} \tag{4.16}$$

where N is the number of turns
μ_0 is the permeability of free space
μ_{rT} is the relative permeability of the partial core inductor
A_c is the cross sectional area of the core
l_c is the length of the core

The relative permeability of the partial core inductor μ_{rT} is found from the reluctance of the magnetic circuit including the core and the free space at both ends of the core. Liew [2001]

The reluctance of the core is

$$R_{core} = \frac{l_c}{\mu_0 \mu_{rc} A_c} \tag{4.17}$$

where μ_{rc} is the relative permeability of the core

The reluctance of the free space at the ends of the core is

$$R_{air} = 1.69356 \times 10^5 \left[\frac{1}{A_c}\right]^{0.345} \left[\frac{1}{l_c}\right]^{0.31} \tag{4.18}$$

The overall reluctance of the partial core inductor is

$$R_T = R_{core} + 2R_{air} \tag{4.19}$$

This is equivalent to a flux path through a homogeneous medium of relative permeability μ_{rT}

$$R_{core} = \frac{l_T}{\mu_0 \mu_{rT} A_c} \tag{4.20}$$

where l_T is the overall flux path length

$$\begin{aligned} l_T &= l_c + 2l_{air} \\ &\approx l_c \qquad (\text{since } l_c \gg 2l_{air}) \end{aligned} \tag{4.21}$$

Rearranging Equation 4.19 gives

$$\mu_{rT} = \frac{l_c}{\mu_0 R_T A_c} \tag{4.22}$$

And the magnetising reactance for 1-leg partial core inductor can be found from (4.16).

Equation 4.16 assumes that the partial core length is the same length as the winding. In practical inductor designs it has been found useful to extend the core beyond the winding length to enable insulation and mounting arrangements and may also provide an improvement in the quality factor as shown in Chapter 3. Therefore it is necessary to include the contribution of the added core length.

In Experiment 2 it was shown that magnetising reactance is approximately proportional to core length or weight. To accommodate the added core length, it is necessary to separate the winding length from the core length in the model. The following approach produces a useful result.

The core area is adjusted to maintain the correct core volume for any given length of core.

$$A_c' = \frac{A_c \times l_c}{l_w} \tag{4.23}$$

where A_c' is the modified core cross-sectional area
A_c is the actual core cross-sectional area
l_c is the actual core length
l_w is the winding length

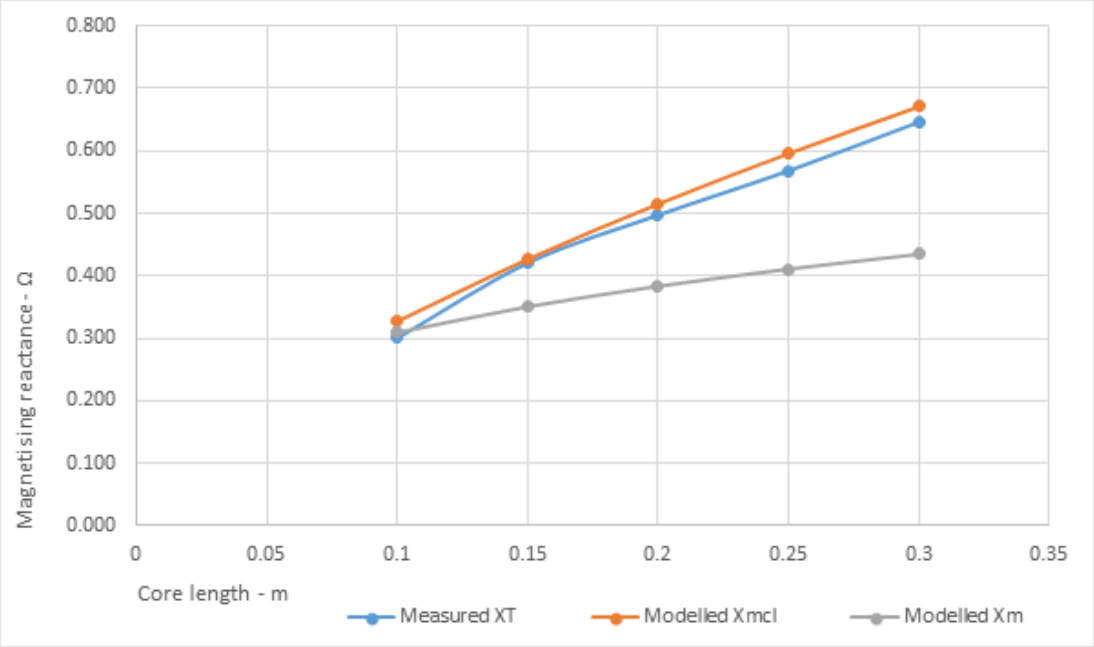

Figure 4.30 Revised calculation of P2 magnetising reactance vs core length

A'_c is substituted into the core and air reluctance expressions,

$$R'_{core} = \frac{l_c}{\mu_0 \mu_{rc} A'_c} \tag{4.24}$$

and

$$R'_{air} = 1.69356 \times 10^5 \frac{1}{A'_c}^{0.345} \frac{1}{l_c}^{0.31} \tag{4.25}$$

$$R'_T = R'_{core} + 2R'_{air} \tag{4.26}$$

$$\mu'_{rT} = \frac{l_c}{\mu_0 R'_T A'_c} \tag{4.27}$$

and

$$X_{mcl} = \frac{\omega N^2 \mu_0 \mu_r T' A'_c}{l_c} \tag{4.28}$$

where X_{mcl} is the magnetising reactance taking core length into consideration

Refer to Figure 4.30 for a comparison of the P2 measured total reactance to the calculated reactance of equation 4.16 and the revised X_{mcl} of equation 4.28. Figure 4.30 shows a better alignment of X_{mcl} with the measured result for the P2 winding. The model does tend to over-estimate the magnetising reactance by 9% for a 100mm length

core, however this is compensated for in the formulation of the 3-phase inductor reactance to follow.

4.7.3 Leakage reactance

Estimations of the leakage reactance in a partial core inductor are based on the formulations derived for full core transformers taking into consideration only the primary winding. This approach is considered valid because the calculation based on only the magnetic energy contained within the volume of the winding, which falls to zero elsewhere. Connelly [1965]

Energy contained within the winding is

$$W_p = \frac{\mu_0 l_p}{2 l_{core}} \cdot \frac{\pi \tau}{3} \cdot (Ni)^2 \tag{4.29}$$

where W_p is the energy contained in the winding
τ is the winding thickness factor
L_{core} is the core length inside the winding
N is the number of winding turns
I is the sinusoidal current in the winding

For a single winding, the winding thickness factor is calculated as follows

$$\tau = \frac{w_1 d_1}{3} \tag{4.30}$$

where w_1 is the mean diameter of the winding
d_1 is the thickness of the winding

The leakage inductance is related to the energy contained in the winding by

$$W_p = \frac{1}{2} L i^2 \tag{4.31}$$

and

$$L = \frac{\mu_0 N^2}{l_{core}} \cdot \frac{\pi w_1 d_1}{3} \tag{4.32}$$

and from

$$X_{leak} = \omega L \tag{4.33}$$

$$X_{leak} = \frac{\omega \mu_0 N^2}{l_{core}} \cdot \frac{\pi w_1 d_1}{3} \tag{4.34}$$

Table 4.11 P5 and P6 magnetising reactance factor

Frequency	$X_m factor$	$50Hz$	$250Hz$	$550Hz$	$800Hz$
P5 1-leg					
Model XT	1	0.42Ω	2.08Ω	4.58Ω	6.67Ω
Measured XT	-	0.37Ω	1.83Ω	4.01Ω	5.83Ω
Revised model XT	0.874	0.36Ω	1.82Ω	4.01Ω	5.83Ω
P5 3-leg					
Measured XT	-	0.63Ω	3.13Ω	6.88Ω	10.02Ω
Revised model XT	1.507	0.63Ω	3.13Ω	6.89Ω	10.02Ω
P6 1-leg					
Model XT	1	0.31Ω	1.54Ω	3.39Ω	4.93Ω
Measured XT	-	0.32Ω	1.27Ω	2.76Ω	3.99Ω
Revised model XT	0.805	0.25Ω	1.23Ω	2.75Ω	3.99Ω
P6 3-leg					
Measured XT	-	0.37Ω	1.73Ω	3.78Ω	5.46Ω
Revised model XT	1.125	0.35Ω	1.73Ω	3.80Ω	5.53Ω

The calculated leakage reactance applies to one single winding of a partial or full core inductor.

This estimation of leakage reactance does not take into account the effect of neighbouring windings in the case of a 3-phase inductor.

4.8 FORMULATION OF 3-PHASE PARTIAL CORE INDUCTOR REACTANCE

The 1-leg model is compared to measured results for 1-leg and 3-phase P5 and P6 inductors in Table 4.11 The edge winding configuration is chosen for both windings due to it having lowest resistances associated with the winding and core. In this example, resistance can be neglected as they have a negligible influence on the results.

It can be seen that with the inclusion of a magnetising reactance factor, the model and measurements align closely. The 1-leg partial core inductor appears to have a lower inductance than the model predicts, while the 3-phase inductance is higher.

It has been shown that the inductance of a 3-phase inductor is influenced by the separation distance of the cores. Therefore the $X_m factor$ demonstrates that varying the magnetising reactance produces useful results in the estimation of 3-phase partial core inductance.

Figure 4.28 shows small but observable changes in flux profiles towards the ends of the winding when comparing 1-leg and 3-phase inductors. It is therefore proposed that

Table 4.12 P5 and P6 reluctance exponent reduction term

P5 3-phase		
Core separation - d	Corrected exponent	Exponent reduction term - p
$0.016m$	0.285	0.060
$0.025m$	0.304	0.041
$0.033m$	0.315	0.030
P6 3-phase		
Core separation - d	Corrected exponent	Exponent reduction term - p
$0.028m$	0.320	0.026
$0.033m$	0.324	0.021
$0.038m$	0.329	0.017
$0.044m$	0.329	0.016

magnetising reactance is altered by proximity of windings due to changes in reluctance of the air path at the ends of the winding.

The formulation of the reluctance of the air path is based on the assumption that the flux density is only significant near both ends of the core. The reluctance of the air path at the core ends diminishes as the windings are brought closer together.

$$R_{air} = 1.69356 \times 10^5 \left[\frac{1}{A_c}\right]^{0.345-p} \left[\frac{1}{l_c}\right]^{0} .31 \tag{4.35}$$

By modifying the air reluctance term in the model for the core end (highlighted in red), an air reluctance is found to produce the correct magnetising reactance for each core separation distance. For each core separation, the exponent reduction term p is found for each P5 and P6 winding in a 3-leg, 3-phase arrangement as shown in Table 4.12.

It is reasoned that since the relationship between core separation and the air reluctance is geometric in nature, i.e. separation of core ends, a solution can be found to relate the separation variable with term p. Refer to Figure 4.31 for a proposed geometry that produces a useful relationship between core separation and the core end exponent reduction term p. The area of effect A_e is defined as the localised flux effect at the core end.

$$A_e = \pi \left(r + d\right)^2 \tag{4.36}$$

where A_e is the Area of Effect

The area of influence A_i is defined as a nominal area that contains the three core

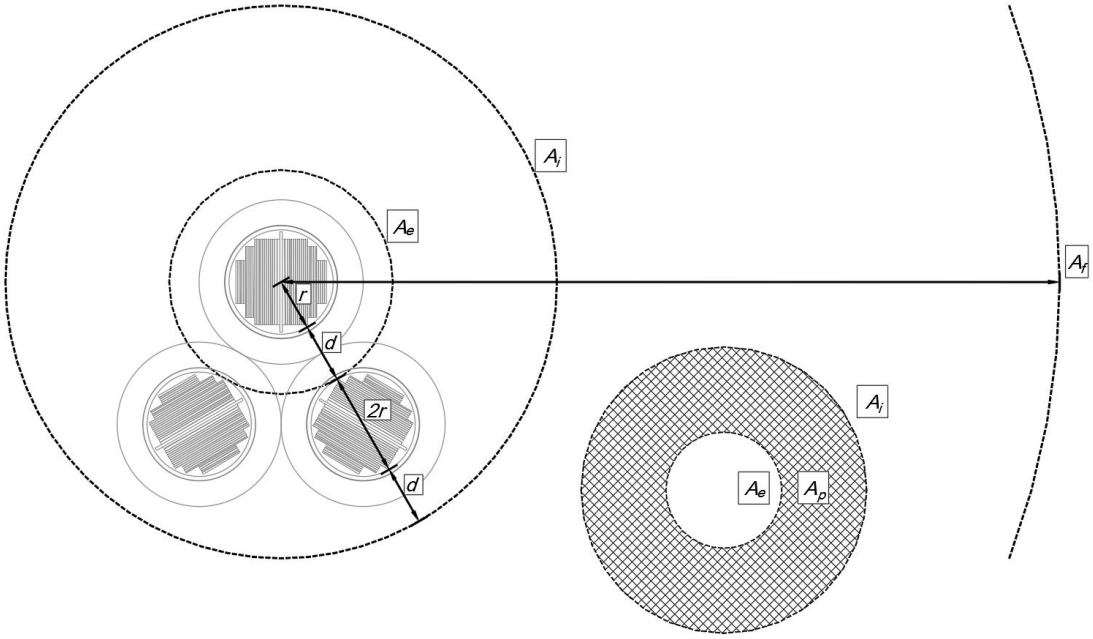

Figure 4.31 Defining the 3-phase partial core geometric relationship of core separation

end effects.

$$A_i = \pi (3r + 2d)^2 \tag{4.37}$$

where A_i is the Area of Influence

The region bounded between the Area of Influence and the Area of Effect defines the geometric relationship between the cross sectional area of the core and the proximity of the cores, and is named the air reluctance Area of Proportionality A_p.

$$A_p = A_i - A_e \tag{4.38}$$

where A_p is the area of proportionality, thus

$$A_p = \pi \left(8r^2 + 10rd + 3d^2\right) \tag{4.39}$$

The air reluctance exponent reduction term p has an exponential relationship to the area of proportionality in the general form,

$$p = a \left(\frac{A_p}{A_f}\right)^b \tag{4.40}$$

where A_f is the area of free space nominally taken as $1.0m^2$. Therefore p is dimensionless.

Table 4.13 P5 and P6 solutions for constants a and b

P5 3-phase (reference P6 $d = 0.033$)					
Core separation - d	-	0.016m	0.025m	0.033m	Average
a	-	0.000875	0.000761	0.00076	0.000799
b	-	-1.0344	-1.0799	-1.0802	-1.06483
P6 3-phase (reference P5 $d = 0.016$)					
Core separation - d	0.028	0.033m	0.038m	0.044m	Average
a	0.0011	0.000875	0.000618	0.00010	0.000898
b	-0.9876	-1.0344	-1.1194	-1.010	-1.03785
Average values					
a	0.000848				
b	-1.051				

The constant a, and exponential b, can be found by solving for winding P5 and P6 simultaneously. A solution for simultaneous equations in P5, for example, has the form,

$$a = p_5 \left(\frac{A_{p5}}{A_f} \right)^b \tag{4.41}$$

and,

$$b = \frac{log(p_5/p_6)}{log(A_p6/A_p5)} \tag{4.42}$$

Depending on the particular points of reference taken for d, a number of similar results were found as shown in Table 4.13 The average values of a and b are found for this sample range of d.

Refer to Figure 4.32 plotting the solutions obtained for the air reluctance exponential reduction factor p. The general solution is compared to the values of p obtained from the model as shown in Table 4.12. There are boundaries on core separation distance. The cores cannot be brought closer than the thickness of the windings and insulation, and p cannot be less than a value that produces the actual 1-leg magnetising reactance of the inductor.

In the case of practical 3-phase inductors, the core separation distance would typically be in the vicinity of the winding and insulation thickness to obtain the optimal inductance for a given winding.

To test the validity of this formulation, a new 3-leg inductor, P7 is constructed and tested and the results are presented in Table 4.14.

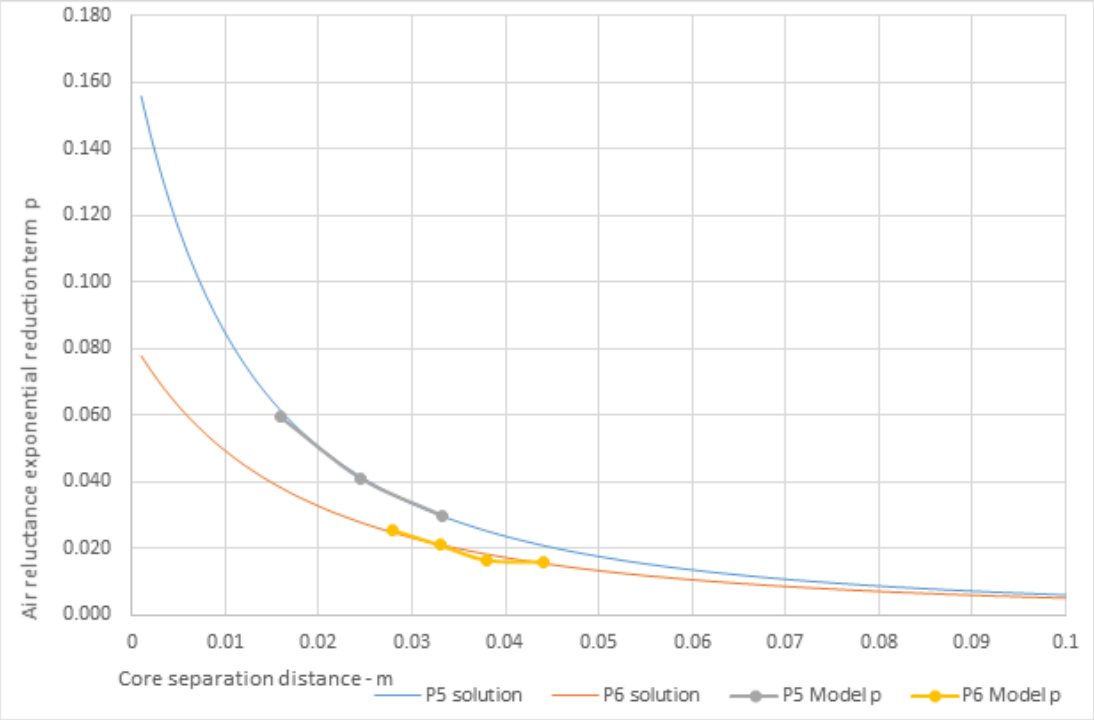

Figure 4.32 Air reluctance reduction term p vs core separation for the general solution and measured results of P5 and P6

Table 4.14 P5, P6 & P7 3-phase inductance vs separation

Device	P5	P6	P7
Physical			
Core separation - d	0.016	0.028m	0.034m
Core cross section	0.000804m^2	0.001569m^2	0.00208m^2
Core length	0.25m	0.215m	0.022m
Winding conductor width	2.5mm	2.5mm	3.55mm
Winding conductor height	5mm	12.5mm	15mm
Turns	90	71	51
Winding aspect ratio	50	16.9	13.5
Electrical			
Measured inductance	1.99mH	1.22mH	0.64mH
Modelled inductance	2.02mH	1.19mH	0.66mH

4.8.1 Conclusion

Modelling the derived air reluctance exponent reduction term p provides a close approximation for magnetising reactance for 3-phase inductors constructed with the following parameters:

- Flat stacked core steel lamination with star orientation
- Edge wound rectangular conductor in a single layer
- 3-phase inductor application
- Triangular winding arrangement with equal core separation distances

4.9 FORMULATION OF 3-PHASE PARTIAL CORE INDUCTOR RESISTANCE

4.9.1 Introduction

Over the years there have been many contributions toward developing a coherent theory of resistance in partial core inductors. To date the work has focussed on losses that occur due to *dc* resistance in the winding and losses in the core. Slemon [1966] Core losses comprise hysteresis loss and eddy current loss due to axial flux along the length of each core lamination. Previous work has also shown there is also a core loss component due to the emanation of flux orthogonal to the axial flux.Huo [2009]

In this work, search coils in both the axial and orthogonal planes have measured the proportionality of these fields along the length of a partial core winding thus supporting the notion of an orthogonal flux component.

This work has also shown there is an eddy current loss in the winding which becomes more significant as frequency increases. The characteristic of an eddy current loss can be modelled by the addition of resistance in parallel with the magnetising reactance as a loss coupled by induction. There may well be other effects causing loss such as proximity effect and skin effect, however these are likely to become more prominent at much higher frequencies and have not been considered here.

Therefore the conclusion reached at this point is that the standard model for hysteresis and eddy current loss is useful only as far as axial contributions to the loss are concerned. New formulations are sought to estimate the magnitude of orthogonal loss contributions in the winding and core.

The approach taken in this work is to demonstrate the magnitude of these orthogonal loss contributions by experimental means and derive an empirical basis for their calculation. It is recognised that this approach has its limitations and these are highlighted by examples of larger devices where the model departs from reality. Nevertheless, a useful estimation of winding eddy current resistance is proposed along

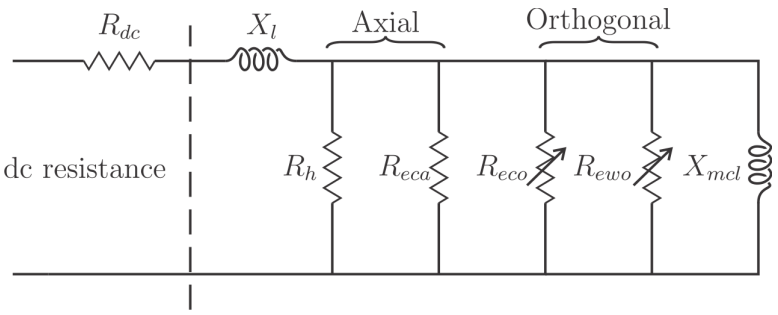

Figure 4.33 Modified Steinmetz equivalent circuit core 3-phase partial core inductors

with a proportionality constant dependent on the separation distance of the cores in a 3-phase device.

Orthogonal eddy current loss estimation in the core is obtained by the proportionality of volume of core material to winding material. These two new terms provide a good starting point for estimating total losses in the 3-phase partial core inductor.

4.9.2 AC resistance in a partial core device

Refer to Figure 4.33 for the transformer equivalent circuit with modifications proposed in this work. R_{dc} is the winding *dc* resistance and is in series with the total device. This resistance can be subtracted directly from the total measured resistance of any device and the balance of the resistance is therefore defined as *ac* resistance.

The *ac* resistance comprises the parallel combination of each resistive effect in the core and winding.

Hysteresis power loss: Nasar and Boldera [1989]

$$P_h = 1.38 \times 10^{-9} \nu_{core}^{-1.5} \gamma_{core} f B_{core}^{1.84} \tag{4.43}$$

where ν_{core} is the core volume
γ_{core} is the core material density

The hysteresis resistance is therefore,

$$R_h = \frac{e_1^2}{P_{hpc}} \tag{4.44}$$

where e_1 is the emf across the magnetising reactance

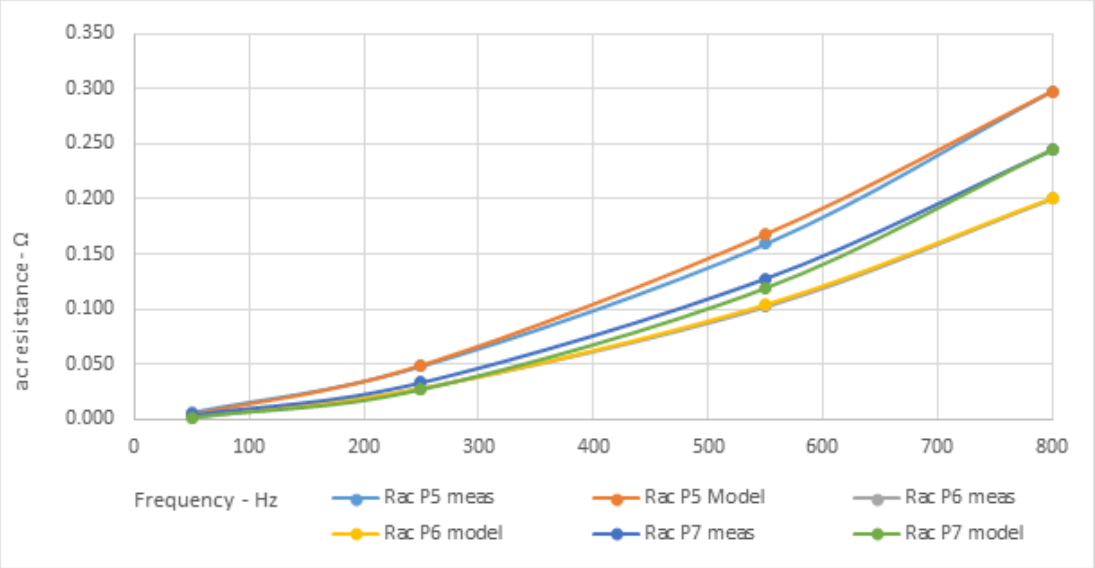

Figure 4.34 P5, P6 and P7 modelled and measured total resistance vs frequency

Core eddy current loss axial: Slemon [1966]

$$R_{eca} = \frac{e_1^2}{P_{ec}} = \frac{N^2 A_c 12 \rho_c}{l_{fc} c_{lam}^2} \tag{4.45}$$

Note that for the low values of inductance used in this analysis, the winding *dc* resistance and leakage reactance are small compared to the magnetising reactance and therefore the emf e_1 is practically the same as the applied voltage in all cases.

By calculating the effects of R_h and R_{eca} in each of the experimental inductors, and combining with an additional resistance R_{eo}, the total orthogonal eddy current loss resistance, the total *ac* resistance is obtained. Refer to Table 4.15 for the calculated values of R_{eo} obtained in experimental windings P5, P6 and P7 at $250Hz$.

Values shown for R_{eo} were found by adjusting the R_{eo} value until the total equivalent series *ac* resistance matches the measured *ac* resistance at each frequency. Refer to Figure 4.34 to obtain a view of the match between measured and estimated values. It can be seen that the size of the core and winding have a significant bearing on the *ac* resistance characteristic of the devices with P6 having the lowest *ac* resistance. Also note the effect of increasing the core separation distance in Table 4.15. The orthogonal resistance increases with increasing core separation. Factor q is introduced further on.

Having quantified the total orthogonal eddy current loss resistance, it is necessary to proportion the resistance between the core and the winding. To start with the winding eddy current orthogonal resistance is defined by the following expression based on the

Table 4.15 P5, P6 & P7 resistance vs separation at 250Hz

Device	P5	P6	P7
1-leg (infinite separation)			
R_h	278Ω	258Ω	229Ω
R_{eca}	1141Ω	1661Ω	1113Ω
R_{eo}	831Ω	304Ω	78Ω
q	0.426	0.381	0.395
3-phase (16mm separation)			
R_h	278Ω		
R_{eca}	1141Ω		
R_{eo}	452Ω		
q	0.232		
3-phase (25mm separation)			
R_h	278Ω		
R_{eca}	1141Ω		
R_{eo}	529Ω		
q	0.271		
3-phase (29mm separation)			
R_h		258Ω	
R_{eca}		1661Ω	
R_{eo}		218Ω	
q		0.274	
3-phase (33mm separation)			
R_h	278Ω	258Ω	
R_{eca}	1141Ω	1661Ω	
R_{eo}	532Ω	235Ω	
q	0.273	0.295	
3-phase (35mm separation)			
R_h			229Ω
R_{eca}			1113Ω
R_{eo}			44Ω
q			0.224
3-phase (38mm separation)			
R_h		258Ω	
R_{eca}		1661Ω	
R_{eo}		261Ω	
q		0.238	
3-phase (42mm separation)			
R_h		258Ω	
R_{eca}		1661Ω	
R_{eo}		272Ω	
q		0.240	

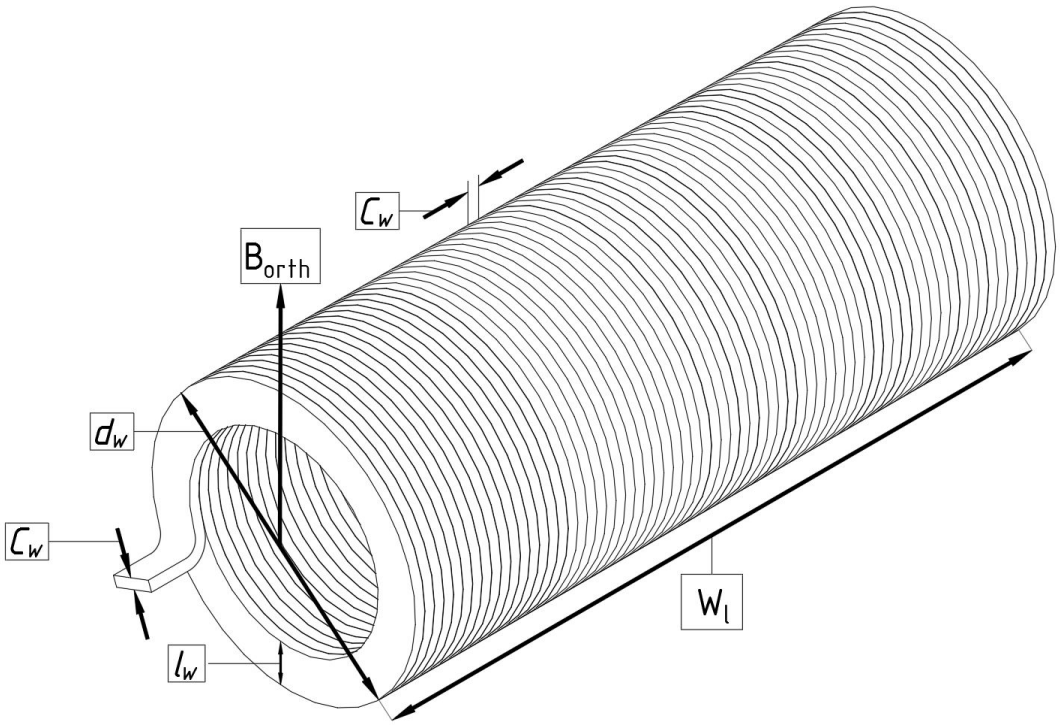

Figure 4.35 Defining the physical parameters for winding eddy current resistance

same formula used for core axial eddy current loss resistance. With the plane of the flux rotated perpendicular to the axial flux, each turn is treated in the same way as a lamination in the core. In this way the same expression can be used to obtain the winding eddy current resistance.

$$R_{ewo} = \frac{e_1^2}{P_{ewo}} \qquad (4.46)$$
$$= q \times \frac{N^2 A_w 12 \rho_w}{l_w c_w^2}$$

where	A_w	is the surface area of the winding ($\pi \times d_w \times W_l$)
	ρ_w	is the resistivity of the winding material
	l_w	is the length of the winding (thickness)
	C_w	is the width of the winding turn
	q	is the winding eddy current resistance factor

Refer to Figure 4.35 for a diagram of the winding dimensions defined in Equation 4.46. The parameters for winding eddy current resistance are analogous to core axial eddy current resistance as shown in Figure 4.36. In addition, the core orthogonal loss resistance is defined as being in proportion to the winding orthogonal resistance based on the assumption that a similar orthogonal field cuts through both the core and winding

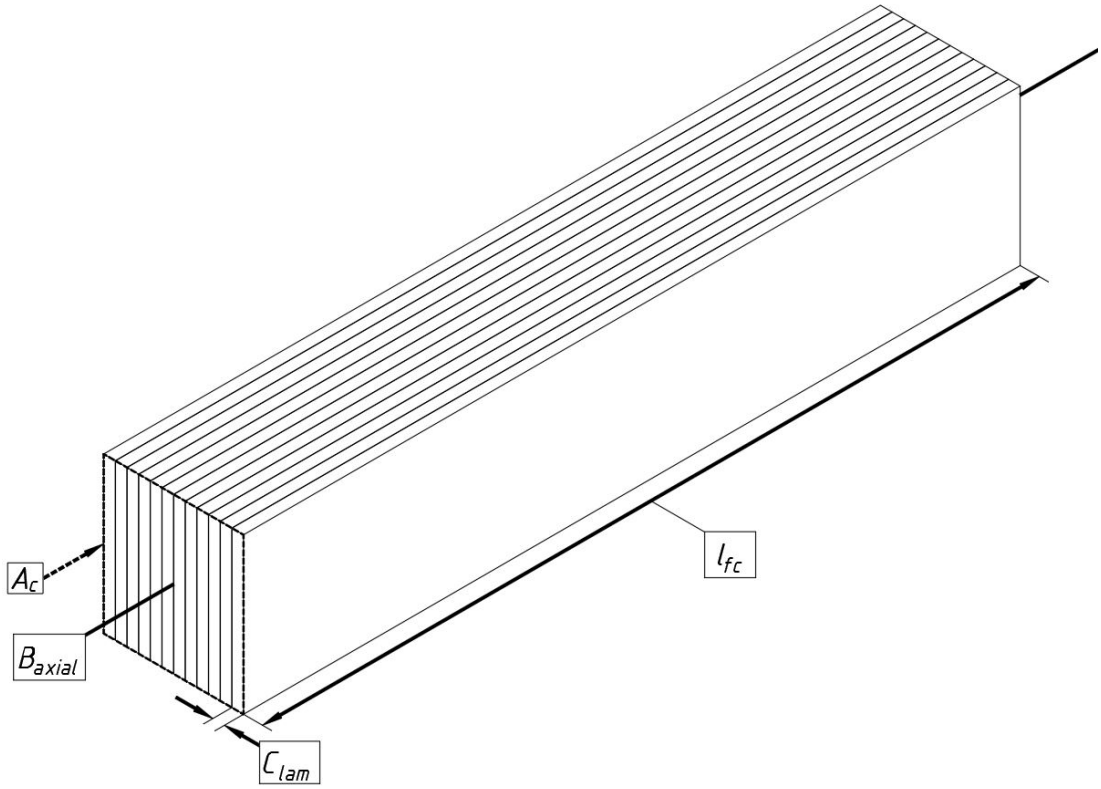

Figure 4.36 Physical parameters for core axial eddy current resistance

volumes. In other words, the orthogonal eddy current losses apparent in the winding, are due to the orthogonal flux set up by the core. Therefore, approximately the same orthogonal flux occurs in the core material. As a first order approximation, the ratio of power loss in the winding and core due to induction, as measured by the calorific method in Chapter 3, enables a comparative estimation of power loss in the core.

The core orthogonal resistive effect is estimated by the volumetric ratio of winding material to core material.

$$R_{eco} = C \times V_{wc} \times R_{ewo} \tag{4.47}$$

where R_{eco} is the core orthogonal eddy current loss resistance
V_{wc} is the ratio of winding volume to core volume
C is the core orthogonal resistance constant determined by (4.49)

$$V_{wc} = \frac{V_{winding}}{V_{core}} \tag{4.48}$$

where $V_{winding}$ is the volume of the winding
V_{core} is the volume of the core, and,

$$C = \frac{R_{eco}}{V_{wc} \times R_{ewo}} \tag{4.49}$$

In the case of the 3-phase P6 device, it was shown by the calorific method that the relative resistances where,

$$C = \frac{790}{V_{wc} \times 238}$$

and,

$$V_{wc} = \frac{0.000562m^3}{0.000342m^3} = 1.64$$

therefore,

$$C = \frac{790}{1.64 \times 238} = 2.02$$

The calculated winding orthogonal resistance is calculated by,

$$R_{ewo} = q \times \frac{71^2 \times 0.000562 \times 12 \times 2.65 \times 10^{-8}}{0.0125 \times 0.0025^2} = q \times 1122\Omega$$

and,

$$R_{eco} = q \times 2.02 \times 1.64 \times 1122 = q \times 3717\Omega$$

where q is the winding eddy current resistance factor

R_{ewo} and R_{eco} are corrected by factor q to produce values that when added into the modified Steinmetz equivalent circuit, the total series equivalent resistance matches that measured at each frequency. The value of q is therefore determined for each core separation distance for P5, P6 and P7 as shown in Table 4.15.

A scatter graph of the points produced by each factor q against the distance of separation is shown in Figure 4.37. The linear correlation coefficient for this data is calculated to be $R^2_{value} = +0.98$.

The solution to the line of best fit relates the core separation distance to the winding orthogonal eddy current resistance by the simple linear relation,

$$q = \frac{4.4 \times d}{d_r} + 0.155 \tag{4.50}$$

where d is the core separation distance in m
d_r is a relative distance $\gg d$ chosen to be $1m$.

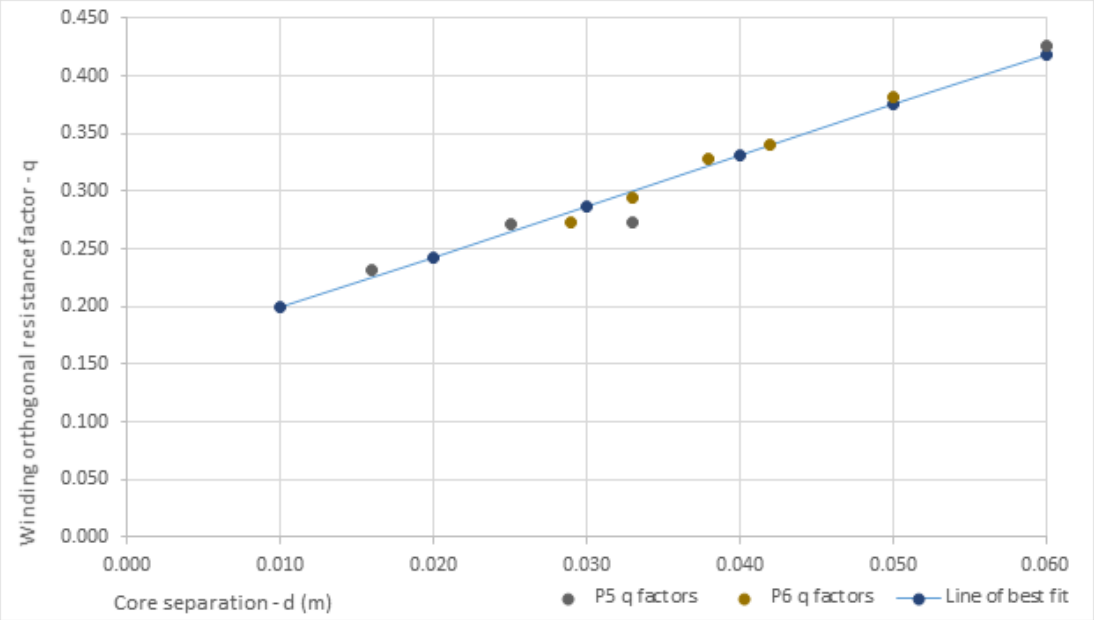

Figure 4.37 Scatter graph of q vs core separation shown with line of best fit

Therefore q is dimensionless.

Refer to Table 4.16 for a comparison of the results obtained for q and V_{wc} for each test inductor and how they influence the total series ac resistance of the inductor.

4.9.3 Discussion

P5 and P6 calculated series equivalent resistance compares well to measured values due to the factor q being derived based on measurements of these inductors. P7 however shows that the result extrapolated for q is too high and therefore the modified resistance R_{series} is too low. The model is not complete therefore and may have limited use around a certain range of sizes of core and winding.

4.9.4 Conclusion

The estimation of winding eddy current resistance shows a good correspondence to the general trend of measured results. The approximation of core orthogonal eddy current loss based on a volumetric assessment compared to winding orthogonal eddy current loss is not justified other than by one set of experimental results for P6 3-phase, and therefore, for this researcher, the subject requires further research, collaborations for learning, and theory development.

Table 4.16 P5, P6 & P7 3-phase resistances' comparison vs core separation at 250Hz

Core separation d	0. 16m	0.025m	0.033m	
P5 3-phase				
q	0.225	0.265	0.300	
V_{wc}	0.895	0.895	0.895	
R_{ewo}	681Ω	801Ω	908Ω	
R_{eco}	1240Ω	1458Ω	1651Ω	
R_{series} (Standard model)	0.044Ω	0.034Ω	0.029Ω	
R_{series} (Modified model)	0.067Ω	0.048Ω	0.040Ω	
R_{series} (Measured)	0.067Ω	0.049Ω	0.041Ω	
Core separation d	0.029m	0.033m	0.038m	0.042m
P6 3-phase				
q	0.283	0.300	0.322	0.340
V_{wc}	1.652	1.652	1.652	1.652
R_{ewo}	293Ω	311Ω	334Ω	352Ω
R_{eco}	983Ω	1044Ω	1120Ω	1181Ω
R_{series} (Standard model)	0.015Ω	0.0145Ω	0.0140Ω	0.0136Ω
R_{series} (Modified model)	0.030Ω	0.028Ω	0.026Ω	0.025Ω
R_{series} (Measured)	0.031Ω	0.028Ω	0.026Ω	0.025Ω
Core separation d	0.035m			
P7 3-phase				
q	0.309			
V_{wc}	1.696			
R_{ewo}	78Ω			
R_{eco}	270Ω			
R_{series} (Standard model)	0.005Ω			
R_{series} (Modified model)	0.021Ω			
R_{series} (Measured)	0.033Ω			

4.10 CHAPTER 4 CONCLUSION

In this chapter the effect of localised heating at the ends of a partial core inductor were determined to be induction losses caused mainly by eddy current heating. The heating effect was further studied by a calorimetric method to determine the proportion of heating that occurs in the winding and core along the length of the winding.

While these experiments were not conducted under precise conditions, the results provide a good indication of the relative proportion of heating in the windings and core. Eddy current loss in the winding becomes more significant with increasing frequency, but at $50Hz$ was not particularly significant in the units tested. At harmonic frequencies however, the winding loss effects were significant and would need to be considered in the project inductor designs. The inductors tested in this chapter were all of edge winding formation type due to this being the more efficient winding. Wider width conductors become less efficient and dissipate greater eddy current losses which were shown in Chapter 3 to be more significant at $50Hz$.

An estimation of winding eddy current resistance was formulated based on the same approach used to formulate core axial eddy current loss resistance. In addition, orthogonal core losses were estimated by a simple volumetric approach based on the winding orthogonal eddy current loss resistance. The approach is simple and improves loss estimations, however is not proven beyond the prototypes it was modelled on.

3-phase magnetising reactance was modelled based on core separation between the limbs of the inductor. An exponent reduction term was proposed to modify the air reluctance calculation. The results of the three inductors test suggest this approach may be useful in determining the inductance of 3-phase inductors where core separation must be adjusted to accommodate the size of the winding.

Core length was decoupled from winding length in the calculation of magnetising reactance to enable the effect of cores that are longer than the winding to be calculated.

The outcome of this chapter is two new resistance terms and a modified magnetising reactance to add to the transformer equivalent circuit that enables 3-phase partial core inductors to be designed with good accuracy and therefore, provide a path to design optimisation.

Chapter 5

OPTIMISATION OF 3-LEG PARTIAL CORE INDUCTORS

5.1 OVERVIEW

This chapter begins by developing an automated software routine to calculate the correct size of core for a given number of turns of a given size conductor, operational current and frequency. The routine calculates the core size required to achieve a target peak flux density for each number of turns in a specified range of turns.

This is followed by an analysis of the optimal conductor size and number of winding layers to achieve a specified inductance as determined for the project inductor in Chapter 6. The chapter concludes with a general prediction on the effect of conductor width and winding layers on the efficiency of 3-phase partial core inductors.

5.2 INTRODUCTION

Throughout this work the goal has been to quantify the performance of partial core inductors in power engineering applications. In this chapter, a software routine is developed to explore the optimal design of an inductor for such an application based on the formulations developed in Chapter 4. The formulations enable calculation of theoretical equivalent circuit elements in the device model, and the optimisation routine automates a rapid trial of incremental physical change until a target solution is found. As a basis for comparison, a commercially built gapped core inductor is tested, measured and weighed as described in Chapter 6.

The project inductor has a specific purpose with a required inductance and current carrying capability at mains frequency and also for the harmonic frequencies it may encounter at maximum rated conditions in service. Based on modelling of the reactive and resistive characteristic of the project inductor, it is possible to determine the weight, size and power loss in trial designs for a given inductance. Therefore various parameters of the winding and core may be altered to observe any trends that occur and where the

point of optimal electrical performance coincides with optimal physical weight, size and cost.

From these comparisons, a target design may be achieved for a given device. To make meaningful comparisons, it is necessary for the model to consider each physical parameter of the core and winding, as altering any dimensional aspect alters the electrical performance of the device. Due to the complexity of these interactions, the only useful way to perform the required number of calculations is to have a complete model linking each electrical element to the relevant physical parameters of the winding and core.

The work in this chapter sets out a design approach to quickly establish the optimal performance of an inductor over a range of winding turns, with peak flux density held constant for the given current and frequency by altering the core cross sectional area. This enables comparison of different windings thereby enabling the optimal inductor design to be found.

For the project inductor, the inductance value is defined along with the current it must carry at each frequency. For a given current and frequency, the voltage developed across the magnetising reactance of the inductor enables the flux density of a given core cross sectional area to be calculated. Altering the core cross sectional area, will alter the inductance and therefore the voltage dropped across the inductor which in turn alters the peak flux density in the core.

The design routine uses a Microsoft excel spreadsheet with a macro routine to automatically step through the trial data until a solution is found for each number of turns in the range.

5.3 COMPUTER DESIGN ROUTINE

The following parameters are set:

1. Target core peak flux density B
2. Winding conductor current density J
3. Winding conductor cross sectional area to achieve J at design current
4. Winding conductor width W_w and height W_h to achieve the required cross sectional area
5. Starting core cross sectional area A_c and increment size
6. Starting number of turns N in the winding, increment value (t), and maximum N
7. Number of layers of winding
8. Insulation thicknesses and winding separation distance
9. Operational temperature

Therefore a winding of N turns of conductor width W_w defines the core length and therefore the reactance and resistance of the partial core inductor can be calculated.

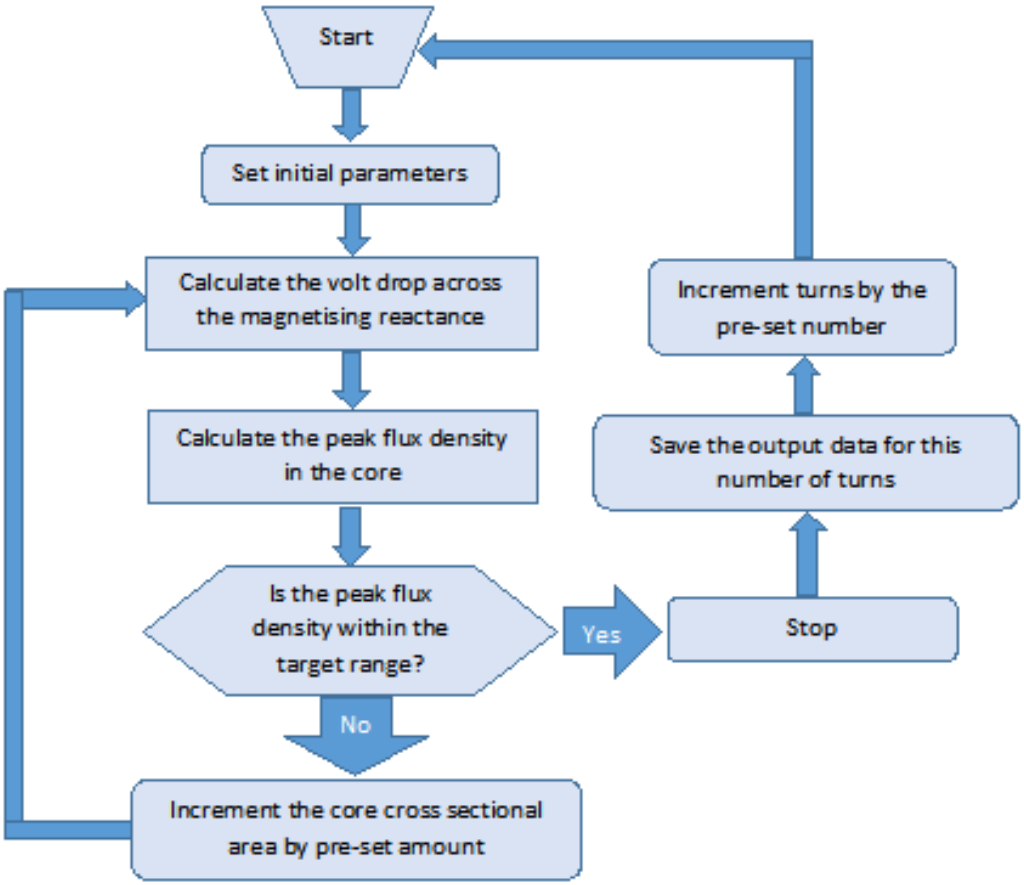

Figure 5.1 Optimisation design routine

Using the modified Steinmetz model of Figure 4.33 developed in Chapter 4, the application of design current and frequency enables calculation of the voltage developed across the magnetising reactance and therefore peak flux density (PFD) in the core.

5.3.1 Design routine process

Figure 5.1 outlines the optimisation design routine. The routine first calculates the voltage drop across the magnetising reactance at starting conditions. This voltage value is then input to the model and a core PFD is calculated based on the stating conditions. Is it greater than the target PFD?

If yes, then the core cross sectional area is too small. Therefore increment the core cross sectional area and recalculate the voltage drop based on the increased magnetising reactance. Input the revised voltage and recalculate the core PFD and compare with the target PFD.

This process of incremental core cross sectional area increase repeats until the calculated core PFD converges on the target core PFD. At this point the winding of

N turns has the maximum possible inductance for a core of given size to achieve the target PFD at rated current and frequency.

The power loss in the core and winding can be calculated from the modelled resistances and therefore the performance of the design may be calculated for N turns. The weights of the core and winding may also be calculated along with any other attribute of the device for N turns.

With these results recorded as a snap shot, the winding turns count is incremented by a set amount t, and the process is repeated for this new inductor of $N + t$ turns. The increased number of turns increases the length of the core which also has the effect of increasing the inductance of the device. A higher voltage drop across the core magnetising reactance therefore requires an increased core cross sectional area which further increases the device inductance and so forth. Again the core cross sectional area is incremented until the target PFD is achieved and these results captured as before.

This process is repeated over a set range of winding turns as defined at the start of the design routine. A picture therefore emerges of the performance of the inductor for a given winding conductor dimension. The whole process may therefore be repeated with different winding conductor dimensions to compare the electrical performance and weight/cost attributes of the devices in the design range. It can be therefore be shown that the optimal performance of a partial core inductor of given inductance and current rating is set primarily by the winding conductor cross sectional area, width and material.

Table 5.1 provides the initial model conditions for the P6 winding.

Refer to Table 5.2 where the range is set to 5 and results are returned for each increment of winding turns 71 through 75.

The last two lines of Table 5.2 demonstrate the motive for optimisation. By increasing the number of turns, the cost per inductance reduces, however, the winding surface power loss density increases. Temperature rise is approximately proportional to surface power loss density and minimal temperature rise is desirable.

5.3.2 Effect of winding conductor width and material

Power inductors carrying tens of amperes usually employ strip conductor of a rectangular cross section in the winding. Rectangular conductor may be wound flat with the widest face in contact with the winding former, or on edge in which case the narrowest face is to the former.

Qualitative experiments at the beginning of this work have shown that a significant improvement in power loss reduction can be achieved by edge winding formation. The following analysis utilises the design routine to examine the effect of adjusting the width of the conductor while keeping the total cross sectional area of the conductor constant.

Table 5.1 P6 3-phase winding initial conditions

Parameter	Initial conditions
Target peak flux density	$0.8T$
Set winding current density	$1.50A/mm^2$
Conductor width	$2.5mm$
Conductor height	$12.5mm$
Winding insulation thickness	$0.06mm$
Winding width factor	1.15
Initial winding turns	71
Winding resistivity	$2.65 \times 10^{-8}\Omega m$
Winding layers number	1
Core additional length	$6mm$
Initial core CSA	$600mm^2$
Core lamination thickness	$0.228mm$
Frequency	$50Hz$
Winding density	$3000kg/m^3$
Interwinding gap	$1.0mm$
Winding former thickness	$1.5mm$
Winding material cost	$15\$/kg$
Core material cost	$10\$/kg$
Operating temperature	$30°C$

Table 5.2 P6 optimisation routine over 5 iterations

Iteration	1	2	3	4	5
Parameter					
Turns	71	72	73	74	75
Inductance	$1.15mH$	$1.19mH$	$1.23mH$	$1.28mH$	$1.32mH$
Total impedance	0.360Ω	0.374Ω	0.387Ω	$0.0.401\Omega$	0.416Ω
Current	$46.9A$	$46.9A$	$46.9A$	$46.9A$	$46.9A$
Voltage developed	$16.9V$	$17.5V$	$18.2V$	$18.8V$	$19.5V$
Peak flux density	$0.800T$	$0.800T$	$0.800T$	$0.800T$	0.796
Winding dc resistance	0.0127Ω	0.0130Ω	0.0133Ω	0.0136Ω	0.0139Ω
Winding ac resistance	0.0004Ω	0.0004Ω	0.0004Ω	0.0004Ω	0.0005Ω
Core loss resistance	0.0019Ω	0.0020Ω	0.0021Ω	0.0022Ω	0.0022Ω
Total loss resistance	0.0151Ω	0.0155Ω	0.0158Ω	0.0162Ω	0.0166Ω
Power loss per leg	$33.2W$	$34.0W$	$34.8W$	$35.6W$	$36.5W$
Quality factor	23.9	24.2	24.4	24.7	25.0
Core CSA	$1340mm^2$	$1370mm^2$	$1400mm^2$	$1430mm^2$	$1470mm^2$
Core length	$214.7mm$	$217.2mm$	$219.7mm$	$222.2mm$	$224.5mm$
Core weight	$2.19kg$	$2.26kg$	$2.34kg$	$2.41kg$	$2.51kg$
Winding weight	$1.41kg$	$1.44kg$	$1.47kg$	$1.50kg$	$1.54kg$
Total weight 3-phase	$10.78kg$	$11.10kg$	$11.43kg$	$11.75kg$	$12.15kg$
Total cost	\$128.9	\$132.6	\$136.3	140.1	\$144.6
Cost per mH	\$112.1	\$111.4	\$110.8	\$109.4	\$109.5
Surface power density	$0.063W/cm^2$	$0.064W/cm^2$	$0.064W/cm^2$	$0.064W/cm^2$	$0.065W/cm^2$

Table 5.3 Project inductor design constants

Winding material	Aluminium	Copper
Parameter		
Target inductance	$1.23mH$	$1.23mH$
Design current at $50Hz$	$49.5A$	$49.5A$
Design current at $250Hz$	$18.4A$	$18.4A$
Design current at $350Hz$	$6.6A$	$6.6A$
Design current at $550Hz$	$2.4A$	$2.4A$
Peak flux density	$0.800T$	$0.800T$
Conductor current density	$1.5A/mm^2$	$1.5A/mm^2$
Conductor resistivity	$2.65 \times 10^{-8}\Omega m$	$1.85 \times 10^{-8}\Omega m$
Core resistivity	$1.60 \times 10^{-7}\Omega m$	$1.60 \times 10^{-7}\Omega m$
Conductor density	$3000kg/m^3$	$9000kg/m^3$
Core density	$7600kg/m^3$	$7600kg/m^3$
Conductor cost per kg	\$15	\$15
Core cost per kg	\$10	\$10

The wider the conductor, the less height the conductor will have, and therefore the closer the cores in a 3-phase configuration. However, a wider conductor requires more core length and each of these parameters have a bearing on the final point at which the required inductance is achieved and how large the core must be for the target PFD.

The inductance chosen for this examination is based on the design specification presented in Chapter 6 for a 33kVAr detuning reactor for a 400V system. The designs are generated based on the constants shown in Table 5.3.

Note that the price of aluminium price per kg was chosen to be the same as for copper. The metals trade index typically shows aluminium is one third the price of copper, however in the prototypes built, the price paid for aluminium conductor was nearly twice that for copper per kg. Due to the wide range of possible pricing without knowing the true value of drawn aluminium conductor, the price was kept the same as copper to enable a cost comparison based on relative weight alone. If it turns out that aluminium conductor is in fact cheaper to purchase, then the benefit of aluminium windings is even more favourable.

Comparison with commercially built reactors shows that many manufacturers offer both copper and aluminium winding materials. Devices with aluminium windings weigh less, and cost less. For this analysis, the partial core windings are modelled in both aluminium and copper and compared with a commercial reactor manufactured by a reputable Indian company referred to in this thesis as the “Vinidhan” reactor or “V” in the figures that follow.

The following simulations were run for aluminium and copper windings of 1 and 2 layers:

1. Surface power density in W/cm^2 at maximum rated conditions
2. Total material cost as a % of the estimated Vinidhan reactor materials cost
3. Power loss at mains frequency ($50Hz$) in W
4. Total power loss including harmonic frequencies $250Hz$, $350Hz$ and $550Hz$ in W
5. Total weight of the core and windings in kg
6. Individual weights of the core and windings in kg

5.4 COMPARISON WITH COMMERCIALLY BUILT REACTOR

5.4.1 Aluminium winding comparison

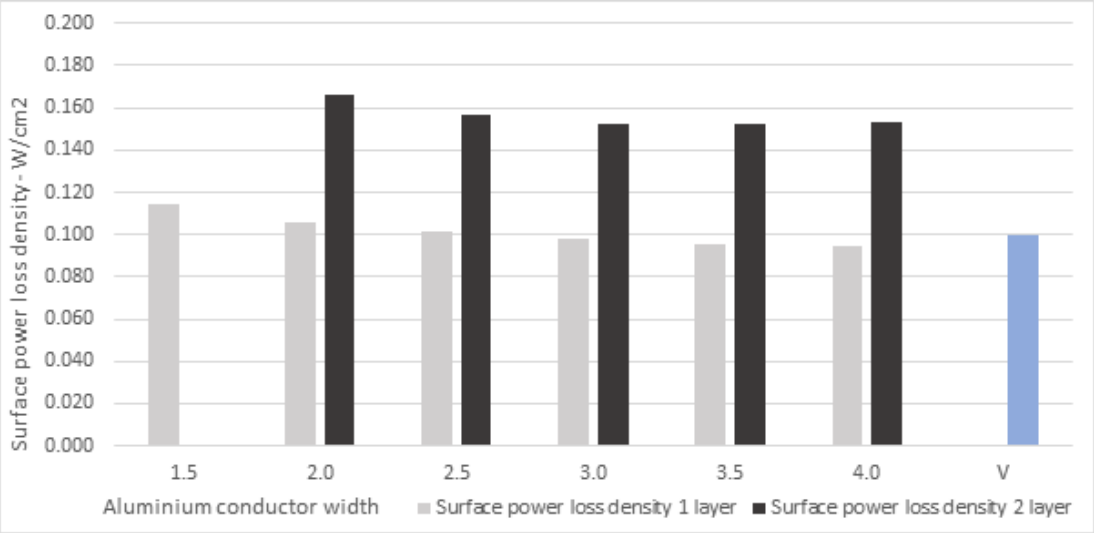

Figure 5.2 Aluminium winding surface power density

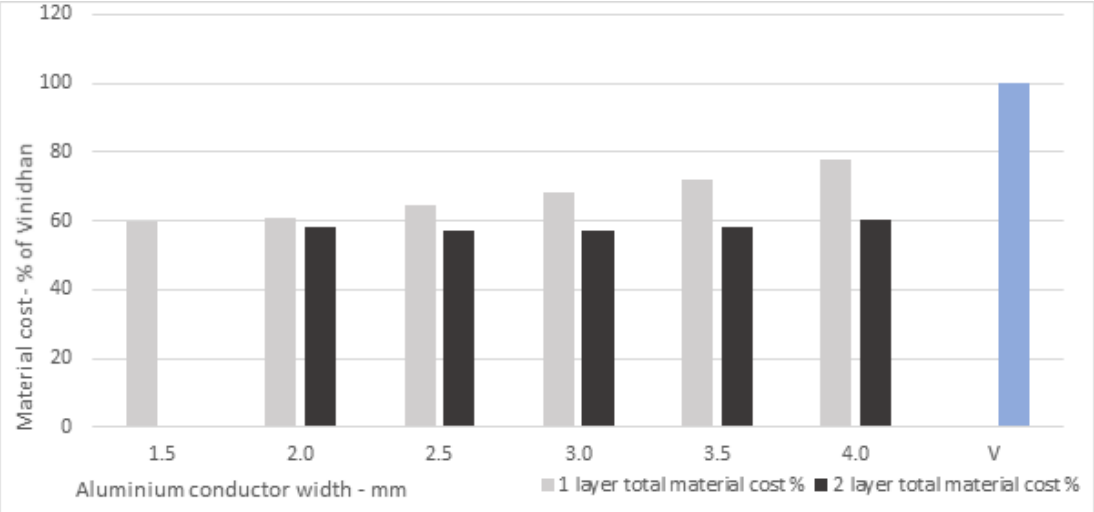

Figure 5.3 Aluminium winding material cost % of Vinidhan

Observations

Single layer aluminium windings produce around 30% less surface power loss density than 2 layer windings and around the same compared to the Vinidhan unit "V".

A narrower winding costs less in 1 layer units. For the 2 layer unit the optimal cost is around the 2.5 to 3.0mm width for aluminium conductor, however 2 layer units are significantly less efficient.

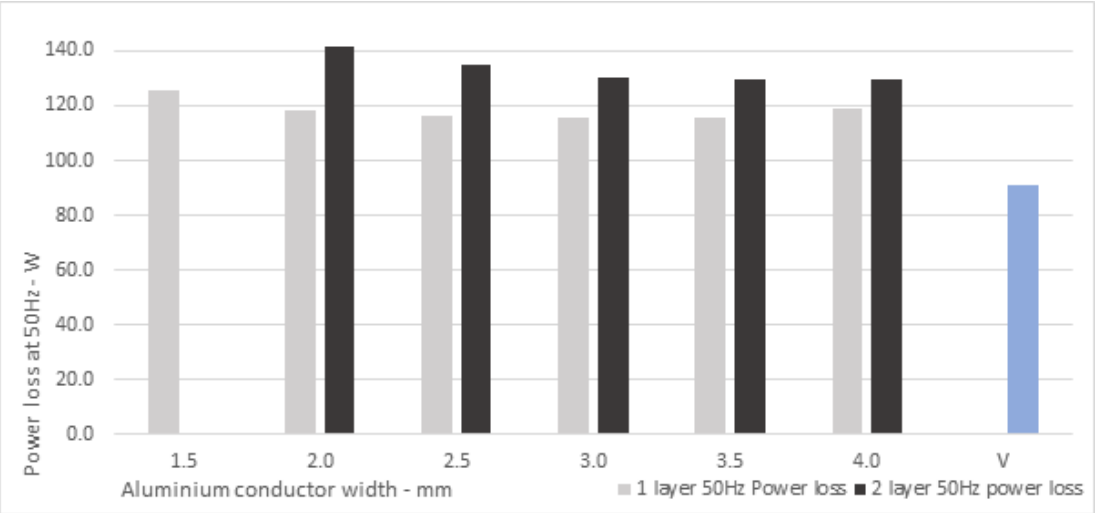

Figure 5.4 Aluminium winding power loss at $50Hz$

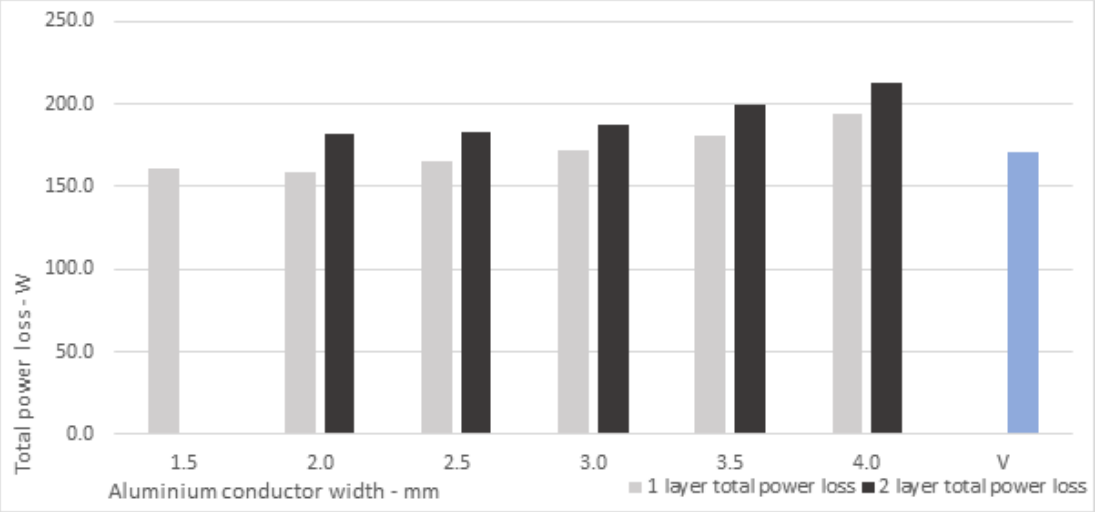

Figure 5.5 Aluminium winding total power loss including harmonics

Observations

Optimal power loss at 50Hz is achieved with a 1 layer aluminium winding width around 2.5 to 3.0mm and is around 30% more lossy than the Vinidhan unit. Optimal 2 layer aluminium winding width is around 3.5mm and is significantly more lossy at 50Hz.

A 1 layer aluminium winding also has a lower total power loss compared to the 2 layer unit in the presence of harmonic currents. 1 layer total winding loss is comparable to the Vinidhan unit at around 2.0 to 2.5mm conductor width.

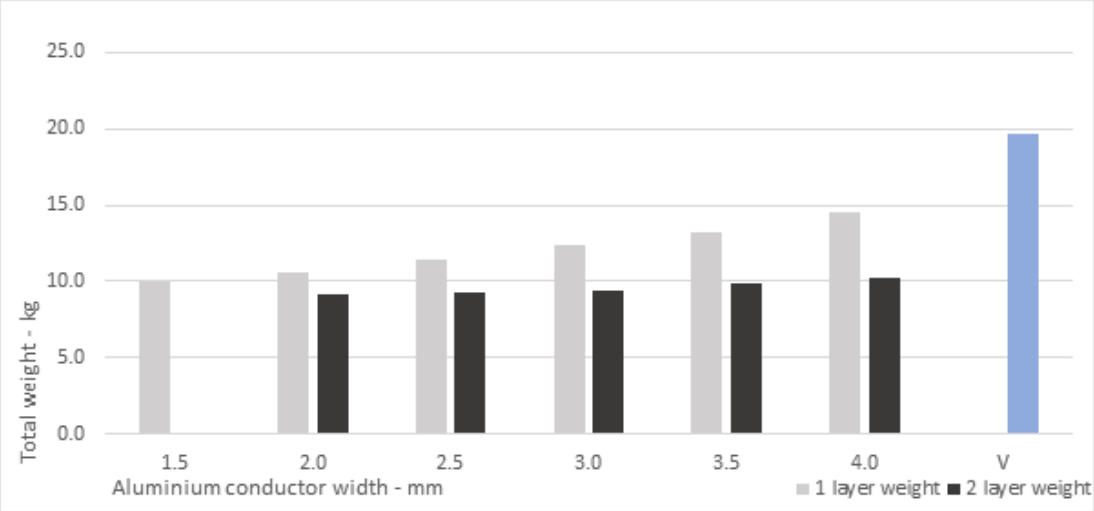

Figure 5.6 Aluminium winding total material weight of a 3-phase unit

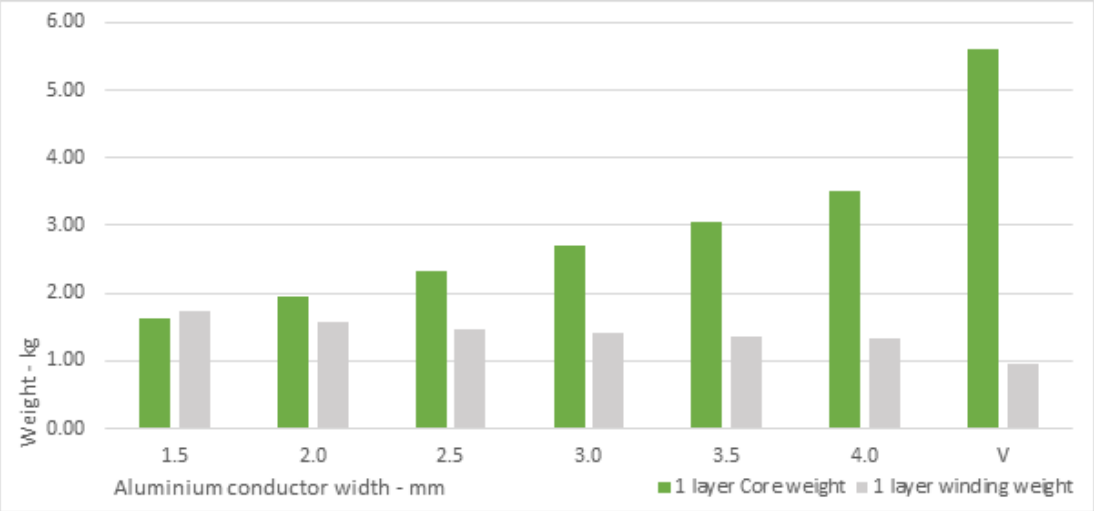

Figure 5.7 Aluminium winding and core weights

Observations

The 2 layer winding is generally lighter than the 1 layer winding due to a reduction of core steel. Both 1 and 2 layer units become lighter with a reduced conductor width and 2 layer windings are up to 50% lighter than the Vinidhan unit with an aluminium winding.

It is interesting to note the general progression of reducing winding weight necessitating greater core weight to achieve the same inductance and power rating.

5.4.2 Copper winding comparison

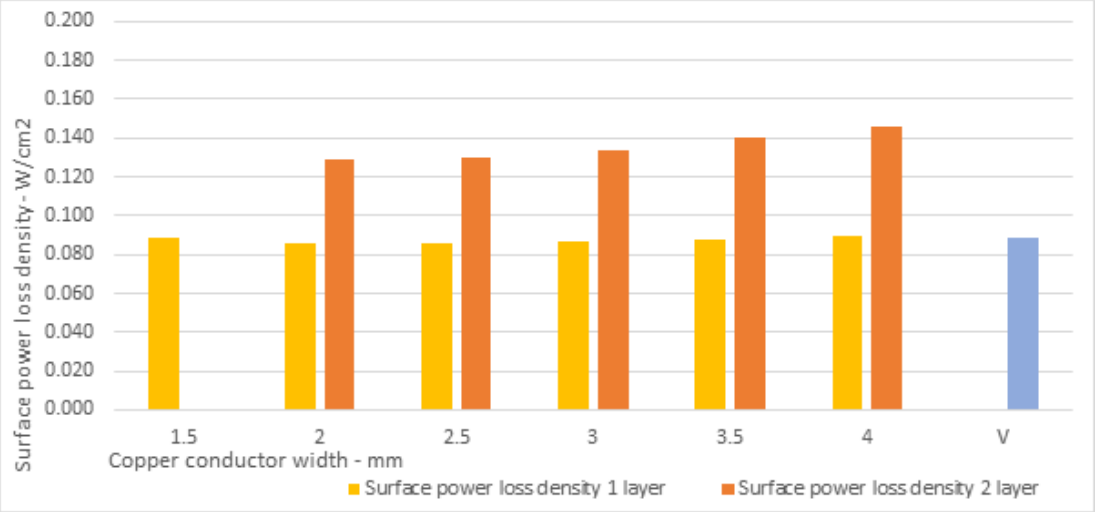

Figure 5.8 Copper winding surface power loss density

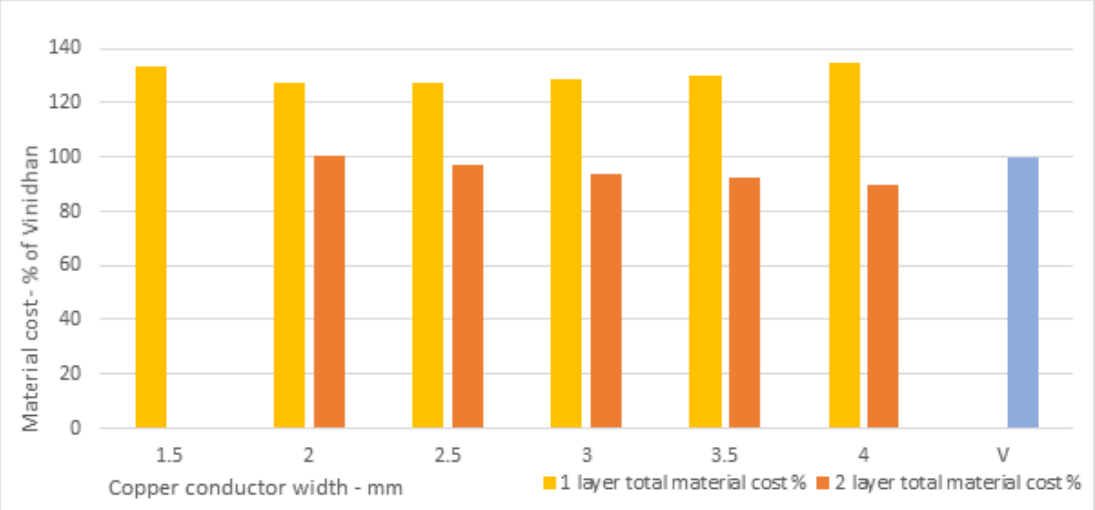

Figure 5.9 Copper winding material cost % of Vinidhan

Observations

Single layer copper windings produce around 30% less surface power loss density than 2 layer windings and around the same compared to the Vinidhan unit with a copper winding.

Copper windings have a different cost profile to aluminium windings. 1 layer copper windings have an optimum width of around 2.0 to 2.5mm but are still 25 to 30% more expensive than 2 layer windings.

2 layer copper windings reduce in cost as conductor width increases however this accompanied by a higher surface power loss density.

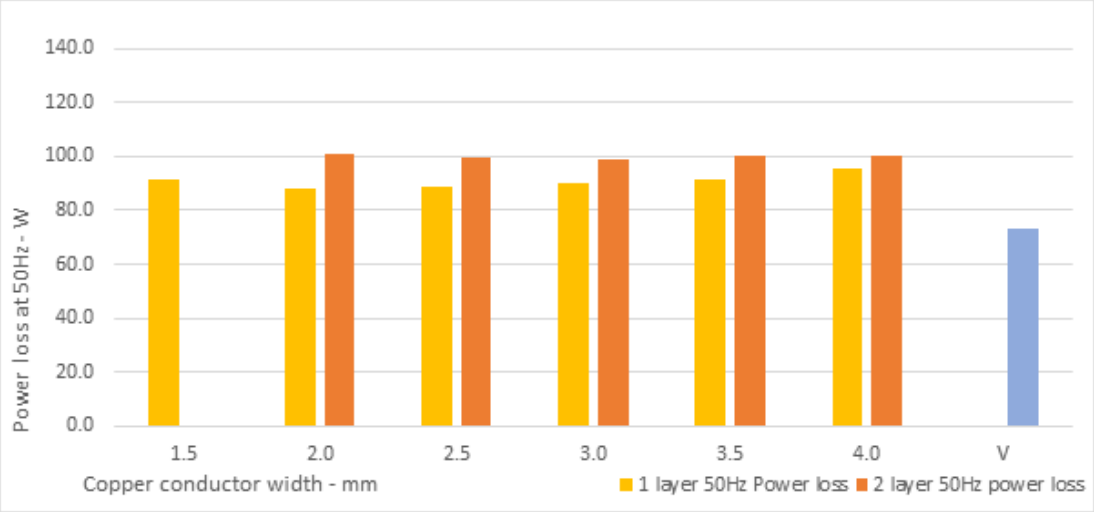

Figure 5.10 Copper winding power loss at $50Hz$

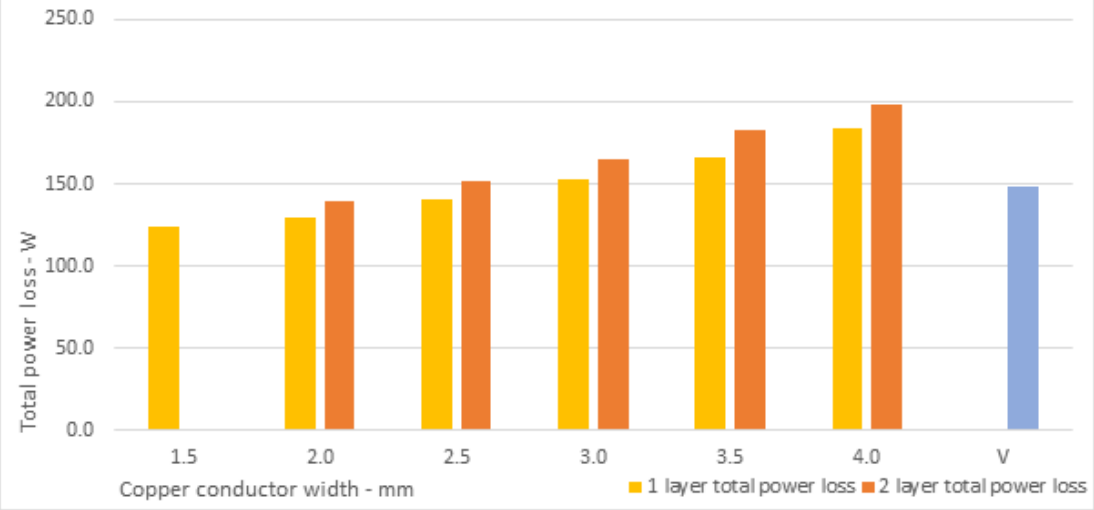

Figure 5.11 Copper winding total power loss including harmonics

Observations

Optimal power loss at 50Hz is achieved with a 1 layer copper winding width around 2.0 to 2.5mm and is around 20% more lossy than the Vinidhan unit with a copper winding. Optimal 2 layer copper winding width is around 3.0mm and is 5 to 10% more lossy at 50Hz compared to the 1 layer winding.

A 1 layer copper winding also has a lower total power loss compared to the 2 layer unit in the presence of harmonic currents. 1 layer total winding loss is comparable or better than the Vinidhan unit at around 2.0 to 3.0mm conductor width.

Copper windings produce lower power loss compared to aluminium windings by 30 to 40%.

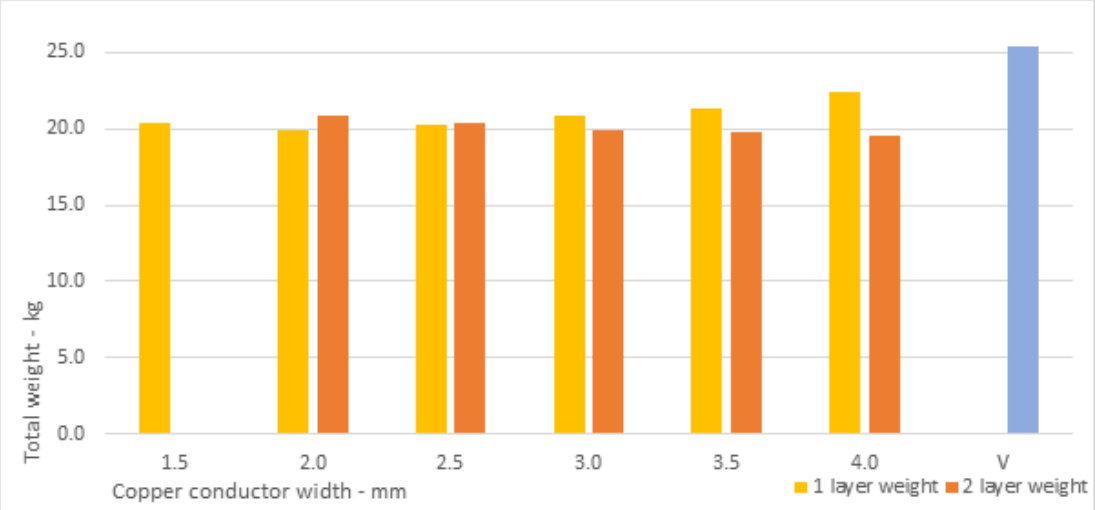

Figure 5.12 Copper winding material weight of a 3-phase inductor

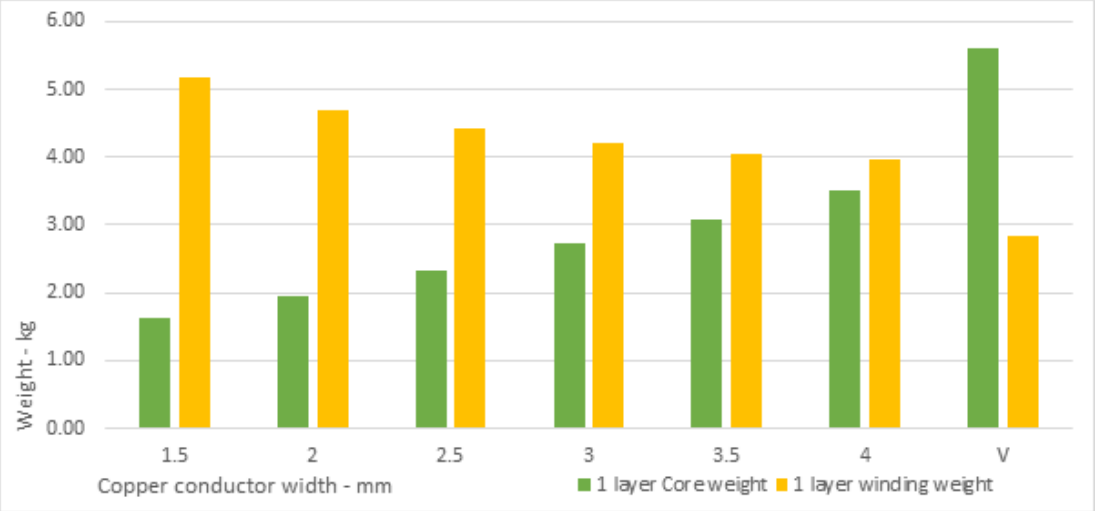

Figure 5.13 Copper winding and core weights for a 1 layer per leg

Observations

Devices with 1 and 2 layer copper windings are more similar in total weight and weigh around 20% less than the Vinidhan unit with a copper winding. 2 layer units become lighter with an increased conductor width, however 1 layer units increase in weight with conductor width with an optimum at around 2.0mm.

A similar general progression of reducing winding weight with increasing core weight occurs with copper windings as it did with aluminium windings.

5.5 DISCUSSION

In terms of power inductors for an application such as a detuning reactor in power factor correction systems, the key performance requirement other than value for money,

is minimal temperature rise. Temperature rise is due to power loss in the inductor and the ability to dissipate the heat generated. Figures 5.2 and 5.8 show surface power loss density in Watts per cm^2, and as a first order approximation, the temperature rise of the reactor is assumed to be proportional to power loss density.

Based on this approximation, single layer windings perform better in both aluminium and copper windings. Single layer windings also dissipate less power at both 50Hz and at harmonic frequencies.

Value for money is also an important consideration and in the examples shown, the copper winding inductors are all considerably more expensive than a comparable Vinidhan unit wound with aluminium windings.

Refer to Figures 5.14 and 5.15 for a comparison of performance and cost for 1 layer windings in aluminium and copper, 2 layer winding in aluminium and the Vinidhan unit. While copper conductor provides the lowest surface power loss density, it comes at significant additional cost. The 2 layer aluminium winding offers a cost benefit over the 1 layer unit, however there is a significant increase in surface power loss density as a result.

There is a significant cost benefit in choosing a 1 layer aluminium conductor of widths 2.5 to 3.0mm when compared to the Vinidhan unit. In this range, the 1 layer unit also has comparable surface power loss densities to the Vinidhan unit making this a logical choice for prototyping.

The effect of temperature rise has not been examined in detail in the section. The trial data has been produced at an operational temperature of 30°C to enable direct comparison with the Vinidhan as measured on the test bench over a short duration. Temperature rise effects are significant however and are discussed in more detail in Chapter 7.

5.6 CONCLUSION TO CHAPTER 5

An analysis produced by a computer aided design routine shows that the optimal design for a 3-leg partial core inductor can be found by comparing winding conductor widths, conductor material and the number of layers of winding. It appears that single layer windings are the most efficient while 2 layer windings offer the lowest cost. Copper windings are significantly heavier and therefore more costly to the point that there would be no cost benefit in using the partial core approach, however, lower power loss figures may be achieved with copper windings compared to the Vinidhan reactor with aluminium windings.

To confirm the usefulness of these comparisons, it is proposed that two trial units be tested to compare with the modelled results. The first offers the best performance for cost and the other offers the lowest cost, but at reduced efficiency.

1. 1 layer aluminium winding of 2.5mm width
2. 2 layer aluminium winding of 3.5mm width

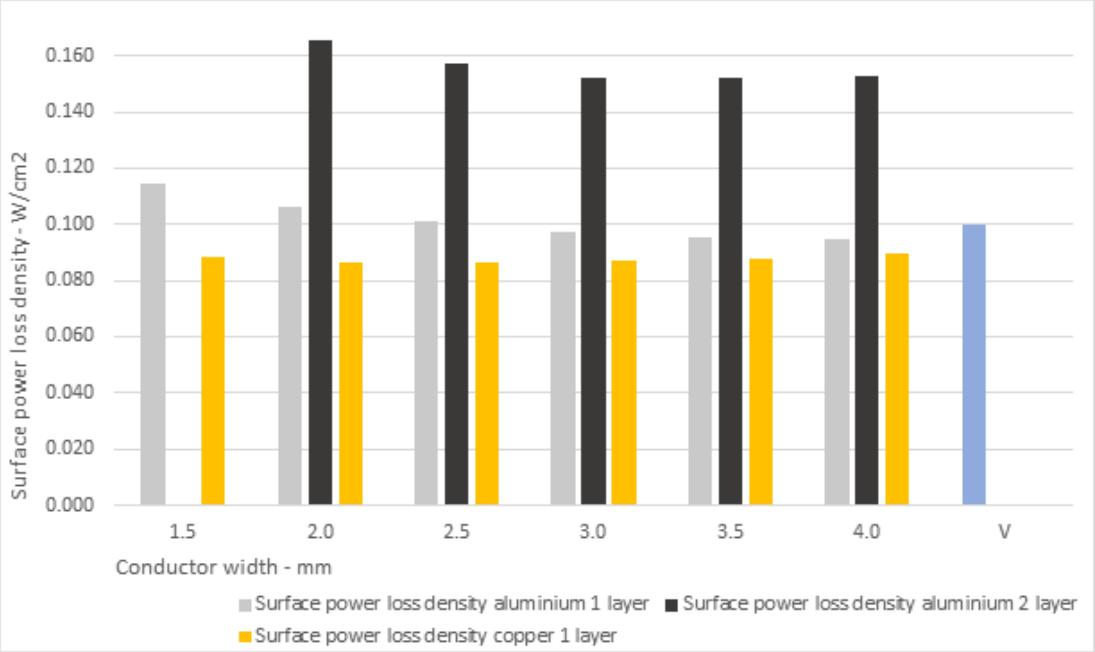

Figure 5.14 Surface power loss density for aluminium 1 layer, 2 layer and copper 1 layer

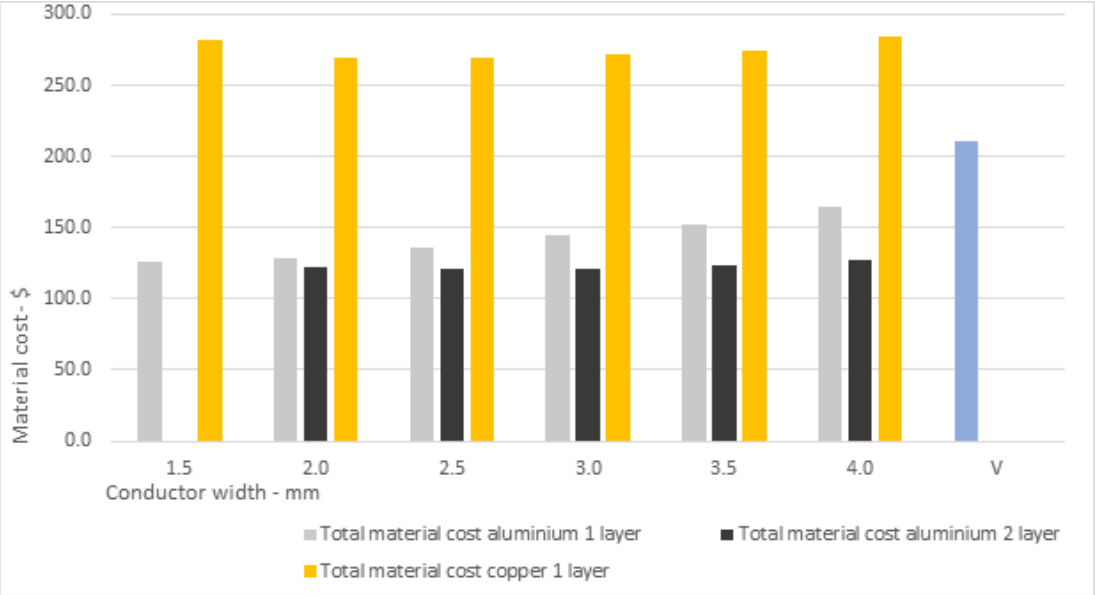

Figure 5.15 Total material cost for aluminium 1 layer, 2 layer and copper 1 layer

Refer to Chapter 7 where full designs are prepared and tested.

Chapter 6

DESIGN APPLICATION

6.1 OVERVIEW

The chapter begins by defining an application for the project inductor and the maximum rated conditions it should be able to tolerate continuously in service.

A desktop investigation is carried out on a commercially available reactor based on published data. A commercially available unit is obtained and testing is carried out to confirm quoted specifications align with the measured performance.

An analysis of the commercial reactor material weight and cost is also made so it is possible to use this device as a benchmark to which the project inductor may be compared.

The chapter concludes with a design specification for the project inductor.

6.2 PROJECT INDUCTOR APPLICATION

Due to the wide variety of possible applications in which partial core technology might be applied, it is necessary to limit the enquiry to a specific application as each will have its own particular design requirements. In this thesis it is proposed that the partial core inductor be applied as a detuning reactor for a capacitor bank in a 400V, 50Hz, 3-phase power system. There are a number of reasons to choose this specific application which include:

1. Viability of research and testing
2. Low inductance and applied voltage requirement
3. Widely used commercial application
4. Examination of technology performance with harmonic currents

Low voltage detuned capacitor banks typically draw a fundamental current of between 10A to 100A and therefore device efficiency is of particular importance, especially where harmonic current flow must also be considered. The application of partial core

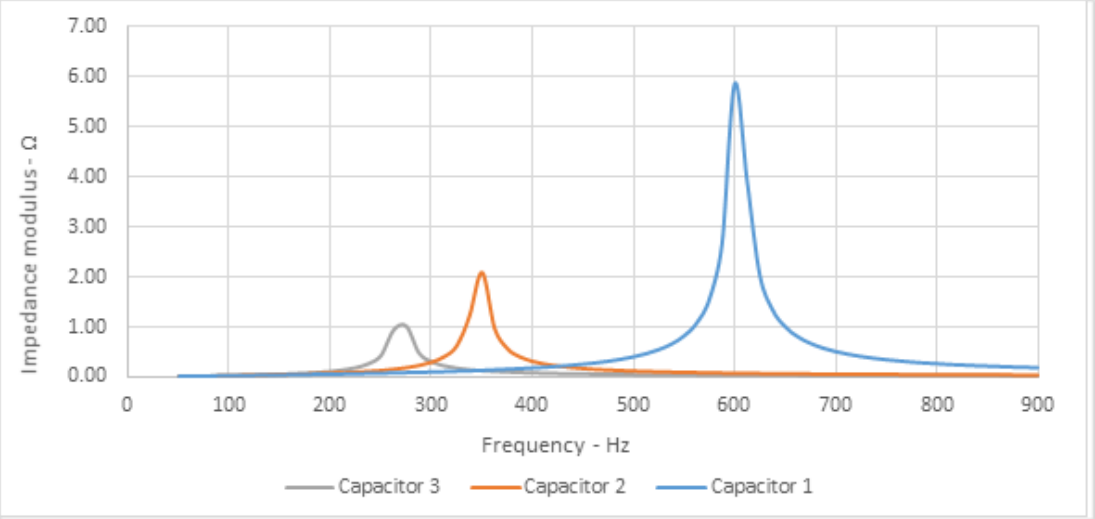

Figure 6.1 Frequency response of LV power system with differently rated banks of capacitance connected

technology to this application may therefore be judged by its merits in terms of device efficiency and any benefit there may be in terms of weight, size and materials cost.

6.3 THE PURPOSE OF A DETUNING REACTOR

When a capacitor bank is connected to a power system there will be a frequency at which it will form a natural resonance with a typically inductive power systemArrillaga and Watson [2003] Gonen [2008]. In low voltage systems this inductive nature is largely due to the leakage reactance of the distribution transformer and associated network as well as the connected loads. Capacitance is connected to a low voltage system to compensate for the inductive reactance of the connected load and thus improve the power factor of the installation presented to the supply. Systems with near unity power factor operate most efficiently and therefore capacitor banks may be connected automatically to regulate the power factor and maintain voltage controlRosa [2006].

The connection of capacitor banks will alter the resonant frequency of the local network and may give rise to serious over voltage where the system resonant frequency is close to any signal that may be present on the power system. It is often the case that harmonic voltages are present and these voltages may be amplified if the coincident amount of capacitance is connected. As an example, refer to Figure 6.1 and accompanying Tables 6.1 and 6.2 of data relating to a typical power system configuration and response as presented in the following Section 6.7 - Developing a system model.

The results in Table 6.2 show that significant harmonic resonance occurs between the mains supply and the capacitor banks at different harmonic frequencies depending on the amount of capacitance connected, despite the levels of harmonic distortion being less than half acceptable levels. Harmonic currents such as these may give rise to overheating

Table 6.1 Basic power system parameters.

HV supply capacity	240	MVA
Transformer rating	1	MVA
Transformer % impedance	5	% pu
Mains cable % impedance	2	% pu
Mains voltage 1st order no load	415	V
Mains borne harmonic voltage		
5^{th} order	3%, 7.2	V
7^{th} order	2%, 4.8	V
11^{th} order	1%, 2.4	V
13^{th} order	1%, 2.4	V

Table 6.2 Modelled system performance with each bank of capacitor connected.

	No Capacitor	Capacitor 1	Capacitor 2	Capacitor 3	Units
Capacitor rating	0	87	269	459	kVAr
Load rating	600	600	600	600	kW
Load power factor	0.8	0.8	0.8	0.8	lag
Total power factor	0.8	0.86	0.95	1	lag
Mains voltage 1st order	397.8	400.4	405.5	410.7	V
Mains current 1st order	1078.1	1014.5	921.9	891.1	A
Mains current 5^{th} order	10.0	21.0	77.8	**279.3**	A
Mains current 7^{th} order	4.8	23.3	**276.7**	**198.0**	A
Mains current 11^{th} order	1.6	42.3	35.6	26.3	A
Mains current 13^{th} order	1.3	**360.9**	24.1	20.1	A

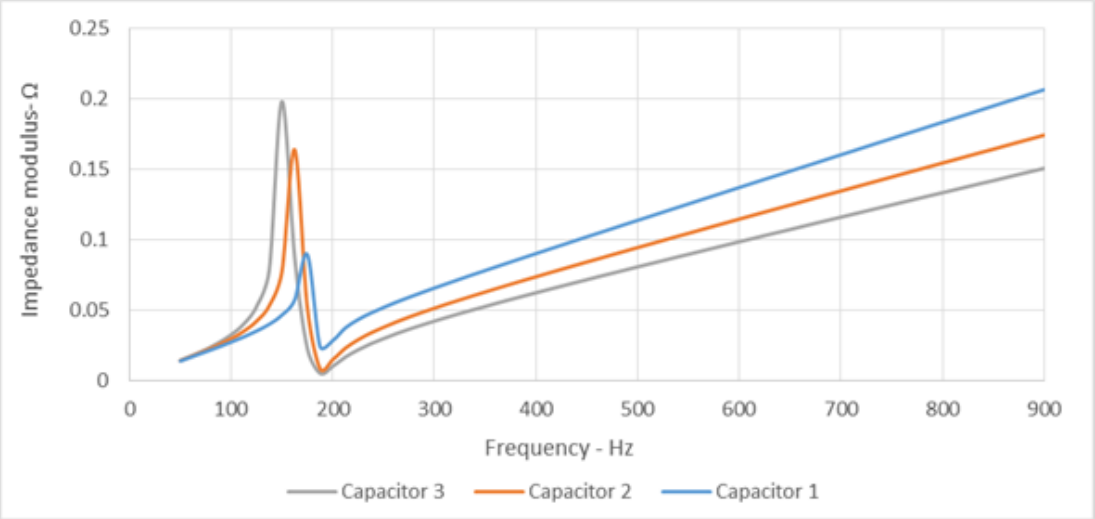

Figure 6.2 System impedance with detuned capacitor banks

of capacitors, transformers and nuisance tripping of protective devicesMunoz [2007].

The addition of detuning reactors in series with the capacitor bank creates a series tuned circuit which is tuned to some frequency usually below the first significant harmonic; e.g. the 5^{th}. Above the tuned frequency of the detuning reactor and capacitor bank combination, the circuit appears as inductive reactance and therefore cannot resonate with any other inductive part of the network. The detuning reactor also presents a series reactance to the capacitor which limits harmonic current flow and reduces inrush current during switching. Resistance inherent in the inductor may also help dampen any switching oscillation if the reactor has sufficient resistanceGonen [2008]. Refer to Figure 6.2 showing the system impedance with capacitor banks fitted with detuning reactors.

Two system resonance conditions occur when detuning reactors are fitted.

1. At the tuned frequency of the detuning reactor and capacitor bank there is a series resonance which produces a low impedance to the system Rosa [2006]. As the size of the capacitor bank increases, this impedance diminishes and lowers the total system impedance. For a detuned reactor of 7% reactance, this frequency is 189Hz. There is usually little in the way of voltage on a power system around this frequency to cause an elevated current flow in the capacitor bank.

2. A parallel resonance between the system and the capacitor occurs below the detuning frequency. The magnitude of the impedance is high, however and there is little in the way of non-triplen voltage on the power system at these frequencies to cause current flow in delta connected capacitor banks usually employed in low voltage systems.

Table 6.2 is compared with the Table 6.3 where 7% detuning reactors are fitted.

Table 6.3 Comparison with 7% detuning reactors fitted to the capacitor banks.

	No Capacitor	Capacitor 1	Capacitor 2	Capacitor 3	Units
Capacitor rating	0	87	269	459	kVAr
Load rating	600	600	600	600	kW
Load power factor	0.8	0.8	0.8	0.8	lag
Total power factor	0.8	0.86	0.95	1	lag
Mains voltage 1st order	397.8	400.6	406.1	411.7	V
Mains current 1st order	1078.1	1010.4	916.0	895.2	A
Mains current 5^{th} order	10.0	28.5	52.2	66.6	A
Mains current 7^{th} order	4.8	10.5	19.0	25.0	A
Mains current 11^{th} order	1.6	3.0	5.4	7.1	A
Mains current 13^{th} order	1.3	2.5	4.4	5.9	A

Resonance between the supply and the capacitor banks has been eliminated and the total harmonic voltage distortion appearing at the low voltage busbar is approximately halved. This is due to detuned capacitor banks reducing the total impedance of the low voltage busbar at harmonic frequencies. Note that the reactive power rating of the capacitor banks in Table 6.3 is higher due to the detuning reactor increasing the terminal voltage at the capacitor bank, and also, due to an elevation of the busbar voltage at fundamental frequency.

Detuning reactors are a well proven method of eliminating the amplification of harmonic currents in power systems that require the connection of capacitors. However, due to the significant tolerance of power system voltages and harmonic voltage levels, it is necessary to design a detuning reactor to accommodate these so they do not overheat or suffer magnetic saturation. Gonen [2008] In the following section, a specification is developed for the design of a detuning reactor which will be used for the partial core inductor design.

6.4 DETERMINING THE SPECIFICATION FOR A DETUNING REACTOR

6.4.1 Tuning frequency

Detuning reactors are specified as a percentage p of the 50Hz reactance of the capacitor bank to which they are to be connected. Electronicon

$$p(\%) = 100\% \times \frac{X_L}{X_C} \tag{6.1}$$

where X_L is the inductive reactance
X_C is the capacitive reactance

Note that X_C is the equivalent star connected reactance for a delta connected capacitor bank.

The % reactance determines the tuning of the reactor and capacitor bank combination. Typical detuning reactance values are 5.7% (210Hz), 7% (189Hz) and 14% (135Hz). The value selected is somewhat dependent on the application, however in New Zealand the default standard is 7% reactance. Power systems that have higher levels of harmonic distortion on the supply may require a higher reactance such as 14% particularly if the harmonic distortion is mains borne. If the distortion is due to operation of the connected load, and there is low background distortion, then a lower tuning such as 5.7% may be more appropriate.

For the purpose of this work, a standard reactance of 7% is chosen because it is a common rating and the ability to benchmark against commercial units is more readily achieved.

6.4.2 Power rating

A detuning reactor is connected in series with the capacitor bank and will carry the full load current of the capacitor bank continuously. It will also carry any harmonic current that is caused to flow by the presence of harmonic voltage distortion on the supply along with the relative impedance of the detuned circuit in relation to the supply impedance.

The power handling capability of a detuning reactor is determined by the maximum continuous load drawn by the capacitor bank at the maximum rated voltage including harmonic distortion. In practice this is determined by the maximum permissible temperature the reactor may reach under maximum operational conditions, which often includes allowance for forced air cooling. Typical values of power loss are in the range of 4 to 6W/kVAr of capacitor bank load. Electronicon

The reactor design must have considerable power handling headroom above standard system voltage conditions. For example, based on the results shown in Tables 6.9 and 6.10, a capacitor bank rated at 31.2kVAr at 400V may cause the reactor to dissipate 2.4W/kVAr x 31.2kVAr = 74W. However under the conditions of a 10% over voltage and the presence of maximum rated harmonic distortion, the power loss may rise to 4.6W/kVAr. As the voltage has increased, the effective reactive load of the capacitor bank has also increased. In this case, a 10% increase in voltage to 440V increases the capacitor bank rating to 37.8kVAr. Therefore the maximum power loss of the reactor is 4.6W/kVAr x 37.8kVAr = 173W. This is more than double the power dissipation capability at nominal fundamental conditions.

Table 6.4 New Zealand low voltage supply tolerance.

Standard voltage	−6%	+6%
Phase to phase	376V	424V
Phase to neutral	216.2V	243.8V

6.4.3 Linearity

Linearity performance largely determines the quality of the reactor and its susceptibility to ferromagnetic-resonance. Gonen [2008] Some manufacturers publish the linearity performance of a reactor to demonstrate that it normally operates well below the point of saturation.

For 7% reactors an acceptable linearity is defined as the reactor having no less than 95% of its rated inductance when carrying around 1.8 times its normal operational current at standard voltage. A value of 1.8 typically requires the reactor to operate at or below a peak flux density of 0.9T at standard rated voltage.

6.4.4 System voltage and frequency

It is necessary to define the operational limits in terms of system voltages and harmonic levels the detuning reactor and capacitor bank must tolerate.

6.4.4.1 Prescribed limits of system voltage

New Zealand

The following limits are set by the Electricity (Safety) Regulations 2012 under legislation by the Electricity Act.

Fundamental voltage at 50Hz may vary by ± 6% from the agreed supply voltage as shown in Table 6.4. The regulations define the standard low voltage for multiple phase MEN systems to be 400V between any two phases and 230V between phases and neutral.

Australia

The following limits are set by the Electricity Supply (Safety and Network Management) Regulation 2008(NSW). Although there are a number of jurisdictions, this one is indicative.

Fundamental voltage at 50Hz may vary by +10% and −6% from the agreed supply voltage as shown in Table 6.5. The regulations define the standard low voltage for multiple phase MEN systems to be 400V between any two phases and 230V between phases and neutral.

Table 6.5 Australian low voltage supply tolerance.

Standard voltage	−6%	+10%
Phase to phase	376V	440V
Phase to neutral	216.2V	253V

Note that the Australian system voltage was harmonised with the IEC program to achieve an international standard system voltage of 230/400V under AS60038 published on the 23rd February 2000.

Proposed voltage limits for the detuning reactor

So that a detuning reactor may be compatible with the voltage supply in New Zealand or Australia, and indeed any country which has adopted the IEC standard voltage system of 230/400V, it is proposed that the Australian low voltage supply tolerance be adopted in this work. The normal operational voltage is therefore 230/400V and the maximum design voltage is 253/440V.

6.4.4.2 Power Quality limits for New Zealand and Australia

In terms of harmonic distortion, the limits are prescribed under AS/NZS 61000.3.6 "Limits - Assessment of emission limits for distorting loads in MV and HV power systems".

The standard is written for power distribution companies and provides guidance on levels of harmonic distortion for low, medium and high voltage systems and the compatibility of connection of consumer loads. There is a statistical probability of system disturbance levels and a corresponding statistical probability of equipment immunity to such disturbances. If the probability densities of the system disturbance and equipment immunity can be sufficiently separated there is a zone in the middle where compatibility of equipment connected to the network exists. The standard takes into account the probability that high levels of disturbance may occur only rarely and for short periods of time rather than prescribe absolute limits of harmonic distortion. Gosbell et al. [1999] Watson et al. [2012]

The standard does however set planning levels for distributors as a means of guidance as to what may be realistically achieved in terms of allowing equipment manufacturers the ability to set reliable immunity levels for their equipment. Refer to Table 6.6 for an extract of the planning levels provided in the standard for odd order harmonics for low and medium voltage supplies.

The equipment immunity levels proposed are based on data provided by manufacturers for detuning chokes as the level at which the reactor must operate continuously. Electronicon

It is therefore proposed that these immunity levels be adopted in this work.

Table 6.6 Network planning levels for harmonics and proposed immunity levels.

Planning levels Odd harmonic - non-triplen		Equipment Immunity Level
Order h	Harmonic voltage %	Harmonic voltage %
5	5	6
7	4	5
11	3	3.5
13	2.5	3
17	1.6	2
19	1.2	1.5

6.5 CHOOSING A CAPACITOR BANK RATING

In commercially available automatic power factor correction systems (APFC) produced for the low voltage market, a system capacity may range from between 37.5 kVAr to 1MVAr and above. To obtain automatic control of the reactive power, capacitor banks are switched in stages to provide the optimal level of compensation. The resolution of the APFC depends on the system requirement and capacitor banks are available in a number of sizes to suit the particular application. Typical capacitor banks sizes are 6.25kVAr, 12.5kVAr, 16.5kVAr, 25kVAr, 33kVAr, 50kVAr, 66kVAr, 75kVAr and 100kVAr. Capacitors

For the purpose of this work it is proposed that one capacitor bank size be chosen to match with a detuning reactor design. It is desirable to choose a capacitor bank with as large a rating as possible to be of practical use, however, not too large that it may offer less resolution in a complete system. A capacitor bank size of nominal rating 33kVAr at 400V, 50Hz is sufficiently large and was chosen to suit available materials and enable full load testing with the available equipment.

Power capacitors are manufactured to standard values to suit the general need of the industry. The capacitors selected for this work are based on standard sizes manufactured by Schneider Electric but are also available from KBR and many others. These capacitors are designed for power factor correction applications and tolerate the typical voltages experienced in electric power systems. The voltage rating selected enables plenty of headroom between the terminal voltage that develops due to the connection of a detuning reactor, and maximum voltage levels, including harmonics, which may occur in service. To meet allowable limits, the maximum continuous current of the capacitor should not exceed 135% of its rated current at rated voltage. However experience has shown that for reliable continuous operation, the capacitor current under maximum rated conditions should not exceed the capacitor rating I_N at full rated voltage U_N.

Figure 6.3 Capacitor bank comprising 2 x 25kVAr 525V delta connected capacitors

Table 6.7 Effective ratings of the selected capacitor bank with 7% detuning reactor

System voltage	Effective capacitor power
400V	31.2kVAr
405V	32.0kVAr
410V	32.8kVAr
415V	33.6kVAr
440V	37.8kVAr

6.5.1 Capacitor bank selection

The selected capacitors are 2 x Schneider Electric 3-phase, delta connected capacitor type BLRCH250A300B52 (2 x 25kVAr at 525V). The rated current of the capacitor bank is 55.0A at 525V. Refer to Figure 6.3.

This selection gives an effective power of $29.02kVAr$ at $400V$ without any detuning reactor. With 7% detuning reactor the effective power of the capacitor bank is shown in Table 6.7.

The 3-phase capacitors each comprise $3 \times 96.2\mu F$ delta connected capacitor modules giving a total of $3 \times 192.4\mu F$ of delta connected capacitors in the capacitor bank.

At 50Hz the reactance of the capacitor bank is calculated by obtaining the equivalent capacitance as if the capacitor bank were built as a star connected unit as follows.

1. Capacitor rating at 400V is 29.02kVAr. Line current is 41.89A
2. Reactance of each star connected leg is $230.9/41.89 = 5.51\Omega$
3. At 50Hz the capacitance of the star leg is $577.35\mu F$ ($3\times$ delta leg value)

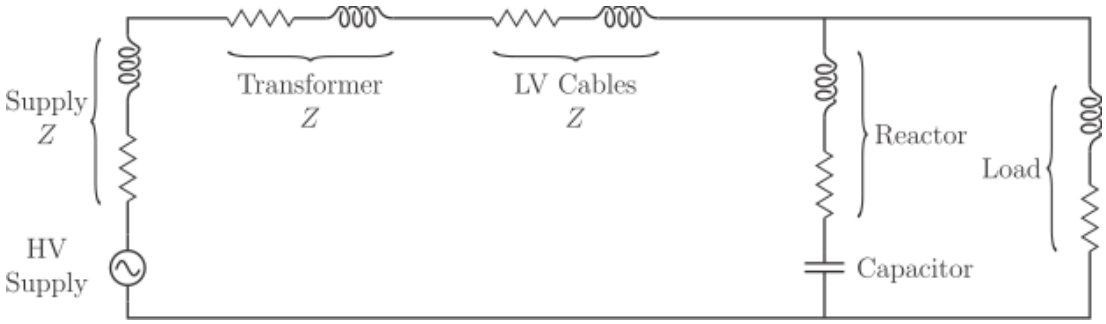

Figure 6.4 System model equivalent circuit

6.6 INDUCTANCE OF THE DETUNING REACTOR WITH THE SELECTED CAPACITOR BANK

To calculate the inductance of the detuning reactor with a 7% reactance: Electronicon

At 50Hz,

$$p(\%) = 100 \times \frac{X_L}{X_C} \tag{6.2}$$

therefore,

$$X_L = \frac{p \times X_C}{100} = \frac{7 \times 5.51}{100} = 0.3859\Omega$$

The inductance of one leg of the detuning reactor is:

$$X_L = 2 \times \pi \times f \times L \tag{6.3}$$

therefore,

$$L = \frac{X_L}{(2 \times \pi \times f} = \frac{0.3859}{(2 \times \pi \times 50} = 0.001229H,$$

or 1.229mH per leg.

With the reactance values of the chosen capacitor and detuning reactor calculated, it is now possible to evaluate the power system parameters that will affect the power handling design of the detuning reactor.

6.7 DEVELOPING A SYSTEM MODEL

A system model is developed to estimate the steady state performance of the power system, load and capacitor bank as shown in Figure 6.4 Detjen et al. [2001]

The high voltage supply impedance and transformer ratings are taken from an actual installation. In practice the permutations of system configuration are nearly

endless and vary constantly depending on the actual connected load at any time, along with network switching configurations and upgrades.

In addition, there is a distinction between the sources of harmonic distortion. Harmonic distortion can either be 1) borne on the high voltage reticulation due to harmonic contributions made by polluting neighbouring consumers, or, 2) it can be produced within the installation itself by the operation of non-linear load. Djeghloud et al. [2014]

In the case of 1) mains borne harmonic distortion, harmonics present as a voltage source and any connected load that conducts harmonic current such as detuned capacitor banks, will draw the full current in proportion the voltage presented. Harmonic voltage at the low voltage busbar will vary in proportion to the load, causing harmonic voltage to be dropped across the high voltage supply, transformer and mains cables.

In the localised case 2), a harmonic voltage is developed on the low voltage busbar in proportion to non-linear loads injecting harmonic current into the impedance of the system. Harmonic current is proportioned between the system and conducting loads depending on the relative impedance of each system element.

In practice there is often a mix of both scenarios. In terms of this analysis however, the former case of 1) voltage source, is chosen due to the need to define harmonic voltage levels presented to the detuned capacitor bank.

The method of analysis is straightforward; a high voltage source with adjustable source impedance is modelled with connection to a step-down transformer and mains cable, each with defined impedance. The impedances are modelled as resistive and reactive components so that the effective reactance may be estimated across a range of frequencies. Similarly the load and capacitor bank are modelled in the same way so that the effect of each harmonic order may be examined.

The model is constructed on an Excel spreadsheet with impedance calculations starting with load then combining the capacitor bank, the mains cable, transformer secondary which in turn is reflected to the transformer primary and finally combined with the high voltage source impedance. A fundamental voltage and harmonic voltages are then applied as a high voltage source and the voltages and currents throughout the network may be analysed at each node by impedance at each frequency. To produce sufficient resolution, the impedances are calculated in 12.5Hz increments so that a simultaneous response of the system at each pertinent frequency may be obtained.

The model has been tested by comparison to laboratory measurements relating to the performance of the capacitor and detuning reactor and found to be in close agreement, sufficient to show the model is an effective tool for this purpose.

Refer to Table 6.8 detailing the system used in this analysis. A relatively strong supply was chosen to minimise the voltages dropped across the supply. As the purpose of this study is to determine the effect of a prescribed fundamental and harmonic voltage

Table 6.8 Power system parameters

HV supply capacity	240	MVA
HV supply voltage	11	kV
Transformer rating	1	MVA
Transformer % impedance	5	% pu
Mains cable % impedance	2	% pu
Mains voltage 1st order no load	415	V
Harmonic voltage 5^{th} order	6	%
Harmonic voltage 7^{th} order	5	%
Harmonic voltage 11^{th} order	3.5	%
Harmonic voltage 13^{th} order	3	%
LV system load		
Load rating	600	kW
Load power factor	0.8	lag

on the detuned capacitor bank, no consideration is given to possible voltages that may develop under other scenarios. For example it is recognised that a high impedance supply feeding a large proportion of non-linear load may give rise to very high harmonic voltages at the low voltage busbar. However if these harmonic voltages are higher than the prescribed limits under law, then in this case, the non-linear load should be treated to minimise the disturbance it may create. Therefore the prescribed equipment immunity levels given in Table 6.6 apply.

Tables 6.9 and 6.10 gives the outputs of the model in terms of the voltages applied to the detuned capacitor bank and developed across the individual components. Note the total maximum rms current of 53.4A does not exceed the capacitor bank rated current at rated voltage (55A at 525V).

6.7.1 Comparison with manufacturer data

A data sheet was obtained for a reactor from Vinidhan International and is presented in Appendix B. The Vinidhan reactor is of the same rating as the project inductor and is shown in Figure 6.5. The measured performance of the Vinidhan reactor is presented in Tables 6.11 and 6.12.

In summary, the data provided by manufacturers agrees well with the modelled estimations. The main area in question however is the power dissipation figure provided as it is not clear if it includes maximum harmonic current.

Testing is carried out at each frequency to determine the power dissipation at the target currents provided in Table 6.9 at rated conditions, and in Table 6.10 for maximium conditions.

A summation of the power dissipation at each frequency provides the total power dissipation and also enables the effective resistance per leg to be determined at each

Table 6.9 Detuning reactor design conditions at rated voltage

Voltage	Busbar	Reactor	Capacitor
Mains phase to neutral	$230V$	$17.4V$	$430V$
Harmonic voltage 5^{th} order	$13.9V$	$32.3V$	$18.5V$
Harmonic voltage 7^{th} order	$11.5V$	$16.3V$	$4.8V$
Harmonic voltage 11^{th} order	$8.1V$	$9.2V$	$1.1V$
Harmonic voltage 13^{th} order	$6.9V$	$7.6V$	$0.6V$
Total harmonic distortion	9.1%		

Current	Reactor	
Mains $50Hz$	$45.1A$	
Harmonic current 5^{th} order	$16.8A$	
Harmonic current 7^{th} order	$6.0A$	
Harmonic current 11^{th} order	$2.2A$	
Harmonic current 13^{th} order	$1.5A$	
Total rms current	$48.5A$	
Total reactive power		$31.2kVAr$

Table 6.10 Detuning reactor design conditions at maximum voltage

Voltage	Busbar	Reactor	Capacitor
Mains phase to neutral	$253V$	$19.3V$	$473V$
Harmonic voltage 5^{th} order	$15.2V$	$35.6V$	$20.3V$
Harmonic voltage 7^{th} order	$12.7V$	$17.9V$	$5.2V$
Harmonic voltage 11^{th} order	$8.9V$	$10.1V$	$1.2V$
Harmonic voltage 13^{th} order	$7.6V$	$8.3V$	$0.7V$
Total harmonic distortion	9.1%		

Current	Reactor	
Mains $50Hz$	$49.5A$	
Harmonic current 5^{th} order	$18.4A$	
Harmonic current 7^{th} order	$6.6A$	
Harmonic current 11^{th} order	$2.4A$	
Harmonic current 13^{th} order	$1.7A$	
Total rms current	$53.4A$	
Total reactive power		$37.8kVAr$

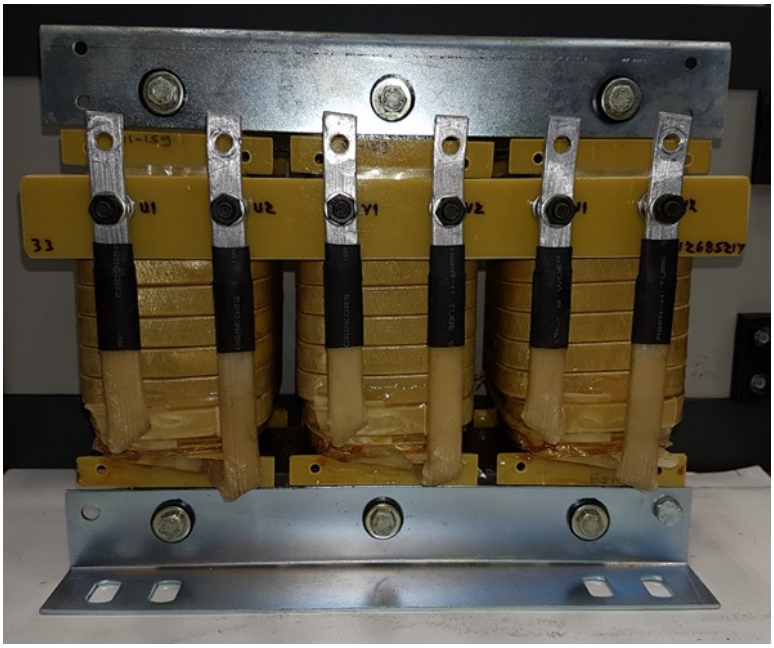

Figure 6.5 Vinidhan 33kVAr, 415V 50Hz reactor

frequency as shown in Figure 6.6. The Vinidhan reactor quality factor is shown in Figure 6.7. Refer to Tables 6.11 and 6.12 for the results of these tests.

The data sheet for the Vinidhan reactor provided in Appendix B, claims a total power dissipation of 86W at 51.6A. based on the result shown in Table 6.12 it is concluded that this figure confirms the power dissipation at 50Hz only. When harmonic current is added the dissipation was measured to be 173W. It can be seen than adding harmonic currents at the prescribed immunity level, effectively doubles the power dissipation of this reactor.

Including harmonic power dissipation at maximum rated current, the power loss of this inductor is 4.6W/kVAr which is comparable to the range of loss specified by Electronicon data sheet which is also included in Appendix B.

6.7.2 Linearity

Refer to Table 6.11 showing the measured values of inductance as 3-phase applied voltage at 50Hz is increased across the each winding of the reactor.

As shown in Table 6.13, the inductance of the Vinidhan reactor falls to 95% of its I_N value at around 200% I_N. Compared to the Electronicon specification, this is a good solid result as 180% I_N is a typical benchmark of performance.

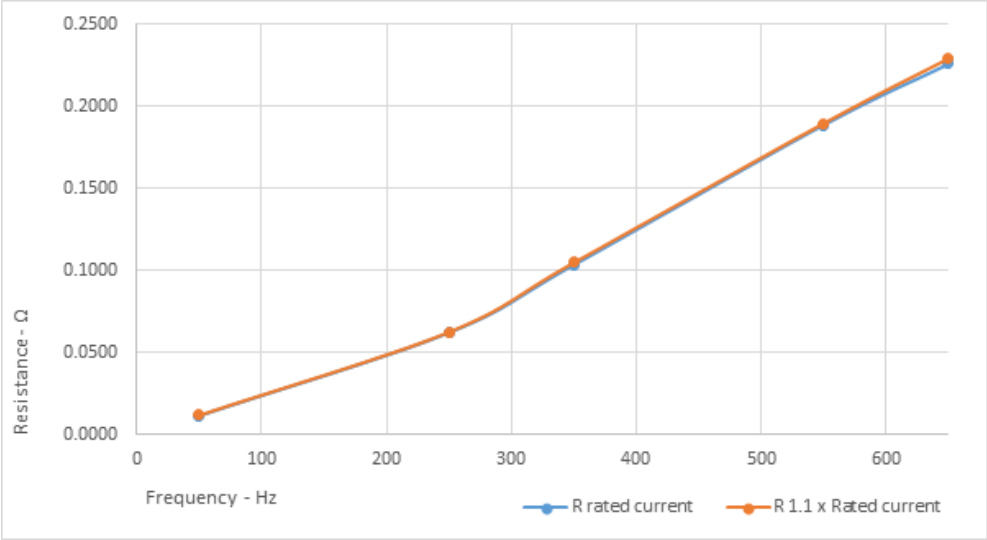

Figure 6.6 Vinidhan $33kVAr$ total resistance vs frequency

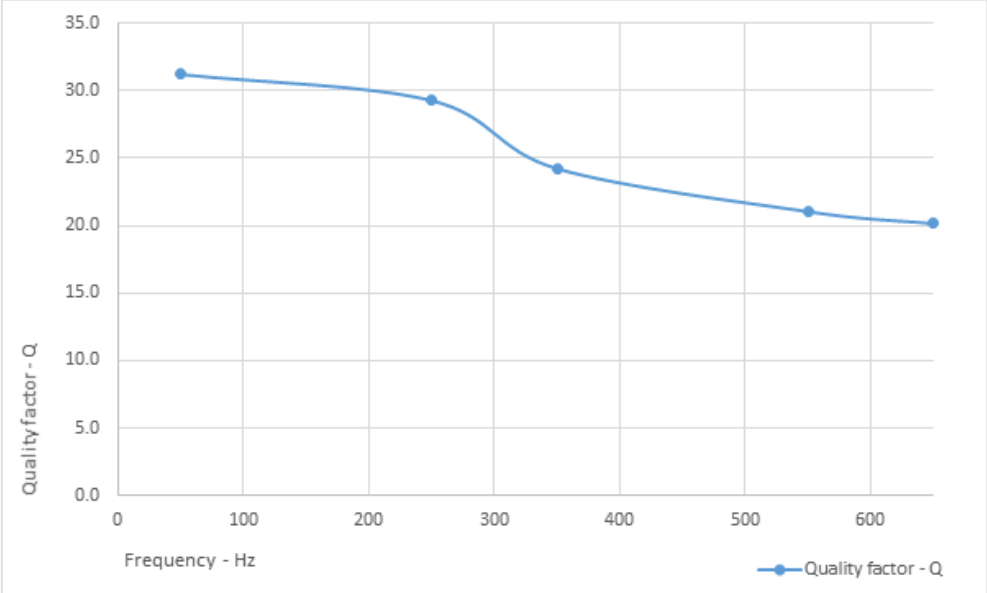

Figure 6.7 Vinidhan $33kVAr$ quality factor vs frequency

Table 6.11 Measured power dissipation of Vinidhan reactor at rated current

Vinidhan - YV17K33 - 33kVAr at 415V					
Frequency	$50Hz$	$250Hz$	$350Hz$	$550Hz$	$650Hz$
Calculated current	$46.8A$	$17.1A$	$6.2A$	$2.2A$	$1.6A$
Calculated inductance	$1.238mH$	$1.238mH$	$1.238mH$	$1.238mH$	$1.238mH$
Measurements					
Average current	$46.1A$	$17.0A$	$6.2A$	$2.2A$	$1.6A$
Average reactor voltage	$17.0V$	$31.2V$	$15.7V$	$8.6V$	$7.3V$
Power 3-phase	$74W$	$54W$	$11.8W$	$2.7W$	$1.7W$
Average leg resistance	0.012Ω	0.062Ω	0.014Ω	0.189Ω	0.226Ω
Average leg inductance	$1.174mH$	$1.168mH$	$1.159mH$	$0142mH$	$1.134mH$
Total power 3-phase	$144W$				

Table 6.12 Measured power dissipation of Vinidhan reactor at maximum current

Vinidhan - YV17K33 - 33kVAr at 415V					
Frequency	$50Hz$	$250Hz$	$350Hz$	$550Hz$	$650Hz$
Calculated current	$51.6A$	$18.4A$	$6.6A$	$2.4A$	$1.7A$
Calculated inductance	$1.238mH$	$1.238mH$	$1.238mH$	$1.238mH$	$1.238mH$
Measurements					
Average current	$50.6A$	$18.3A$	$6.6A$	$2.4A$	$1.7A$
Average reactor voltage	$18.7V$	$33.6V$	$16.8V$	$9.5V$	$7.9V$
Power 3-phase	$91W$	$63W$	$13.7W$	$3.3W$	$2.0W$
Average leg resistance	0.012Ω	0.063Ω	0.015Ω	0.190Ω	0.230Ω
Average leg inductance	$1.176mH$	$1.167mH$	$1.156mH$	$1.156mH$	$1.131mH$
Total power 3-phase	$173W$				

Table 6.13 Measured linearity of Vinidhan reactor

Vinidhan - YV17K33 - 33kVAr at 415V $I_N = 46.6A$ at $50Hz$			
Measurements			
Voltage	Current	$\%L$ to L_N	$\%I$ to I_N
$8.56V$	$22.9A$	101%	49%
$11.54V$	$30.59A$	101%	66%
$14.28V$	$38.27A$	101%	82%
$16.92V$	$45.8A$	100%	98%
$19.75V$	$53.2A$	100%	114%
$22.79V$	$61.7A$	100%	132%
$25.57V$	$69.7A$	99%	150%
$29.1V$	$80.1A$	98%	172%
$32.55V$	$91.2A$	97%	196%
$36.44V$	$113.6A$	87%	244%

Table 6.14 Vinidhan reactor component weight estimation

Vinidhan - YV17K33 - 33kVAr at 415V Component weights		
Steel core		
Item	Limb	Cross arm
Quantity	3	2
Width	$0.04m$	$0.04m$
Depth	$0.065m$	$0.065m$
Length	$0.136m$	$0.220m$
Volume	$0.001061m^3$	$0.001144m^3$
Weigth	$8.1kg$	$8.1kg$
Total core weight	$16.8kg$	
Miscellaneous items	$1.4kg$	
Windings	$2.84kg$	
Total weight	$21.0kg$	

Table 6.15 Material cost estimate of the Vinidhan 33kVAr reactor

Vinidhan - YV17K33 - 33kVAr at 415V Component costs		
Steel core	$Cost/kg$	$TotalCost$
$16.8kg$	\$10	\$168.00
Winding		
$16.8kg$	\$15	\$42.60
Total cost		\$210.60

Table 6.16 Project reactor specification

Parameter	Target value
nominal capacitor bank rating	$33kVAr$ @ $415V$
Capacitor value	$3 \times 192.4\mu F$ of delta connected capacitors
Reactor inductance per leg	$1.23mH$ or 7% reactance
Standard stsyem voltage	$230/400V$
Maximum system voltage	$253/440V$
Maximium continuous rms current	$53.4A$ ($49.5A$ at $50Hz$)
Harmonic current 5^{th} order	$18.4A$
Harmonic current 7^{th} order	$6.6A$
Harmonic current 11^{th} order	$2.4A$
Harmonic current 13^{th} order	$1.7A$
Maximum power loss range	4 to $6W/kVAr$ or around $130W$ to $230W$
Linearity	96% L_N at 200% x L_N
Total weight	Less than $21kg$
Cost	Less than \$210 for core steel and winding

6.7.3 Physical construction

Table 6.14 provides an estimation of the Vinidhan reactor component weights based on measurements of the core and an estimation of the winding weight assessed by the number of turns counted. Table 6.15 provides an estimate of the cost of the Vinidhan 33kVAr reactor based on materials cost per unit weight. Labour and incidental materials were not included.

6.8 SPECIFICATION FOR THE PROJECT INDUCTOR

Refer to Table 6.16 for the specification of the project inductor based on the calculations provided in this chapter and by comparison with the Vinidhan reactor.

6.8.1 Conclusion to Chapter 6

An application for the project partial core inductor has been chosen as a detuning reactor for low voltage capacitor banks. The characteristics of such inductors have been examined both in terms of the required performance based on permissible power system voltage and harmonic voltage disturbance.

A desktop study was made for a commercially made inductor of similar rating to the project inductor and showed that the modelled parameters were in agreement with the data provided except that the power dissipation may not have included the effects of harmonic current.

An experimental study was further conducted on the Vinidhan reactor. The results show that the inductance achieved by the reactor was lower than quoted but within -5% tolerance. The quoted performance for power dissipation may only include the contribution of 50Hz power loss at maximum rated current. This may be acceptable practice, however it highlights the difficulty in knowing exactly how a device may perform when comparing specifications of various products.

The linearity of the Vinidhan unit achieved 95% of rated inductance at $200\% \times I_N$. This is considered to be a solid result which is indicated by the weight of the device. When compared to published data for the Schneider reactor for example, a device of 50kVAr rating also has a total weight of 21kg. The linearity of the Schneider reactor was not tested.

To conclude, a specification was determined for the project inductor based on the calculations of inductance, maximum voltage rating and typical power loss data for a commercial reactor of the project inductor rating. This will form the basis of comparison to the project inductors tested in Chapter 7.

Chapter 7

PROJECT INDUCTOR DESIGN AND PERFORMANCE

7.1 OVERVIEW

In this chapter, designs for two partial core 3-phase reactors are analysed with the fully developed model of Chapter 4, and optimisation routine of Chapter 5. The designs were built and tested. Electrical performance is compared to the model and a commercially available unit. Physical performance in terms of weight and cost are also compared.

A conclusion is reached in terms of cost-effective performance of partial core inductors.

7.2 INTRODUCTION

In this thesis, Chapter 4 defined new circuit elements and modified the Steinmetz equivalent circuit for 3-phase partial core devices. Chapter 5 demonstrated an automated routine for finding the optimal conductor width and material for a given application, and Chapter 6 describes an application and developed a specification for comparing a partial core inductor with a commercially available unit.

Based on the detuning choke specification in Chapter 6, two prototype inductors were built and tested over the course of the research. Whilst characterisation of 1-leg inductance could be approximated at the time of device construction, the affects of 3-phase winding construction on inductance and device resistance were still under examination. The two inductors demonstrate that the revised model predicts the performance of these devices by:

1. Alignment of model to device performance, and,
2. Alignment of optimisation predictions with devices

From the optimisation work done in Chapter 5, it was concluded that to achieve the project inductor specification of Chapter 6, $2.5mm$ wide aluminium conductor wound in a single layer would provide the optimal cost benefit. The most cost effective, but

less efficient design could be achieved with a two layer aluminium winding of $3.5mm$ width conductor. In this chapter the two prototype inductors are tested in terms of alignment with the model and the general prediction of the design routine.

Finally, these designs are compared with a commercially built full-core unit.

7.2.1 Transformer reverse design technique

The transformer reverse design technique has been applied to all inductor designs in the work. It is of particular use due to the ability to design for the available materials, especially when building numerous small, yet different inductors. In particular, it has served invaluably to the computation of incremental designs as produced in the optimisation routines of Chapter 5.

7.2.2 Obtaining Materials

Local manufactures have been very supportive in finding materials in low quantities to enable the various prototypes to be produced. The difficulty of sourcing specific materials should not be underestimated and therefore we are very grateful for this support.

In particular, the sourcing of aluminium conductor of specific sizes proved to be time consuming. Even when a source was found, it could be a matter of two to three months to procure a drum or two of wire. The problem appeared to be due to the need for our small quantities to be consolidated with other orders to make the shipment worthwhile. Paying additional for airfreight may be a worthwhile consideration to better maintain research momentum. As a further general observation, it would be essential to fully research the supply chain sourcing arrangements well before a design for production was contemplated.

The other significant challenge was to source core steel of specific size. The department has a stock of lamination steel widths on drums, however the time required to chop the steel to specific sizes to build cores would have been an impediment to research progress. We are therefore very grateful to the local manufacturer who was not only prepared to supply small quantities of core steel, but was also prepared to slit it into widths and chop it to length with an automatic machine at their disposal. The only limitation being that the width of the steel needed to be in multiples of 5mm to suit the slitting knives available. The steel length could be of any reasonable dimension.

7.2.3 Design development process

As mentioned in the introduction, the prototypes that are presented in this chapter were not built at the conclusion of this work due to the optimisation process carried out in Chapter Five. Rather, the designs were motivated earlier in the research as a means

of validating the various hypotheses developed along the research journey. The first unit built was the two layer winding unit because the theoretical model being tested at the time determined that, with the aluminium conductor selection available, a 2 layer winding would produce the lowest cost design. It is satisfying to see that the optimisation routine does indeed confirm this is the case, however, what was not known at the time was the effect this would have on the ac resistance of the device.

Trials with other 2 and 3 layer designs established that this was a more lossy approach when compared to single layer designs. Therefore the 1 layer design with $2.5mm$ conductor width followed and showed a significant improvement in efficiency, particularly at higher frequencies. It needed a little more core steel, but fewer turns, which also made it more efficient at mains frequency compared to the 2 layer device. Once again, the optimisation routine shows that $2.5mm$ width conductor is in the right range for optimal efficiency.

Therefore the process used to model these two prototypes is presented, but now with the fully developed equivalent circuit and its connection to the physical parameters of the devices.

7.2.4 Material selection

7.2.4.1 Winding conductor

Obtaining winding materials and core steel was not a straightforward matter and is was necessary to choose from the available limited material range. The project inductor specification determines the current to be carried in the conductor, and therefore the required range of conductor cross sectional area narrowed down the options in terms of conductor dimensions.

The project capacitor bank was calculated to draw around $49.5A, 50Hz$ at maximum rated voltage (Table 6.16) and therefore, given a nominal current density of $1.5A/mm^2$ typical for air cooled conductors, a cross sectional area of $33mm^2$ would be required.

At the time of the prototype construction, the target cross sectional area was assessed to be $31mm^2$ which was later shown to be a bit on the low side for maximum continuous operation. Therefore based on a $31mm^2$ cross section, the two conductors chosen were:

1. 1 layer $2.5mm \times 12.5mm = 31.25mm^2$ - at $49.5A$, $= 1.58A/mm^2$
2. 2 layer $3.55mm \times 9mm = 31.95mm^2$ - at $9.5A$, $= 1.55A/mm^2$

It will be shown that when harmonic current is considered, the current density and eddy current heating effects add to further loss, and therefore heat, in the conductor.

7.2.5 Target Peak flux density

It was shown in Chapter 6 that commercially built detuning reactors typically operate at a lower peak flux density to enable a good linearity for a range of over-current. Measurements of inductors with an over-current applied until the inductance falls to 95% nominal inductance, suggest that an operational range of current between 1.36 and $2.20 \times I_N$ is typical depending on the quality of the inductor. This is also supported by manufacturers' claims. Electronicon

It is therefore necessary to design the project inductor at a lower peak flux density than might be optimal for a transformer. In the design of the prototype inductors, a target peak flux density of $0.8T$ was set which is around half of the usual design target of $1.6T$. This effectively doubles the core cross sectional area required, however it was considered necessary to obtain the required linearity. It should also be noted that increasing core cross sectional area increases the inductance of the reactor for a given number of turns. There is an optimal target flux density to achieve the best balance between minimising the core cross section and the length of conductor required to achieve a given inductance, thus there is another design balance point to trade off cost with efficiency. This aspect of design optimisation was not carried out in this work.

Note also the uneven distribution of axial flux, shown in Chapter 4, over the length of the partial core which gives a significantly higher peak flux density toward the centre of the core length. No account has been made of this in these designs, however triplen current distortion was noted in the linearity tests conducted at around $2.0 \times I_N$. The selection of a target peak flux density of $0.8T$ is therefore justified.

7.2.6 Core material

Although a good quality lamination steel was available from a local transformer manufacturer, the slitting equipment was able to slit the steel to multiples of 5mm only. Given the nature of the winding being wound on edge, it was found that a circular former was best in terms of producing a uniform wind. Therefore it was necessary to determine the best utilization of the circular former with laminations with 5mm incremental width.

To further simplify the core making process, as cores needed to be made three at a time, a simple algorithm was devised to optimize the steel packets to just three widths. This was found to minimise constructional cost and yet provide a reasonable packing of the available space.

To further complicate matters, the circular winding former, made by a paper resin process, was only available in standard sizes from the manufacturer in Australia. It was therefore necessary to optimise both the core steel lamination widths with the available tube sizes.

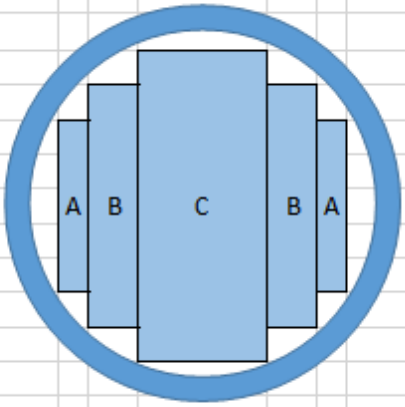

Item	Dimension	Lamination quantity
A width	25mm	16
B width	35mm	31
C width	45mm	88
Lamination thickness	0.23mm	
Former ID	50.8mm	
Former OD	53.8mm	
CSA core	1593mm^2	

Figure 7.1 Optimal core steel and insulating tube dimensions

The optimisation routine example shown in Chapter 5 show that to achieve the operational design current rating of $46.9A$ at $50Hz$, a core cross section of $1330mm^2$ (2 layer) and $1400mm^2$ (1 layer) is required to maintain a peak flux density design target of $0.8T$. At the maximum rated current of $49.4A$, $50Hz$, the core size would need to be $1500mm^2$ for the 1 layer design. Allowing for a little headroom the optimal arrangement was found for insulation tube and steel laminations as shown in Figure 7.1 The inside area of the insulating tube is $2,027mm^2$. Assuming a stacking factor of 95%, this would equate to a core area of $1,925mm^2$. The design core is $1593mm^2$ and therefore is nearly 79% of the total available area. There may be room for significant improvement in the stacking factor of this core, however it would require a wider range of lamination widths, and take considerably longer to build. A six width-of-steel construction may be optimal as well as readily achievable. The core section of Figure 7.1 was used for the 2 layer unit. It turns out that the 1 layer unit had a slightly reduced core cross section of $1470mm^2$ owning to an error during construction.

7.2.7 Operational temperature

In the standard model used in this analysis, the effects of temperature on the core and winding have been set to a value to enable direct comparison of laboratory measurements at room temperature. Short duration trials do not give time for significant temperature rise to occur and therefore the results of the model and experiment can be quickly compared.

Under normal operational conditions, components such as reactors would be expected to operate continuously and therefore the effect of temperature rise must be taken into account. The mechanism of temperature rise can be accounted for by the

increase in resistivity of conductors and core steel as their temperature increases. As the resistivity of the circuit elements increases, so too does the power dissipated by those elements, giving rise to further increase in resistivity and so on. There is a logarithmic increase in resistivity leading to an analogous rise in temperature. Eventually, a stable design will reach an equilibrium point where the dissipation of heat equals the generation of heat and no further temperature rise occurs.

However, if this equilibrium is not reached, the device may continue to heat at a greater rate and become thermally unstable, leading eventually to very high temperatures that may damage insulation and cause the device to malfunction.

For the prototype devices, the actual temperature rise is measured over a reasonable period of time in comparison with the Vinidhan unit. This data gives a very clear indication of the thermal performance of the devices.

To begin with, the designs were based on a temperature of 30°C to enable direct comparison with experimental data over a short run. Later, the measurements were repeated at the conclusion of a thermal trial conducted over several hours. The results demonstrate the importance of taking temperature rise into consideration.

7.2.8 Modelling the prototype inductors

The two prototypes are evaluated using the modified Steinmetz equivalent circuit model developed in Chapter 6. The construction parameters are defined in Table 7.1 for the 1 layer inductor and Table 7.3 for the 2 layer inductor. The results from the model calculations are presented in Table 7.2 for the 1 layer unit and Table 7.4 for the 2 layer unit.

7.3 RESULTS

Figures 7.4 and 7.5 graph the reactance and resistance against frequency for the modelled results and those obtained through measurement. There is a good correlation for reactance and a close correlation for resistance at lower frequencies.

Figure 7.4 shows the comparative reactance of the model and measurement of the 1 layer and 2 layer prototype inductors. There is a close agreement between the reactance values with the model being slightly lower than measurement in both cases.

Figure 7.5 shows the comparative resistance of the model and measurement of the 1 layer and 2 layer prototype inductors without taking the proposed end plate eddy current resistance into account. It will be shown in Figure 7.6 that the net effect of the increased resistance in terms of power loss is not that significant when compared to the commercial Vinidhan unit.

Table 7.1 Prototype 1 layer physical parameters

Parameter	Physical value
Peak flux density target	$0.8T$
Winding current density	$1.58A/mm^2$
Conductor width	$2.5mm$
Conductor height	$12.5mm$
Conductor insulation thickness	$0.03mm$
Winding width factor	1.165
Number of turns	71
Winding resistivity	$2.65 \times 10^{-8}\Omega m$
Number of winding layers	1
Core additional length	$6mm$
Core CSA	$1470mm^2$
Lamination thickness	$0.228mm$
Winding conductor density	$3000kg/m^3$
Core steel density	$7600kg/m^3$
Inter-winding gap	$0.5mm$
Winding former thickness	$1.5mm$
Winding conductor cost	$\$15/kg$
Core steel cost	$\$10/kg$
Operating temerapture	$30°C$

7.3.1 Increase of measured resistance

The measured resistance value is higher than the modelled resistance. This is thought to be due to a difference of construction between the prototype inductors used to develop the model and the project inductors which are held together by stainless steel plates welded to the ends of the core. This method of fixing the cores in position was found to dramatically reduce vibration between the cores - due to the intense fields between them in operation. The welding of the core ends was carried out by the TIG process with 316 stainless steel filler wire. The effect of the stainless steel plates was thought to be minimal at lower frequencies based on observable heating effect.

The end plates did however become much hotter above $550Hz$ and therefore the eddy current loss induced into these end plates will have a bearing on the measured resistance of the project inductors.

To account for this effect, a resistance increase factor is applied to the core loss and winding loss components of the resistance. The new calculated resistance is shown at the bottom of Table 7.2 and Table 7.4. The factor was adjusted until the resistance at each frequency align with those measured. In this way it can be seen that there is more unaccounted for resistance in the 1 layer inductor where the factor is 1.3 compared to the 2 layer inductor where the factor is 1.23.

Refer to Figure 7.2 showing the endplate of the 1 layer reactor, and Figure 7.3 of the

Table 7.2 Prototype 1 layer electrical performance for model vs measurement

Frequency	$50Hz$	$250Hz$	$350Hz$	$550Hz$	$650Hz$
Model results					
Inductance	$1.184mH$	$1.184mH$	$1.184mH$	$1.183mH$	$1.183mH$
Current	$46.4A$	$18.6A$	$6.6A$	$3.5A$	$3.0A$
Voltage developed	$18.4V$	$34.6V$	$17.3V$	$14.3V$	$14.7V$
Peak flux density	$0.794T$	$0.299T$	$0.107T$	$0.056T$	0.049
Winding dc resistance	0.0138Ω	0.0138Ω	0.0138Ω	0.0138Ω	0.0138Ω
Winding ac resistance	0.0004Ω	0.0109Ω	0.0214Ω	0.0529Ω	0.0739Ω
Core loss resistance	0.002Ω	0.0155Ω	0.0273Ω	0.0551Ω	0.0713Ω
Power loss per leg	$39.5W$	$13.9W$	$2.8W$	$1.5W$	$1.5W$
Quality factor	23.0	46.2	41.6	33.6	30.4
Core length	$220mm$	$220mm$	$220mm$	$220mm$	$220mm$
Core weight	$2.50kg$	$2.50kg$	$2.50kg$	$2.50kg$	$2.50kg$
Winding weight	$1.46kg$	$1.46kg$	$1.46kg$	$1.46kg$	$1.464kg$
Total weight 3-phase	$11.70kg$	$11.70kg$	$11.70kg$	$11.70kg$	$11.70kg$
Total cost	\$139.3	\$139.3	\$139.3	139.3	\$139.3
Cost per mH	\$117.70	\$117.70	\$117.70	\$117.70	\$117.80
Surface power density	$0.071W/cm^2$	$0.025W/cm^2$	$0.005W/cm^2$	$0.003W/cm^2$	$0.003W/cm^2$
Total reactance	0.40Ω	1.9Ω	2.6Ω	4.1Ω	4.8Ω
Total loss resistance	0.016Ω	0.040Ω	0.063Ω	0.122Ω	0.159Ω
Measured results					
Total reactance	0.40Ω	1.9Ω	2.6Ω	4.1Ω	4.9Ω
Total loss resistance	0.017Ω	0.047Ω	0.077Ω	0.155Ω	0.204Ω
Apply resistance factor	1.3	1.3	1.3	1.3	1.3
Total reistance with factor	0.017Ω	0.048Ω	0.077Ω	0.154Ω	0.203Ω

Table 7.3 Prototype 2 layer physical parameters

Parameter	Physical value
Peak flux density target	$0.8T$
Winding current density	$1.55A/mm^2$
Conductor width	$3.55mm$
Conductor height	$9.0mm$
Conductor insulation thickness	$0.03mm$
Winding width factor	1.22
Number of turns	80
Winding resistivity	$2.65 \times 10^{-8}\Omega m$
Number of winding layers	2
Core additional length	$0mm$
Core CSA	$1593mm^2$
Lamination thickness	$0.228mm$
Winding conductor density	$3000kg/m^3$
Core steel density	$7600kg/m^3$
Inter-winding gap	$2.0mm$
Winding former thickness	$0.5mm$
Winding conductor cost	$\$15/kg$
Core steel cost	$\$10/kg$
Operating temerapture	$30°C$

2 layer reactor. There is proportionally more end plate present on the 1 layer inductor than on the 2 layer unit. It is therefore proposed that the departure of measured resistance in the model is due to the contribution of eddy current resistance due to the end plates.

7.3.2 Power loss and temperature rise

Optimisation of partial core designs in terms of power loss and temperature rise has been a key design objective in this work. The optimisation work in Chapter 5 predicts that a 1 layer design will produce less power loss per winding surface area and will therefore run cooler as well as dissipating less heat. To test this, Experiment 11 was conducted to compare the power loss and temperature rise of the 1 and 2 layer project inductors, with the Vinidhan reactor.

7.4 EXPERIMENT 11 PART ONE - POWER LOSS COMPARISON

In the first part of the experiment, the power loss for each reactor is compared with the same current at each frequency as determined by the maximum permissible current the reactor shown in Table 6.16. The results are shown in Figure 7.6.

Table 7.4 Prototype 2 layer electrical performance for model vs measurement

Frequency	$50Hz$	$250Hz$	$350Hz$	$550Hz$	$650Hz$
Model results					
Inductance	$1.40mH$	$1.40mH$	$1.40mH$	$1.39mH$	$1.39mH$
Current	$49.5A$	$18.7A$	$6.6A$	$3.5A$	$3.0A$
Voltage developed	$21.7V$	$41.0V$	$20.3V$	$16.9V$	$17.3V$
Peak flux density	$0.767T$	$0.290T$	$0.103T$	$0.054T$	0.047
Winding dc resistance	0.0169Ω	0.0169Ω	0.0169Ω	0.0169Ω	0.0169Ω
Winding ac resistance	0.0011Ω	0.0283Ω	0.0555Ω	0.1368Ω	0.1910Ω
Core loss resistance	0.0017Ω	0.0151Ω	0.0271Ω	0.0572Ω	0.0755Ω
Power loss per leg	$48W$	$21.1W$	$4.3W$	$2.6W$	$2.6W$
Quality factor	22.3	36.4	30.9	22.8	20.1
Core length	$180mm$	$180mm$	$180mm$	$180mm$	$180mm$
Core weight	$2.10kg$	$2.10kg$	$2.10kg$	$2.10kg$	$2.10kg$
Winding weight	$1.87kg$	$1.87kg$	$1.87kg$	$1.87kg$	$1.87kg$
Total weight 3-phase	$11.90kg$	$11.90kg$	$11.90kg$	$11.90kg$	$11.90kg$
Total cost	\$150.0	\$150.0	\$150.0	150.0	\$150.0
Cost per mH	\$107.0	\$107.0	\$107.0	\$107.0	\$107.0
Surface power density	$0.089W/cm^2$	$0.039W/cm^2$	$0.008W/cm^2$	$0.005W/cm^2$	$0.005W/cm^2$
Total reactance	0.44Ω	2.19Ω	3.07Ω	4.82Ω	5.70Ω
Total loss resistance	0.023Ω	0.075Ω	0.115Ω	0.261Ω	0.346Ω
Measured results					
Total reactance	0.46Ω	2.25Ω	3.14Ω	4.91Ω	5.78Ω
Total loss resistance	0.023Ω	0.075Ω	0.115Ω	0.261Ω	0.346Ω
Apply resistance factor	1.23	1.23	1.23	1.23	1.23
Total reistance with factor	0.020Ω	0.070Ω	0.118Ω	0.256Ω	0.345Ω

Figure 7.2 1 layer reactor end plates

Figure 7.3 2 layer reactor end plates

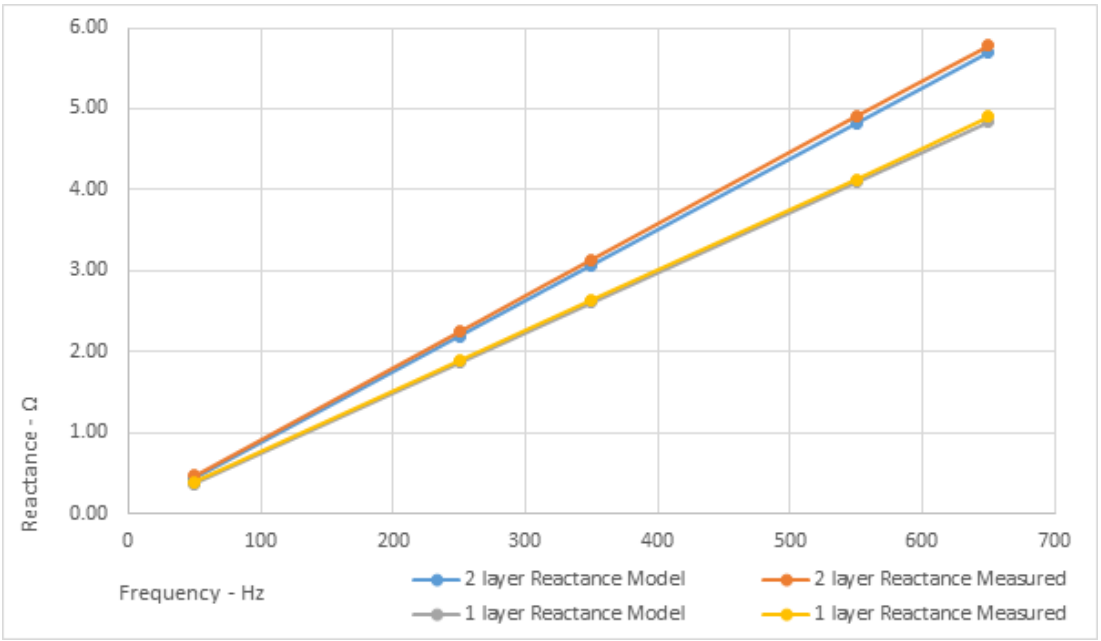

Figure 7.4 Reactance model and measurements vs frequency for 1 layer and 2 layer reactors

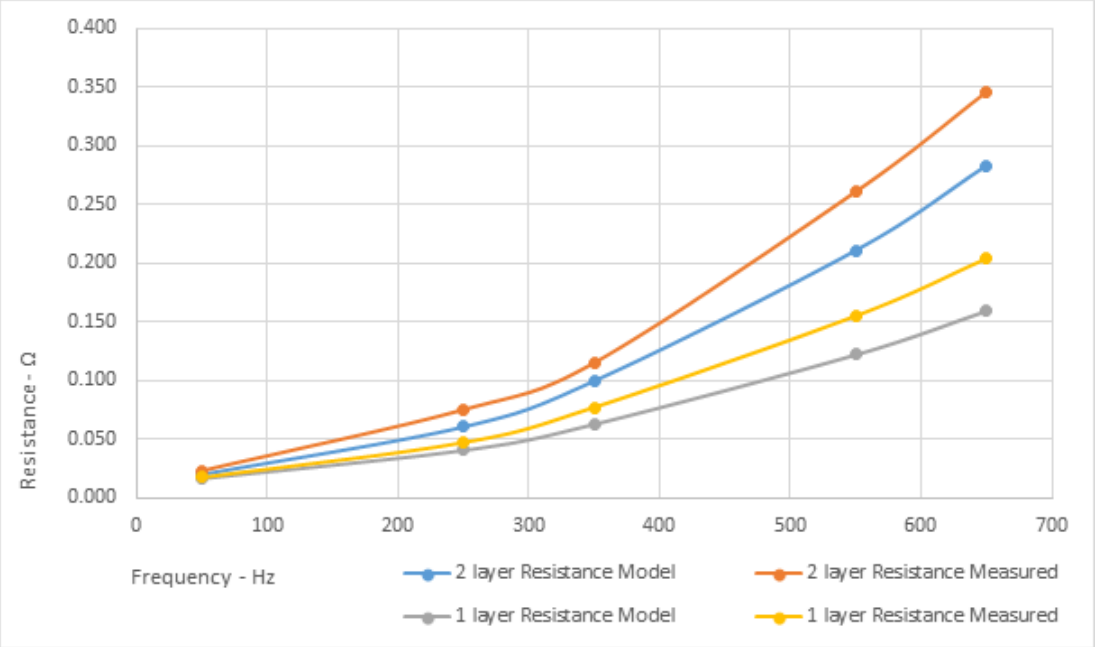

Figure 7.5 Resistance model and measurements vs frequency for 1 layer and 2 layer reactors

Table 7.5 Prototype simultaneous test current

Frequency	$50Hz$	$250Hz$	$350Hz$
Current	$50.4A$	$10.1A$	$7.2A$

The resistance in each reactor has been normalised as though each reactor has the same inductance to enable comparison of power loss. The Vinidhan reactor produces less power loss at 50Hz but dissipates more power at harmonic frequencies. The 1 layer prototype inductor offers improved performance compared to its 2 layer counterpart.

7.5 EXPERIMENT 11 PART TWO - TEMPERATURE RISE

To enable comparison of the test reactors it is necessary to inject them with the same current simultaneously so that experimental conditions are the same. Refer to Figure 7.7 for the experimental setup. The reactors are connected in series and physically separated so as not to influence each other as shown in Figure 7.9.

The test current was produced by the Ametek 3-phase programmable power source. A fundamental current is set by programming the required voltage to generate the current. Harmonic currents can be produced by adjusting the harmonic voltage as a percentage of the fundamental voltage. Due to this configuration it was not possible to produce harmonic voltages higher than the fundamental voltage. Refer to Table 7.5 for the simultaneous test currents applied.

The total power for all three inductors was measured as 520W at the start of the trial and 660W at the trial conclusion. Over a $4.5hr$ period the inductor temperature

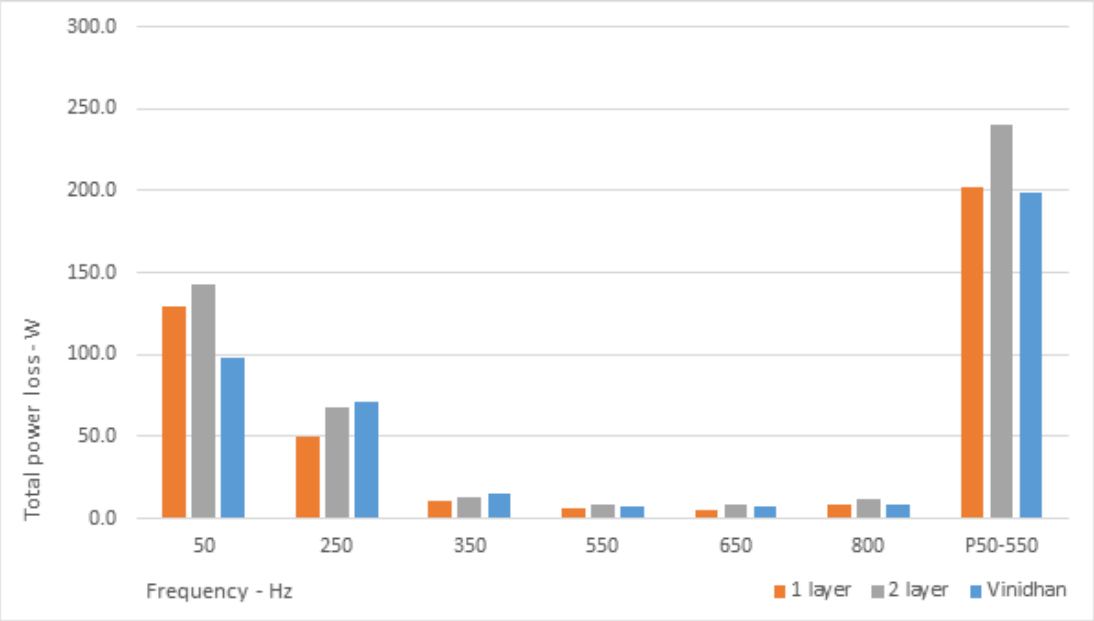

Figure 7.6 Power loss vs harmonic order for 1 layer, 2 layer and Vinidhan reactors

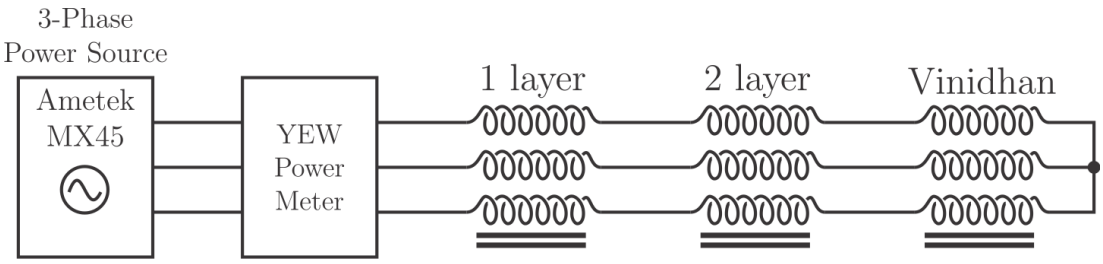

Figure 7.7 Experimental setup connection for temperature rise

Table 7.6 Vinidhan measured surface power density

Frequency	$50Hz$	$250Hz$	$350Hz$
Measured results			
Current	$50.4A$	$10.1A$	$7.2A$
Total power loss	$97.7W$	$20.0W$	$16.9W$
Surface power density	$0.057W/cm^2$	$0.012W/cm^2$	$0.010W/cm^2$
Total power	$135W$		
Surface power loss density	$0.079W/cm^2$		

Table 7.7 Prototype 1 layer modelled surface power density

Frequency	$50Hz$	$250Hz$	$350Hz$
Model results			
Current	$50.4A$	$10.1A$	$7.2A$
Total power loss	$122.7W$	$12.6W$	$9.6W$
Surface power density	$0.074W/cm^2$	$0.008W/cm^2$	$0.006W/cm^2$
Apply resistance factor	1.3	1.3	1.3
Power loss with factor	$129W$	$15W$	$12W$
Total power loss	$155W$		
Surface power loss density	$0.094W/cm^2$		

Table 7.8 Prototype 2 layer modelled surface power density

Frequency	$50Hz$	$250Hz$	$350Hz$
Model results			
Current	$50.4A$	$10.1A$	$7.2A$
Total power loss	$147W$	$19.2W$	$16.2W$
Surface power density	$0.092W/cm^2$	$0.012W/cm^2$	$0.010W/cm^2$
Apply resistance factor	1.23	1.23	1.23
Power loss with factor	$152W$	$23W$	$19W$
Total power loss	$194W$		
Surface power loss density	$0.122W/cm^2$		

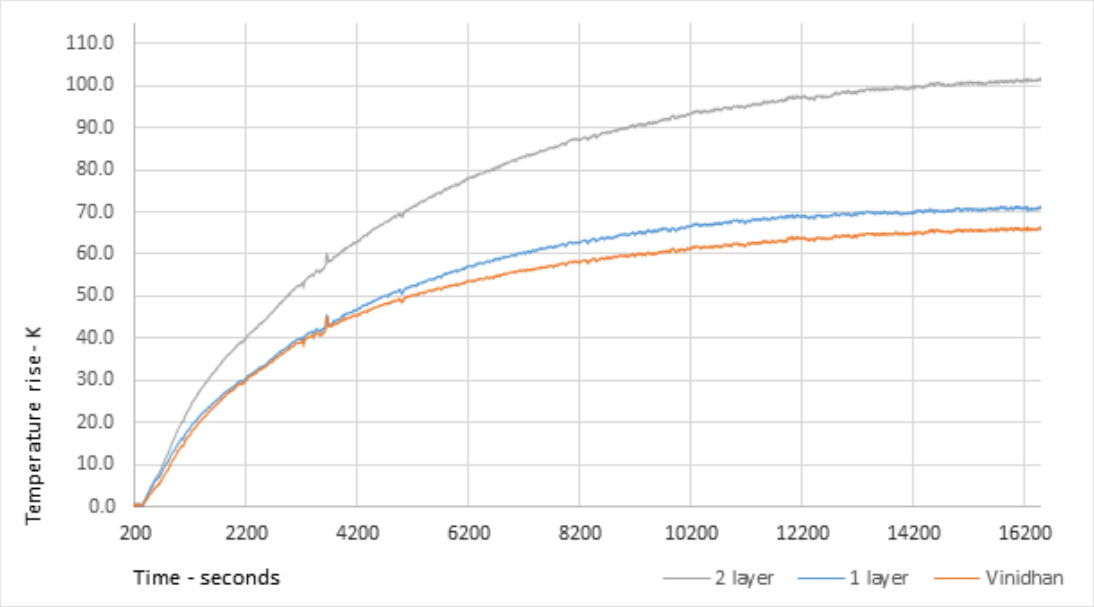

Figure 7.8 Temperature rise vs time over $4.5hrs$ for 1 layer, 2 layer and Vinidhan reactors

Table 7.9 Comparison of reactor power, surface power density and temperature rise

Parameter	Vinidhan	1 layer	2 layer
Total power loss	$135W$	$155W$	$194W$
% power increase cf Vinidhan	0%	15%	44%
Surface power density	$0.079W/cm^2$	$0.094W/cm^2$	$0.122W/cm^2$
% surface power density increase cf Vinidhan	0%	18%	54%
Temperature rise	$66K$	$71K$	$102K$
% temperature rise cf Vinidhan	0%	8%	55%

rise was such as to generate an addition $140W$ over the three units which suggests a 20 to 30% increase in power dissipation due to increased resistance in the devices.

The modelled data is now recalculated based on these currents to obtain the power loss data and surface power density. Refer to Tables 7.6, 7.7 and 7.8.

7.5.1 Discussion

The power, surface power density and temperature rise for the 1 layer and 2 layer reactors are compared to the Vinidhan unit in terms of percentage increase in Table 7.9. Although the harmonic currents are not as high as the prescribed maximum levels, the relative temperature rise and surface power density are comparable to the total estimate of power loss increase between the devices.

Table 7.9 is repeated in Table 7.10 with the projected impact on power loss with

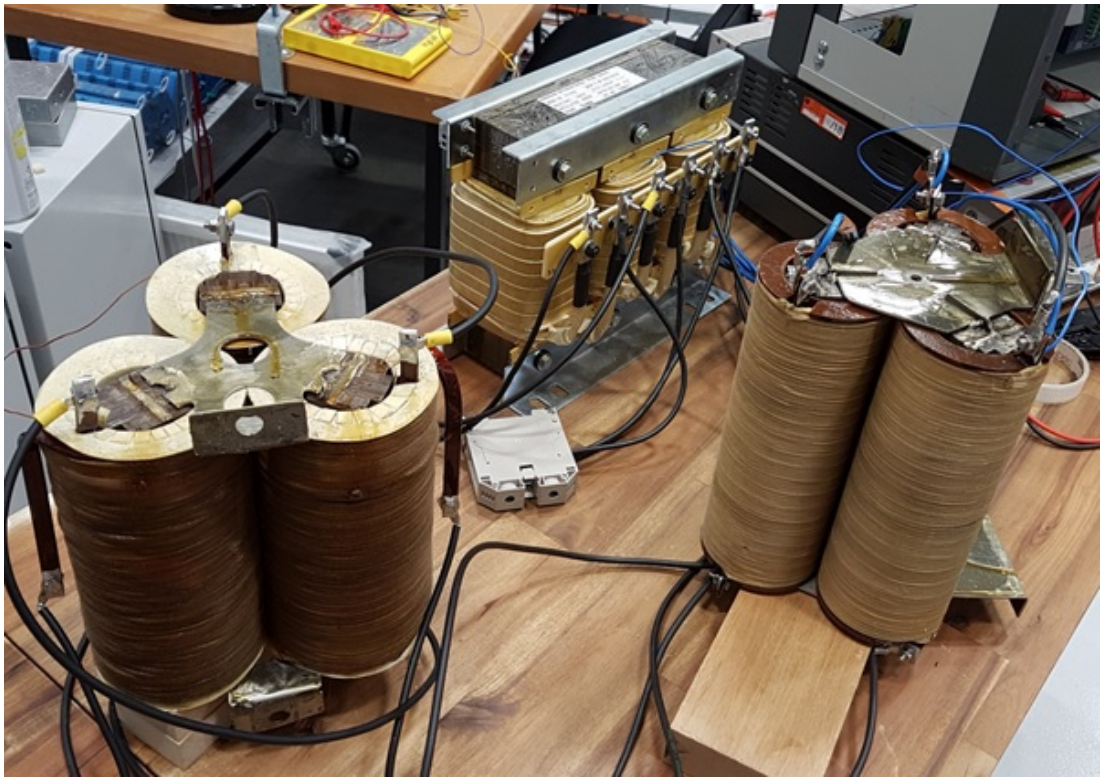

Figure 7.9 Reactors under temperature rise test

the full prescribed harmonic current.

The projections in Table 7.10 show a significant further temperature rise may occur at maximum rated conditions. Based on an assumed ambient temperature of 40°C under operational conditions, the temperature of both the Vinidhan and 1 layer unit would exceed 130°C, which is generally regarded as above acceptable levels. Thermal cut-out devices embedded in commercial reactors are often set to 125°C and would switch off the power to the device above that temperature.

It must also be considered that the temperature rise data taken was based on free air conditions allowing for natural convection to take heat away from the device. It is usual for reactors in these applications to have forced air cooling and therefore operational temperatures would be lower.

Overall the 1 layer partial core device has comparable performance to the Vinidhan reactor in terms of temperature rise at maximum rated conditions including harmonics. At lower levels of harmonic current, the Vinidhan reactor runs cooler due to having lower loss at $50Hz$. The 2 layer reactor would not operate at acceptable temperature rise levels unless there was forced cooling.

Table 7.10 Comparison of reactor power, surface power density and temperature rise at maximum rated conditions

Parameter	Vinidhan	1 layer	2 layer
Total power loss	$190W$	$189W$	$248W$
% power increase cf Vinidhan	41%	41%	84%
Surface power density	$0.112W/cm^2$	$0.114W/cm^2$	$0.156W/cm^2$
% surface power density increase cf Vinidhan	41%	44%	97%
Temperature rise	$93K$	$95K$	$130K$
% temperature rise cf Vinidhan	41%	44%	97%

Table 7.11 Vinidhan linearity performance

Voltage applied	Current	Inductance	% inductance	% Current	Peak flux density
$14.8V$	$38.27A$	$1.188mH$	101%	82.1%	$0.9T$
$16.29V$	$45.8A$	$1.176mH$	100%	98.3%	$1.0T$
$19.75V$	$353.2A$	$1.182mH$	100%	114.2%	$1.2T$
$22.79V$	$61.7A$	$1.176mH$	100%	132.4%	$1.4T$
$25.57V$	$69.7A$	$1.168mH$	99%	149.6%	$1.6T$
$29.1V$	$80.1A$	$1.156mH$	98%	171.9%	$1.8T$
$32.55V$	$91.2A$	$1.136mH$	97%	195.7%	$2.0T * minor$
$36.44V$	$113.6A$	$1.021mH$	87%	243.8%	$2.3T*$

7.5.2 Comparison of linearity

Apart from stable thermal performance, the quality of a reactor may be compared by its linearity at over-current conditions. The Vinidhan, 1 layer and 2 layer reactor are compared in Tables 7.11, 7.12 and 7.13 respectively. *Core saturation noted by the appearance of triplen harmonic current flowing in addition to fundamental current.

Table 7.12 1 layer linearity performance

Voltage applied	Current	Inductance	% inductance	% Current	Peak flux density
$15.2V$	$40.7A$	$1.194mH$	100%	87.3%	$0.7T$
$20.15V$	$53.86A$	$1.191mH$	100%	115.6%	$0.9T$
$25.01V$	$66.8A$	$1.192mH$	100%	143.3%	$1.1T$
$30.12V$	$80.9A$	$1.185mH$	100%	173.6%	$1.3T$
$35.0V$	$92.3A$	$1.207mH$	101%	198.1%	$1.5T*$
$40.15V$	$105.6A$	$1.210mH$	102%	226.6%	$1.7T*$

Table 7.13 2 layer linearity performance

Voltage applied	Current	Inductance	% inductance	% Current	Peak flux density
$14.83V$	$33.11A$	$1.426mH$	100%	71.1%	$0.5T$
$20.3V$	$45.49A$	$1.421mH$	100%	97.6%	$0.7T$
$25.12V$	$56.3A$	$1.420mH$	100%	120.8%	$0.9T$
$30.04V$	$67.5A$	$1.417mH$	100%	144.8%	$1.1T$
$35.04V$	$78.5A$	$1.421mH$	100%	168.5%	$1.2T$
$40.0V$	$88.8A$	$1.434mH$	101%	190.6%	$1.4T * minor$
$45.06V$	$98.0A$	$1.464mH$	103%	210.3%	$1.6T*$
$50.0V$	$107.7A$	$1.478mH$	104%	231.1%	$1.8T*$

7.6 DISCUSSION

The Vinidhan reactor can tolerate nearly $2 \times I_N$ with only a very faint sign of saturation in the current drawn by the reactor. At this point the estimated peak flux density in the core is $2T$ and the inductance of the reactor is around the 95% mark. This would be regarded as good linearity performance against the benchmark of $1.8 \times I_N$. Electronicon

1 layer and 2 layer devices appear to show signs of saturation at lower flux density levels which is consistent with observed axial flux levels being much higher toward the centre of the partial core length. An unusual feature of the partial core performance is the apparent lack of reduction of inductance at higher over-current. In fact the results appear to show the inductance increases at higher over-current. This effect was not examined further at this time, however it may result from the uneven distribution of axial flux in the core and its behaviour at higher flux densities where saturation occurs toward the centre of the core length.

As the measure of linearity performance is defined as the percentage over-current at which the inductance of the reactor falls to 95% of its rated value; as this had not occurred at over 230% of rated current, it is concluded the partial core inductors tested have excellent linearity performance.

7.7 COMPARISON OF PHYSICAL ATTRIBUTES

7.7.1 Weight and materials cost

Refer to Table 7.14 for a comparison of weight and cost for the three reactors. Two costing scenarios are compared with different costs per weight of steel and aluminium winding conductor. It is not known what the actual costs for materials are in a large scale production environment, however these figures have been estimated based on the purchase price of the Vinidhan reactor.

It can be seen that in terms of cost per unit inductance, the 2 layer reactor has the best performance overall. The 1 layer unit is not very different, and depending on the

Table 7.14 Comparison of reactor weight and material cost

Parameter	Vinidhan	1 layer	2 layer
Core weight	$16.8kg$	$7.4kg$	$6.5kg$
Winding weight	$2.84kg$	$4.4kg$	$5.5kg$
Total weight	$19.64kg$	$11.7kg$	$11.9kg$
Core cost at \$10/kg	\$168	\$73.7	\$65.4
Winding cost at \$15/kg	\$42.6	\$65.7	\$81.9
Total cost	\$210.6	\$139.3	\$147.3
Total cost per mH	\$178.5	\$117.1	\$103.8
Core cost at \$5/kg	\$84.0	\$36.8	\$32.7
Winding cost at \$10/kg	\$28.4	\$43.8	\$54.6
Total cost	\$112.4	\$80.6	\$87.3
Total cost per mH	\$95.3	\$67.7	\$61.5

actual cost structure of materials, may be similar to the 2 layer unit if steel is much less expensive than winding conductor.

Overall, it is estimated that the 1 layer reactor offers around 40% reduction in weight and a 30% reduction in materials cost compared to the Vinidhan reactor.

It can be further seen that there is a significant reduction in total weight of the 1 and 2 layer reactors of around 40% compared to Vinidhan.

7.7.2 Physical size

The pictures in Figures 7.10 and 7.11 provide a good comparison of the relative size of the devices. Both footprint and height are important considerations when constructing equipment incorporating reactors. A reduced footprint enables greater equipment density for a given cabinet size, however the height of the device must also be considered if devices are to be stacked vertically. The 1 layer reactor offers the smallest footprint, however is taller than the Vinidhan reactor thus limiting the number of units that may be stacked vertically in a cabinet. Lying the 1 layer unit on its side provides a similar form factor to the Vinidhan reactor but with less height.

Another factor that must be taken into consideration with partial core reactors such as these, is the emanation of stray magnetic fields at the core ends and along the length of the device. At the flux densities used in these reactors, a clearance to neighbouring metal of $50mm$ right around the device was sufficient to minimise the effects of stray magnetic fields being too significant in terms of eddy current heating and induced vibration in steel.

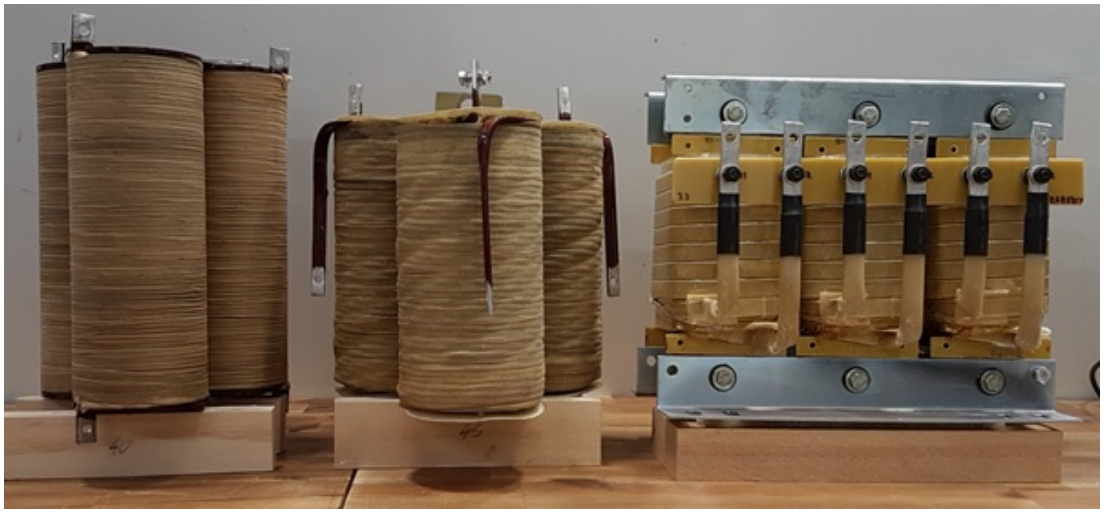

Figure 7.10 Front view of 1 layer, 2 layer and Vinidhan reactors

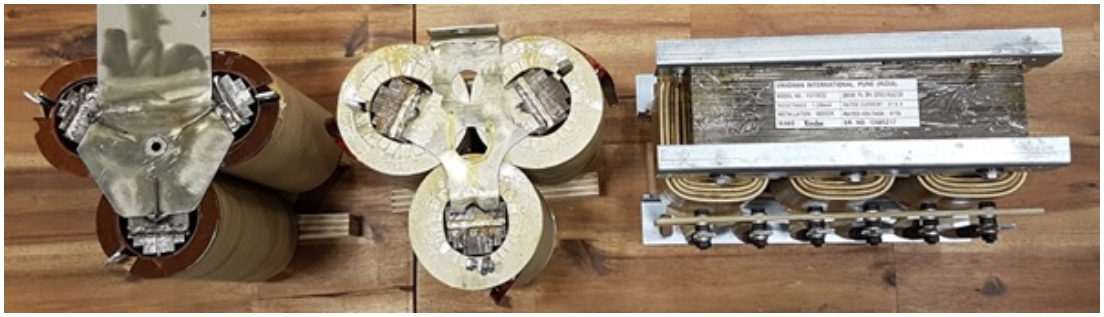

Figure 7.11 Top view of 1 layer, 2 layer and Vinidhan reactors

It was also found necessary to partition adjacent reactors with a steel barrier to prevent interaction of the magnetic fields which can cause unpredictable changes of inductance and temperature rise.

Overall, by the time clearances for stray fields are considered, the physical space required for the 1 layer partial core reactor is similar to the Vinidhan unit.

7.8 CONCLUSION TO CHAPTER 7

3-phase, 1 layer partial core inductors with aluminium windings can provide comparable thermal performance to commercially built reactors when maximum operational conditions are the benchmark of performance. They are less efficient at mains frequency however, and it can be shown that any significant increase in conductor size to compensate for this, may make the design less viable. The partial core reactor has reduced loss at harmonic frequencies compared to the full core reactor tested.

The partial core reactor significantly reduces the weight of core steel by 56%, but has increased winding weight of 55%. An overall reduction of weight in the order of 40% can be achieved. Depending on the cost structure of the materials, the overall cost benefit is in the order of 30%.

The partial core inductor shows excellent linearity performance and may even have a slight increase of inductance at the point of observable core saturation. Further research into this effect would be required however to confirm the mechanism at play.

Spatially, the partial core reactor occupies a smaller volume than the full core reactor, but consideration must be made for stray magnetic field effects which can cause eddy current heating and vibration in neighbouring metal. When appropriate clearances are provided, the partial core reactor occupies a similar spatial volume.

The partial core reactor must also be shielded from neighbouring reactors to prevent interaction of magnetic fields which may lead to changes in device inductance and additional heating. Refer to Figure 7.12 for a picture of a proposed mounting arrangement that achieves shielding of the 1 layer partial core reactor.

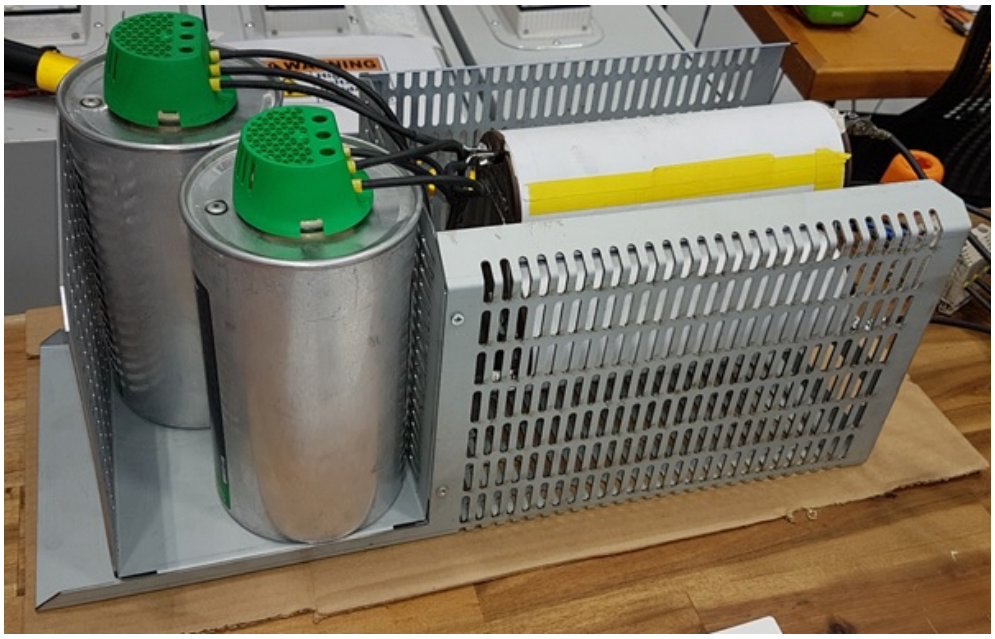

Figure 7.12 Magnetic shielding of the 1 layer reactor with capacitors mounted to the left

Chapter 8

CONCLUSION & FUTURE WORK

8.1 SUMMARY & KEY ACHIEVEMENTS

An optimal design for a 3-phase partial core reactor has been modelled and tested showing that such designs may be feasible. Although the partial core reactor dissipated 32% more heat at the fundamental frequency, if the reactor were to operate at maximum permissible conditions of harmonic distortion, the partial core reactor would dissipate less power than the commercial unit tested and would therefore operate at a lower temperature.

This suggests that partial core technology may be ideally suited to power filtration applications. Further optimisation of the design is possible, and therefore the conclusion of this work is that partial core technology may produce viable designs in power reactors.

The inductive reactance model for a 1-limb partial core reactor was modified to enable 3-limb, 3-phase devices to be modelled depending on the separation of the cores. The units constructed were re-modelled with the fully developed model and were in good agreement with the measured results.

An approach to modelling the winding ac loss resistance for a 3-phase partial core reactor was presented which gave good results in the trial units of Chapter 5, but were not a close fit in the project inductors tested. It is believed that the attachment of the cores by means of a welded stainless steel plate has given rise to the discrepancy and therefore it would be necessary to take such additional metal into consideration in the model, or find a different approach for securing the cores.

A simple estimation of orthogonal core loss resistance was also presented to further correct the circuit theory approach. While this approach has only been tested with a few different windings, the results were acceptable from a design point of view and would enable similar sized designs to be modelled with confidence.

An optimisation routine was developed to enable a range of inductors with incremental winding turns to be modelled based on keeping the core flux density to a constant value. The advantage of this approach is that the actual performance of an inductor can be viewed as the turn count is incremented until the correct inductance is

achieved. When the design inductance is achieved, the number of turns, core length, and core cross sectional area are calculated for a conductor of a given size. Therefore using the formulations developed from circuit theory, an estimation of power loss and device weight can be made. In this way, windings of particular sizes and shapes, material and number of layers can be compared to confirm the most suitable target design. With an optimal target design achieved, it is then possible to develop the working design with the available materials using the Transformer Reverse Design approach.

In the application of the project inductor, an aluminium winding conductor of $2.5mm$ width, wound in a single layer was shown to be the most efficient approach to constructing the partial core inductor to the target specification.

The work shows that the optimal cost-efficient design of a partial core inductance is dependent on the width of the winding conductor.

8.2 REVIEW OF OBJECTIVES

The objective was to apply partial core technology to a 3-phase inductor application and find the factors that influence optimal design.

A significant amount of experimental work has shown the typical behaviour of partial core inductors applied in 3-phase applications and the parameters that govern performance have been identified and modelled.

An optimisation routine was investigated and shown to produce results that were consistent with the model predictions. The modelling enables designs to be evaluated for partial core inductors in the range of sizes examined in this thesis.

8.3 CRITIQUE

The main critique of this work is that the models were developed substantially around the two sizes of devices tested. A third size device was tested and the modelled resistance was found to depart from measured results, although the inductance was in good agreement.

An approach to estimating winding *ac* resistance was presented without theoretical justification. The approach may produce useful estimates for the windings examined but requires further investigation to establish its theoretical validity.

The estimation of orthogonal core loss resistance is only approximate and relates mainly to the size of devices built. It is not by any means a complete picture of core behaviour under the influence of orthogonal flux components and further work is required in this area.

Modelling of the magnetising reactance for 3-phase partial core inductors was developed based on modifying the reluctance term applied to the core cross-sectional

area only, and did not consider the core length. As most of the designs built and tested were of similar length, the results were good but it cannot be concluded that this approach can be scaled-up to devices of greater length.

Despite the lack of theoretical justification for determining the new circuit theory components used in this work, a solution was found that produced a useful practical device. Empirical deduction may be justifiable on the grounds that useful designs may be achieved, however a significant effort is still required to validate new designs until confidence is reached in the proposed model.

8.4 FUTURE WORK

There are a number of areas where the research could be continued. A short description of these follows.

8.4.1 Model

The formulation of 3-phase magnetising and leakage reactance and resistance elements in the circuit theory model have proven to be useful for the range of devices tested. It would be useful to know if such formulations hold true for devices of different sizes and in particular, in the length of devices.

A comparison of FEA simulations with the circuit theory model and other devices may lead to further refinements in the magnetising functions associated with the magnetising and leakage reactance formulated by circuit theory. Such enhancements to circuit theory provide for rapid calculation in the optimisation routine process.

The winding loss resistance and orthogonal core loss resistance were tested over a small range of core and winding sizes. Once again, a more complete theoretical understanding of the geometric relationship between orthogonal flux and the effect on eddy current losses over a wider range of device sizes would enable a more complete picture of device behaviour.

8.4.2 Core

The research of the partial core inductors in this work used only flat steel laminations in the core. It is a well-established fact that where significant leakage fields exist around a core, a core with radial laminations may help to reduce core heating and power loss.

Testing inductors with radially laminated cores may reduce heating in the core but it is unclear if this would reduce heating in the winding, particularly in 3-phase arrangements. It is possible that radial cores may make winding loss worse due to the presence of more intense or more complete radial fields around each core. An investigation of these effects would prove useful.

Significant stray flux emanates around the ends of the cores. Operation of a partial core reactor in close proximity to any metal will cause unwanted heating, vibration and further power loss in the system. An investigation of shielding arrangements may be necessary to limit stay flux effects.

There may also be other lamination orientations that are better suited to the triangular arrangement of 3-phase windings.

8.4.3 Windings

With edge wound rectangular conductor there is deformation in the conductor width when it is bend around the former leading to a small winding creep along the length of the winding. This is due to a thickening of the conductor at the former edge. A method for calculating the creep of the winding would prove useful to better estimate the total winding length. At present the model assumes the top of the conductor stretches, and the bottom of the conductor expands about the centre line of the conductor height.

A more complete solution is required taking into account the mechanical properties of the conductor and possibly the insulation. There may be an optimal conductor shape that minimises this conductor width growth.

8.4.4 Mounting of the windings and cores

The welded stainless steel core brackets provide a solid means of securing the cores and thus minimise vibration and noise, however they introduce greater eddy current heating in the device that may be problematic in terms of controlling temperature rise.

Other methods of mounting the cores to minimise eddy current losses, and yet maintain the required rigidity would be worthwhile examining.

8.4.5 Temperature rise estimation

A method for estimating the temperature rise was presented based on the total power loss of the inductor and the effective surface area of the winding. An iterative calculation was performed until the increased heating due to temperature rise stabilised. Further work on a logarithmic function producing the temperature rise would enable better estimates of device performance to be calculated.

Appendix A

EXPERIMENTAL TECHNIQUE FOR MEASURING AC RESISTANCE OF INDUCTORS

A.1 INTRODUCTION

Measuring ac resistance in power inductors is often difficult due to distinguishing very small resistive values from much higher reactance values. Four techniques have been tested as listed in Figure A.1.

Technique	Equipment	Pros	Cons	Comment
Direct measurement	HP impedance analyser	Simple test at any frequency	Maximum applied voltage 1V	Best to test power inductors at rated voltage
Phase shift measurement	Agilent scope	None	Poor resolution of phase shift	A tiny shift in phase gives rise to a big deviation in resistance
Series resonant method	Capacitor to resonate at prescribed frequency, Agilent scope	Reasonable accuracy with good quality capacitors	Laborious setup procedure	Scope can detect a null phase more easily at series resonance and therefore impedance = resistance
Precision power measurement	YEW power meter	Simple test at rated voltage – good accuracy	None	Power and current measurements enable resistance to be calculated

Figure A.1 Resistance measurement methods trialled

Of the techniques trialled in Figure A.1, the YEW precision power meter has proven to be the easiest and most accurate way to obtain equivalent series *ac* resistance values at rated voltage. To verify the accuracy of this technique, the following experiment was conducted.

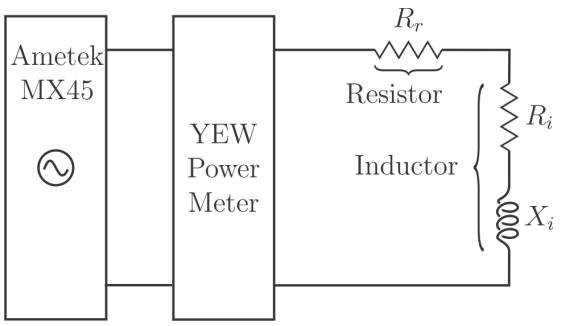

Figure A.2 Experimental circuit for the resistor and inductor trial

A.2 EXPERIMENT 12 - DIFFERENTIATING RESISTANCE AND REACTANCE

A precision resistor and an inductance are each measured individually and connected in series to compare the power measurements obtained by the YEW power meter. The measurements are taken over a range of frequencies at constant current of $40A$, and at *dc* with a Megabras MPK254 micro-Ohmmeter. Refer to Figure A.2 for the test configuration.

A.2.1 Apparatus

1. Power source: Ametek MX45 3-phase power frequency generator
2. Power meter: YEW digital ac power meter Type 2503
3. Standard Resistor: Elliot Bros London (RI 6) Nameplate rating 0.01Ω, $60Amps$
4. Inductor: Single leg of partial core inductor P6

A.2.2 Results

Refer to Table A.1 for measurement results.

In Figure A.3 the Difference trace refers to the difference between the Inductor in series with resistor trace, and the Inductor trace. The difference between these two curves should be equal the the constant value of the resistor as this is what is giving rise to the difference. The Difference plot is very close to the Resistor plot up to 350Hz and above that there is a very small increase in resistance for the Difference measurement. This suggests that the power meter is able to discern the very small added value of the resistance compared to the significantly higher reactance as well as the increase in *ac* resistance produced by the inductor.

A.3 CALCULATION OF RESISTANCE AND INDUCTANCE

The impedance is calculated by $V/I = Z(\Omega)$
The resistance is calculated by $P/I^2 = R(\Omega)$

Table A.1 YEW test results for resistance and reactance vs frequency

Frequency Resistor	dc	$25Hz$	$50Hz$	$150Hz$	$250Hz$	$350Hz$	$550Hz$	$800Hz$
Resistance R	0.0105Ω	0.0105Ω	0.0105Ω	0.0105Ω	0.0105Ω	0.0105Ω	0.0105Ω	0.0105Ω
Inductor								
Series equiv. res. Ri	0.01477Ω	0.0152Ω	0.0154Ω	0.0236Ω	0.0380Ω	0.0560Ω	0.0997Ω	0.1812Ω
Series equiv. react. Xi	-	0.1485Ω	0.2956Ω	0.8887Ω	1.4747Ω	2.0574Ω	3.2127Ω	4.6588Ω
Resistor and Inductor								
Series equiv. res. Rri	0.0248Ω	0.0259Ω	0.0259Ω	0.0341Ω	0.0492Ω	0.0672Ω	0.1122Ω	0.1963Ω
Series equiv. react. Xi	-	0.1500Ω	0.2963Ω	0.8887Ω	1.4746Ω	2.0559Ω	3.2110Ω	4.6555Ω
Difference								
Rri - Ri - R	−0.0005Ω	0.0007Ω	0.0005Ω	0.0005Ω	0.0012Ω	0.0012Ω	0.0025Ω	0.0051Ω
Difference as a % of Rri								
Error %	−1.8%	2.6%	1.9%	1.6%	2.5%	1.8%	2.2%	2.6%

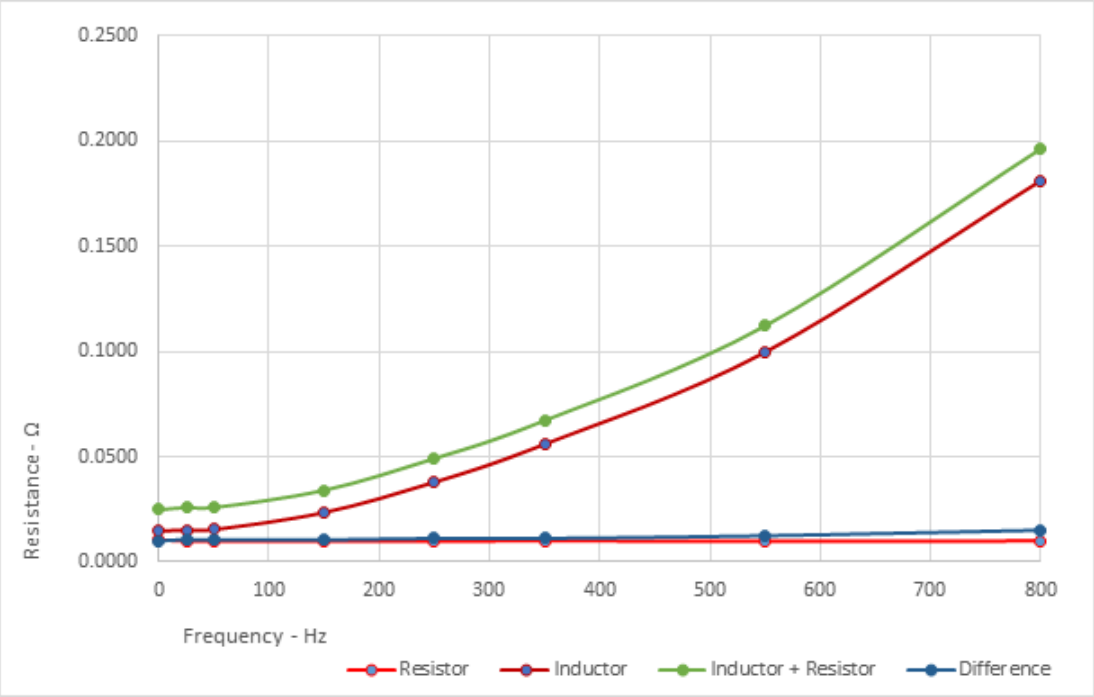

Figure A.3 Test resistor, inductor and combination vs frequency

The reactance is calculated by $(Z^2 - R^2)^{0.5} = X(\Omega)$
The inductance is calculated by $X/\omega = L(H)$

A.4 CONCLUSION

Overall the influence of the inductive reactance causes less than 3% measurement deviation for the actual resistance of the resistor when combined in series with the inductor. For the purposes of resistance measurements in this work, which are mainly comparative, this method gives a sufficiently accurate and straightforward means of determining the *ac* resistance of a device at test frequencies up to the 800Hz limit of the Ametek MX45 source.

Appendix B

MANUFACTURERS DATA

A data sheet for the Vinidhan 33kVAr reactor is provided in Figure B.1. An analysis of the data is presented in Figure B.2.

As discussed in Chapter 6, the manufacturer's data is modelled by the system model developed in this work, and the essential features of the reactor in terms of inductance agree with the model. The rated maximum permissible current may be slightly low when harmonic contribution is included, however the 50Hz rating agrees with the model.

The significant level of harmonic distortion imposed in this work may be considered to be an onerous assessment of the maximum permissible levels that may be occur in practice. However, experience with local network supplies where THDv levels have exceeded 10% suggest that such a tolerance may be warranted.

In the case of levels of harmonic distortion approaching the maximum permissible levels under the Standard, it may be reasonable to expect power dissipation of reactors to double as the results of Chapter 6 have shown.

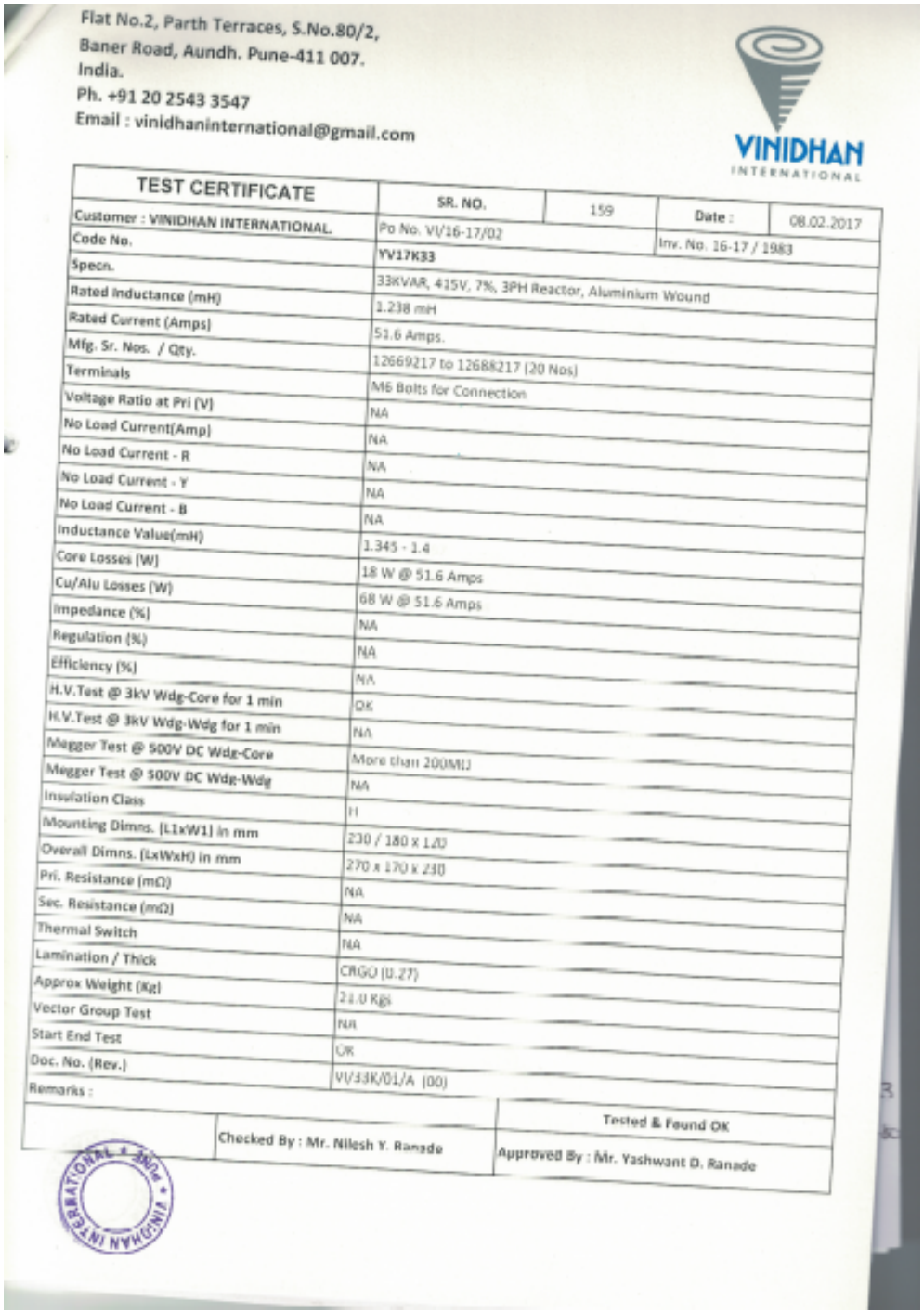

Flat No.2, Parth Terraces, S.No.80/2,
Baner Road, Aundh. Pune-411 007.
India.
Ph. +91 20 2543 3547
Email : vinidhaninternational@gmail.com

VINIDHAN INTERNATIONAL

TEST CERTIFICATE	SR. NO.	159	Date :	08.02.2017
Customer : VINIDHAN INTERNATIONAL.	Po No. VI/16-17/02		Inv. No. 16-17 / 1983	
Code No.	YV17K33			
Specn.	33KVAR, 415V, 7%, 3PH Reactor, Aluminium Wound			
Rated Inductance (mH)	1.238 mH			
Rated Current (Amps)	51.6 Amps.			
Mfg. Sr. Nos. / Qty.	12669217 to 12688217 (20 Nos)			
Terminals	M6 Bolts for Connection			
Voltage Ratio at Pri (V)	NA			
No Load Current(Amp)	NA			
No Load Current - R	NA			
No Load Current - Y	NA			
No Load Current - B	NA			
Inductance Value(mH)	1.345 - 1.4			
Core Losses (W)	18 W @ 51.6 Amps			
Cu/Alu Losses (W)	68 W @ 51.6 Amps			
Impedance (%)	NA			
Regulation (%)	NA			
Efficiency (%)	NA			
H.V.Test @ 3kV Wdg-Core for 1 min	OK			
H.V.Test @ 3kV Wdg-Wdg for 1 min	NA			
Megger Test @ 500V DC Wdg-Core	More than 200MΩ			
Megger Test @ 500V DC Wdg-Wdg	NA			
Insulation Class	H			
Mounting Dimns. (LIxW1) in mm	230 / 180 x 140			
Overall Dimns. (LxWxH) in mm	270 x 170 x 230			
Pri. Resistance (mΩ)	NA			
Sec. Resistance (mΩ)	NA			
Thermal Switch	NA			
Lamination / Thick	CRGO (0.27)			
Approx Weight (Kg)	21.0 Kgs			
Vector Group Test	NA			
Start End Test	OK			
Doc. No. (Rev.)	VI/33K/01/A (00)			
Remarks :			Tested & Found OK	
	Checked By : Mr. Nilesh Y. Ranade		Approved By : Mr. Yashwant D. Ranade	

VINIDHAN INTERNATIONAL * PUNE *

Figure B.1 Manufacturer's data for 33kVAr reactor

Vinidhan International	Term	Units	Manufacturer Data	Thesis Model
Make			Vinidhan International	
Model			YV17K33	
Reactive power rating (detuned)	Q_{LC}	kVAr	33	33.5
Winding material			Aluminim	
Total weight		kg	21	
Rated ambient temperature		°C	Not specified	
Insualtion class			Not specified	
Thermal cutout temperature		°C	Not specified	
System voltage	U_N	V	415	415
System frequency	f	Hz	50	50
% reactance	p	%	7	7.03
Inductance per leg	L_N	mH	3 x 1.238	3 x 1.238
Inductance tolerance between legs		%	Not specified	
Capacitor value	C	µF	3 x 191.7	3 x 191.7
Fundamental rated current	I_N	A	Not specified	46.6
Linearity at current multiple of I_N	L_{LIN}		Not specified	
Maximum rms current*	I_{eff}	A	51.6	54.5 (51.2A, 50Hz)
% of I_N x I_1	I_1	%	Not specified	110.0
% of I_N x I_3	I_3	%	Not specified	3.8
% of I_N x I_5	I_5	%	Not specified	36.9
% of I_N x I_7	I_7	%	Not specified	13.3
% of I_N x I_{11}	I_{11}	%	Not specified	4.8
% of I_N x I_{13}	I_{13}	%	Not specified	3.3
Applied harmonic voltage U_1 % of U_N	U_1	%	Not specified	110
Applied harmonic voltage U_3 % of U_N	U_3	%	Not specified	0.5
Applied harmonic voltage U_5 % of U_N	U_5	%	Not specified	6.0
Applied harmonic voltage U_7 % of U_N	U_7	%	Not specified	5.0
Applied harmonic voltage U_{11} % of U_N	U_{11}	%	Not specified	3.5
Applied harmonic voltage U_{13} % of U_N	U_{13}	%	Not specified	3.0
Power dissipation (full loss at I_{eff})	P_{eff}	W/kVAr	2.10	
Power dissipation (full loss at I_{eff})	P_{eff}	W	86	

Figure B.2 Comparison of manufactuer's data with system model

REFERENCES

Arrillaga, J. and Watson, N.R. (2003), *Power system harmonics*, J. Wiley and Sons, Hoboken, NJ;West Sussex, England;, 2nd ed.

Bell, S. and Bodger, P. (2007), 'Power transformer design using magnetic circuit theory and finite element analysis - a comparison of techniques', University of Canterbury research archives.

Bell, S.C. (2008), *High-voltage partial-core resonant transformers*, PhD thesis, University of Canterbury. Electrical and Electronic Engineering.

Bendre, V., Bell, S., Enright, W. and Bodger, P. (2007), In *AC high potential testing of large hydro generator stators using open core transformers*, University of Ljubljana Elektroinstitute Milan Vidmar Slovenia.

Bodger, P. (2014 lecture notes), 'Electroheaters and transformers', .

Bodger, P., Walker, R. and McInnes, I. (1996), 'Significant technology improvement in fluid heating', .

Bodger, P., Liew, M. and P.T.Johnstone (2000), 'A comparison of conventional and reverse transformer designs', AUPEC 2000 Hobart Australia 29 September 2013.

Bodger, P., Enright, W. and Ho, V. (2005), 'A low voltage, mains frequency, partial core, high temperature, superconducting transformer', .

Capacitors, K.P. (), 'Multicond power capacitors data sheet', .

Chew, E.P. (2010), *Superconducting Transformer Design and Construction*, Master's thesis, University of Canterbury. Electrical and Electronic Engineering.

Connelly, F. (1965), *Transformers: Their principles and Design for Light Electrical Engineers*, Ir Issac Pitman and Sons Ltd, London.

Detjen, D., Jacobs, J., Donker, R.W.D. and Mall, H.G. (2001), 'A new hybrid filter to dampen resonnances ans compensate harmoninic currents in industrial power systems with power factor correction equipment', .

Djeghloud, H., Terriche, Y., Larakeb, M. and Bentounsi, A. (2014), 'Laboratory implementation of a hybrid series active power filter system', In *16th International Power Electronics and Motion Conference and Exposition, Antalya, Turkey*, .

Electronicon (), 'PFC reactor theory and product data', .

Enright, W. and Bodger, P. (2005), 'Short time rated and protected high voltage ac testing of generator stators using parallel resonant circuits', .

Ferreira, J.A. (1989), *Skin and Proximity Effect Losses in Transformer and Inductor Windings*, Springer Science+Business Media, Dordrecht.

Gonen, T. (2008), *Electric power distribution system engineering*, CRC Press, Boca Raton, 2nd ed.

Gosbell, V.J., Muttik, P. and Geddey, D. (1999), 'A review of the new australian harmonic standard as/nzs 61000.3.6', Universities Power Engineering Conference, AUPEC, Australasian.

Hase, Y. (2013), *Handbook of power systems engineering with power electronics applications*, John Wiley, Hoboken, NJ, 2nd ed.

Heathcote, M.J. (2007), *J and P Transformer Book*, Newnes, GB, 13th ed.

Huo, X.T.B. (2009), *New Model of Eddy Current Loss Calculation and Applications for Partial Core Transformers*, Master's thesis, University of Canterbury. Electrical and Electronic Engineering.

Irani, Y. (2017), *Cascaded partial core resonant transformers.*, PhD thesis, University of Canterbury. Electrical and Electronic Engineering.

Irani, Y., Lapthorn, A. and Bodger, P. (2013), 'A comparison of vlf and 50 hz field testing of medium voltage cables', EEA Conference and Exhibition 2015 June Wellington.

Lapthorn, A. and Bodger, P. (2009), 'A comparison between the circuit theory model and finite element model reactive components', .

Lapthorn, A. and Keenan, K. (2012), 'A radially laminated core for partial core transformers', EEA Conference and Exhibition 2015 June Wellington.

Lapthorn, A.C. (2012), *High Temperature Superconducting Partial Core Transformers*, PhD thesis, University of Canterbury. Electrical and Electronic Engineering.

Liew, M., O'Neill, M. and P.S.Bodger (2001), 'Operating partial core transformers under liquid nitrogen conditions', .

Liew, M.C. (2001), *Reverse design transformer modelling technique with particular application to partial core transformers*, PhD thesis, University of Canterbury. Electrical and Electronic Engineering.

Munoz, A.M. (2007), *Power quality mitigation technologies in a distributed environment*, Springer, London.

Nasar, S. and Boldera, I. (1989), *Electric Machines: Steady State Operation*, Hemisphere Publishing Corporation, USA.

Paul, C., Nasar, S. and Unnewehr, L. (1986), *Introduction to electrical engineering*, McGraw-Hill Inc, Singapore.

Roddy, D. and Coolen, J. (1981), *Electronic Communications Second Edition*, Reston Publishing Company Inc, Reston Virginia.

Rosa, F.C.D.L. (2006), *Harmonics and power systems*, CRC/Taylor and Francis, Boca Raton, FL.

Sham, J.K. (2015), *High Temperature Superconducting Partial Core Transformer and Fault Current Limiter*, PhD thesis, University of Canterbury. Electrical and Electronic Engineering.

Slemon, G. (1966), *Magnetoelectric Devices: Transducers, Transformers and machines*, John Wiley and Sons Inc, USA.

Takau, L. (2015), *Improved modelling of induction and transduction heaters*, PhD thesis, University of Canterbury. Electrical and Electronic Engineering.

Watson, N., Orillaza, J.R.C. and Hardie, S. (2012), 'Harmonic planning levels in New Zealand medium voltage networks', *IEEE transactions on power systems*.

Zhong, M. (2012), *Partial Core Power Transformer*, Master's thesis, University of Canterbury. Electrical and Electronic Engineering.